Development of 2D-3D Numerical Coupling Model for Inundation Flow Analysis and Its Application to Urban Area

By

LEE Dongkeun

2010

Abstract

Inundation disasters due to heavy rainfall are common throughout the world, which contain inundation due to insufficient drainage capacity of sewerage, overflow from a river channel and inundation due to levee failure. Inundation disasters are frequently reported to have brought about extensive property damage and loss of life. Therefore, understanding of mechanism and behavior of inundation flow and research of countermeasures are very important in order to manage inundation disasters and prevent hazards in a river basin. To reduce inundation disasters, it is common to couple structural and non-structural countermeasures and consider various scenarios involving conditions of river and floodplain and variations of flood discharge.

Most of the inundation studies have been related to insufficient drainage capacity of sewerage or levee failure. But, study of inundation flow considering overflow from a river channel is also very important to establish countermeasures against inundation disasters. Hydraulic structures in a river such as pier and girder cause water level rise during flood period. In fact, flood disasters are occurring in all parts of the country. To evaluate effective non-structural preventive countermeasures against inundation disasters, it is necessary to estimate precisely the inundation flow considering overflow from a river channel and complicated flow in a river. To evaluate complicated flow in a river with hydraulic structures, it is necessary to consider three-dimensional flow with free-surface variation. Conducting a three-dimensional simulation for whole domain including river and floodplain is not efficient at all from the point of calculation time and capacity. Therefore, most effective method for this problem is coupling of two-dimensional and three-dimensional models.

So far, inundation analysis models are divided into integrated inundation models and dynamic inundation models. In the former one, flow fields for a floodplain and a river channel are calculated separately and connected by the overtopping formula. The latter one is conducted by the planar inundation analysis on incorporated domain with a floodplain and a river channel. In most of those numerical models, river channel flow has been considered as one-dimensional or two-dimensional flows, and inundation flow in a floodplain or an urban area has been considered as two-dimensional flow. However, at least in a river channel, three-dimensional computation is required for estimation of accurate overflow discharge from a river channel because one- or two-dimensional calculations are insufficient for evaluation of complicated flow around river structures and overtopping flow into a floodplain from a river channel. In this context, the main purpose of this study is to develop a numerical 2D-3D coupling model to

predict inundation phenomenon including overtopping flow from a river channel, which helps to establish the most effective and reliable countermeasures against inundation disasters.

A numerical coupling model is developed to reproduce the inundation flow in a floodplain or urban area considering overflow from a river channel and complicated flow in a river channel. 2D horizontal model and 3D Reynolds Averaged Navier-Stokes (RANS) model are employed for constructing the numerical coupling model. The finite volume method based on unstructured mesh is used in this model. The standard k-ε model and the Volume of Fluid (VOF) method are also employed for turbulence closure and free-surface modeling, respectively. As a coupling method of 2D and 3D models, simultaneous grid method is employed. The 2D domain (floodplain or urban area) and the 3D domain (river channel) are arranged to be connected, and some computational meshes of the 2D domain and the 3D domain are overlapping at the connected area. It is expected that more effective and reliable reproduction of inundation flow is possible by using this method.

First, in order to evaluate the validity of the proposed 3D model, it is applied to a river channel with river structures for estimation of flow considering water level rise by those structures. The laboratory experiments are also conducted to compare with the numerical results. The results of water level, velocity at z=2cm from bottom and free-surface velocity are used for comparison of simulations and experiments. From the results of water level, it is found that the numerical model can reproduce well the tendency of water level profile around hydraulic structures. Also, the numerical results of the velocities show good agreements with the experimental results. In conclusion, the simulated results generally are in good agreement with the experimental results, and it is judged that the proposed 3D numerical model can be useful to investigate the complicated flow in a river channel with hydraulic structures.

Second, inundation flow in a floodplain considering overflow from a river channel is estimated through coupling of 2D and 3D models. The study area includes 3D domain for a river channel and 2D domain for a floodplain. Two domains are connected by the overlapped meshes and calculation is carried out by the simultaneous grid method. The laboratory experiments are also conducted to compare with the numerical results and to estimate inundation flow in the floodplain considering complicated flow in the river channel. The results of water level and free-surface velocity are analyzed to verify the validity of the numerical coupling model and to evaluate the behavior of inundation flow. The simulated results have good agreements with the experimental results. Therefore, the proposed numerical coupling model can predict well

overflow into floodplain from a river channel as well as water level rise caused by the river structures.

Finally, application to actual area is carried out for evaluation of the proposed numerical coupling model. The observed extreme daily and maximum 24 hour precipitation at the observatory during the flood period are 427.5mm and 431.0mm, respectively. The inundation disaster started with overflow around river structures. The effects of river structures need to be investigated because the inundation disaster occurred during repairing work of river structures. The numerical coupling model proposed in this study is applied to this area for understanding the process of inundation and the influence of river structures. It is judged that simulated results generally have good agreements with the previous inundation data. Consequently, the proposed coupling model can be useful also in an actual urban area.

In this study, the numerical analysis and the experimental studies are carried out to investigate the inundation flow considering overflow from a river channel. The numerical coupling model is developed and applied to experimental flumes and an actual urban area. The computational results of inundation flow are in good agreement with the experimental and observed results. Therefore, this proposed model will be helpful to establish non-structural countermeasure systems against inundation flow disasters caused by effects of river structures such as piers and girders of bridges.

Key Words: *inundation flow, overflow, floodplain, urban area, river channel, river structures, laboratory experiments, numerical coupling model*

Acknowledgements

I would like to express my sincere gratitude and appreciation to many people who made this thesis possible.

I would like to express my deepest and sincere gratitude to my supervisor, Professor Dr. Hajime Nakagawa, Disaster Prevention Research Institute (DPRI), Kyoto University, for his continuous guidance, support and encouragement throughout my whole study period.

I am deeply grateful to my thesis reviewers, Professor Keiichi Toda and Professor Masaharu Fujita, Disaster Prevention Research Institute (DPRI), Kyoto University, for their valuable comments and suggestions to refine the thesis.

I wish to express my sincere gratitude to Dr. Kenji Kawaike, Dr. Yasuyuki Baba and Dr. Hao Zhang, for their valuable guidance and suggestions in all aspects of my study. I would also like to express my sincere thank to Dr. Ripendra Awal and Dr. Badri Bhakta Shrestha for their support and help in many aspects. I warmly thank Mr. Satoshi Kohda for his valuable discussions and friendly helps.

I am indebted to my all colleagues of River Disaster Prevention System (RDPS), Disaster Prevention Research Institute (DPRI), Kyoto University for their kind cooperation, helps and unforgettable friendship. I am especially grateful to Mr. Hiroshi Teraguchi, Mr. Hideaki Mizutani, Mr. Ram Krishna Regmi, Mr. Amir Reza Mansoori, Mr. Yeonjung Kim, Mr. Seungsu Lee, Mr. Takaharu Utsumi, Mr. Yasunori Nanbu, Mr. Yasutaka Saito, Mr. Toshimasa Mataga, Mr. Atsushi Shimizu, Mr. Sohshi Yoneda, Mr. Shiro Nakanishi, Mr. Hidenari Sumitomo and Mr. Taichi Tachikawa.

I would like to thank all the professors and friends in the Research Center for Fluvial and Costal Disaster, Disaster Prevention Research Institute of Kyoto University, who have made my academic experience rich and memorable. I would like to thank Mr. Seiji Fujihara, Mr. Kazuhiro Nishimura, Mr. Yoshinori Yoshida, Mrs. Natsuyo Sugimura and all the staffs in Ujigawa Open Laboratory, Disaster Prevention Research Institute of Kyoto University for their support in routine administrative process and experiments.

I gratefully acknowledge the financial support of the Monbukagakusho (Ministry of Education, Culture, Sports, Science and Technology, Japan).

I would like to thank my parents Hakman Lee and Gapnyeon Kwak and all other family members for their encouragement and loving support. Finally, I am deeply grateful to my wife Hyegyeong Park and son Myeonghan Lee for their understanding, contribution and support throughout my study period.

Table of Contents

Chapter 1

Introduction

1.1 General

Nature preservation and development, those are words that mean one of the biggest conflicts for the human. The destruction of nature by the development for improvement of the quality of life is an inevitable result. The consequence could increase the damage of properties and lives of the human. The flood disasters by heavy rainfall are one of the biggest troubles and their resultant damages are also the heaviest among natural disasters occurring in the world. Figure 1.1 shows major flood disasters by heavy rainfall and typhoon which occurred in the world. It is the best to carry out the development with natural preservation, but that is not easy. Therefore, the human have to find the countermeasures to protect the properties and lives. The measures and actions are the most important when a disaster occurs because it is impossible to block occurrence of natural disasters. The research for establishment of those countermeasures is one of the most important issues for present all humankind.

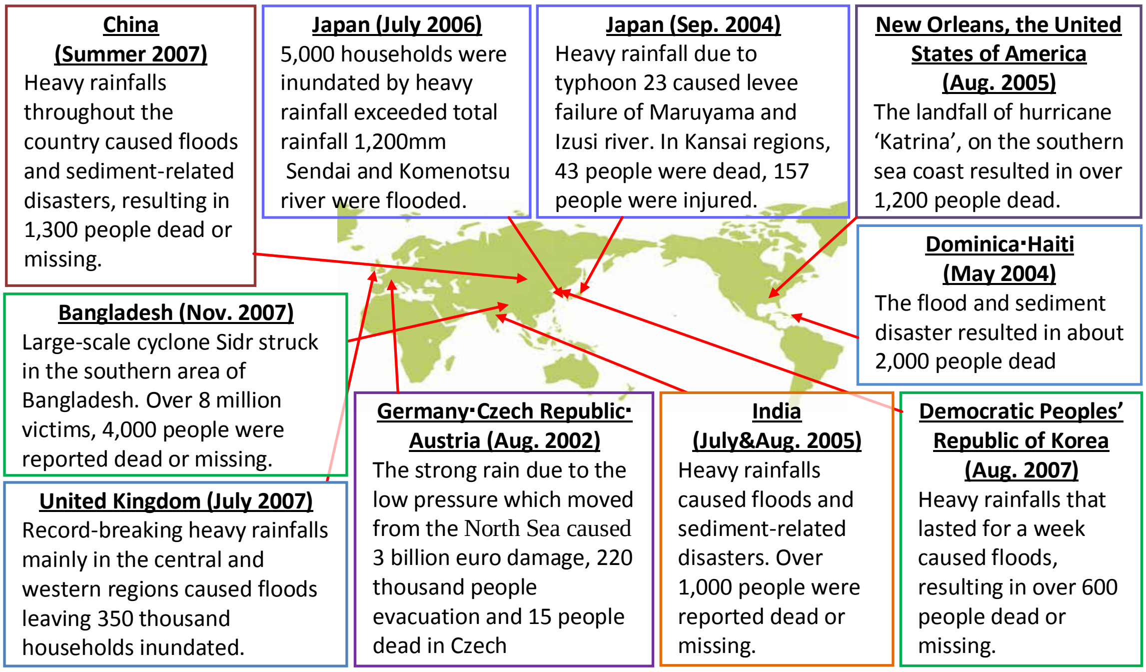

Figure 1.1 Major flood disasters which occurred in the world (*Source: MLIT, Japan)*

Inundation disasters are one of the representative natural disasters. The inundation disasters have been increasing by effects of urbanization and industrialization. Before urbanization and industrialization, rain water infiltrated into ground during flood period and houses were located in safer areas. But, after urbanization and industrialization, increase of flood discharge and quick collection of rain water into river channel occurred because impermeable area increased and water retention function decreased in the river basin. Urbanization and industrialization of the river basin have much effect on discharge hydrograph of the river. Figure 1.2 shows the changes before and after urbanization and industrialization.

Many people have lived in floodplains after urbanization and industrialization, and it has caused increase of damages during flood disasters. Figures 1.3 shows the terrain conditions around the rivers in Japan and United Kingdom.

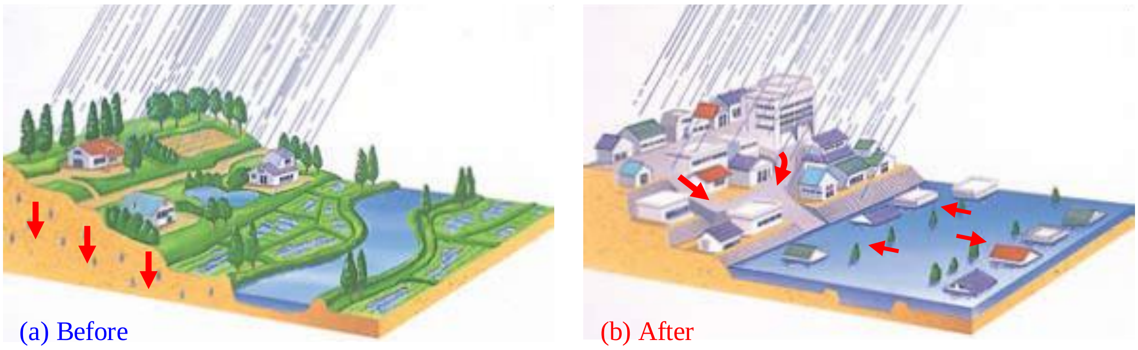

Figure 1.2 Before and after urbanization and industrialization (*Photo Courtesy: MLIT, Japan)*

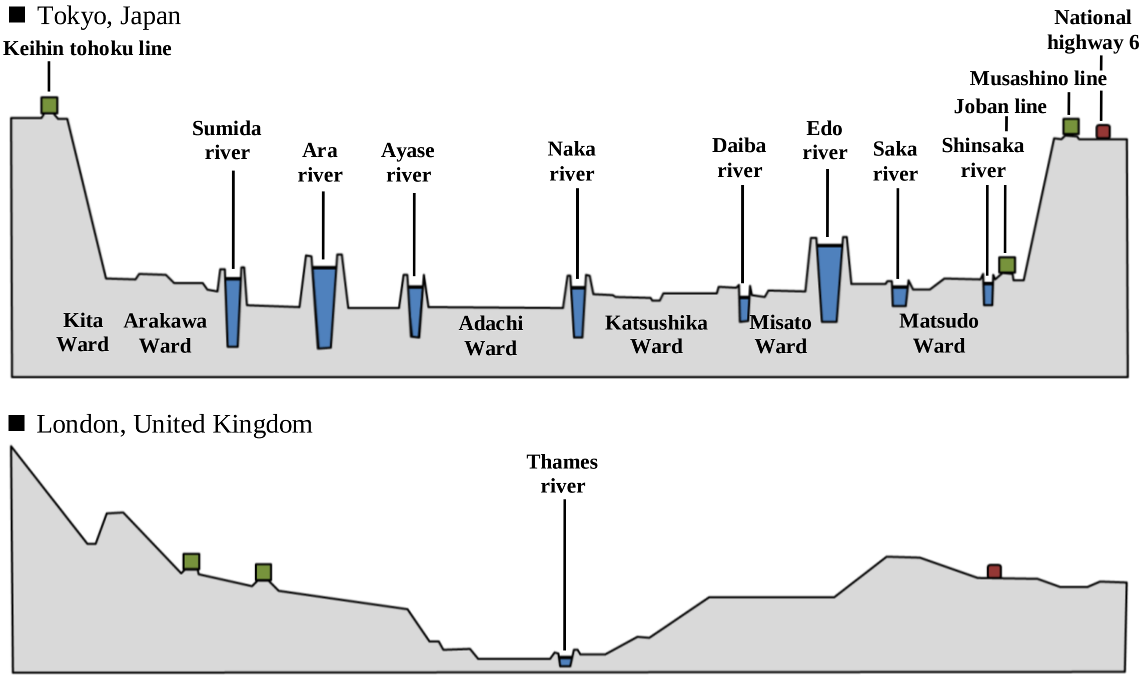

Figure 1.3 Terrain conditions of Japan and United Kingdom (*Source: MLIT, Japan)*

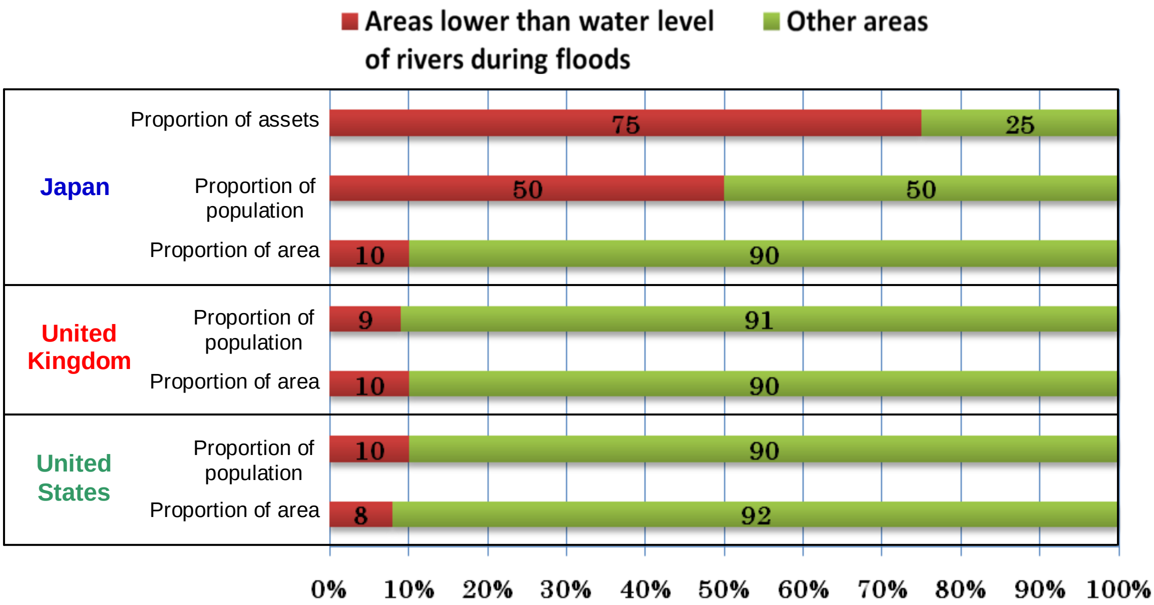

Figure 1.4 Proportion of population and area in low-lying area (*Source: MLIT, Japan)*

As seen in Figure 1.3, the water overflowing an embankment would give the damages directly to people living in a floodplain. Therefore, establishing the inundation measures for residents in a floodplain is very important. In particular, most of urban areas in Japan are located in low-lying areas that are lower than the water level during flooding duration. As shown in Figure 1.4, in Japan, much damage is anticipated when flooding occurs because half of the population and three-quarters of total properties are concentrated in low-lying areas. And thus, establishment of countermeasures when an inundation disaster occurs is more important than any other countries, so Japan has to pay much attention to them.

Japan is surrounded by 40,000km coastal line and is located on the path of typhoons. Also, there are frequent earthquakes in the sea area around Japan and many big cities are faced to bay areas. From ancient times, Japan has experienced many inundation damages due to tsunami, storm surge and heavy rainfall because of such geographical characteristics. Figure 1.5 shows the classification of land-use of Japan. 10 percent of Japanese territory is the flood inundation area and many people is living in this area. Therefore, the establishment of prevention measures against the inundation disasters is more important than any other countries.

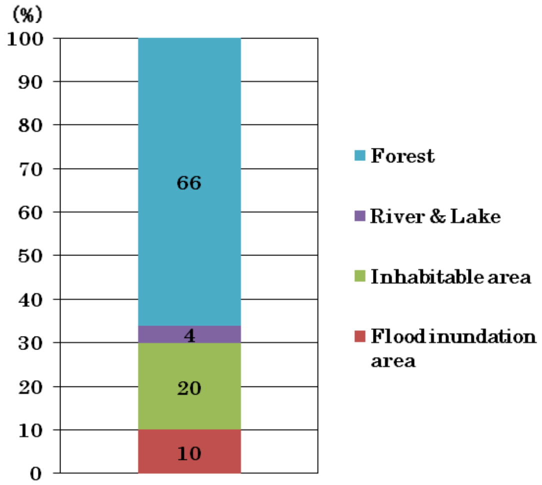

Figure 1.5 Classification of land-use of Japan
(*Source: MLIT, Japan)*

- Hourly maximum rainfall : 93mm,
- Total amount of rainfall (11-12 Sep.) : 567mm

(a) Shonai river, Aichi Pref., Japan (11-12 Sep., 2000)

- Hourly maximum rainfall : 73mm
- Total amount of rainfall (13 July) : 473mm

(b) Ikarashi river, Niigata Pref., Japan (13 July., 2004)

- Hourly maximum rainfall : 50.0~100.0mm
- Total amount of rainfall (18 July) : 338mm

(c) Asuwa river, Fukui Pref., Japan (18 July., 2004)

- Hourly maximum rainfall : 71mm
- Total amount of rainfall (4-8 Sep.) : 1307mm

(d) Mimi river, Miyazaki Pref., Japan (4-8 Sep., 2005)

- Hourly maximum rainfall : 146.5mm
- Total amount of rainfall (26-31 July) : 475mm

(e) Asa river, Hachioji City, Tokyo, Japan (26-31 Aug., 2008)

- Hourly maximum rainfall : 80mm
- Total amount of rainfall (19-26 July) : 702mm

(f) Kusu river, Oitai Pref., Japan (19-26 July, 2009)

Figure 1.6 Major inundation disasters occurred in Japan (*Photo Courtesy: MLIT, Japan)*

Many inundation disasters have occurred in Japan and Figure 1.6 shows those from 2000 to 2009. Inundation disasters by heavy rainfall are frequently occurring in a floodplain connected with a river. Inundation flow analysis in those areas is necessary for construction of preventive measure against urban flood disasters.

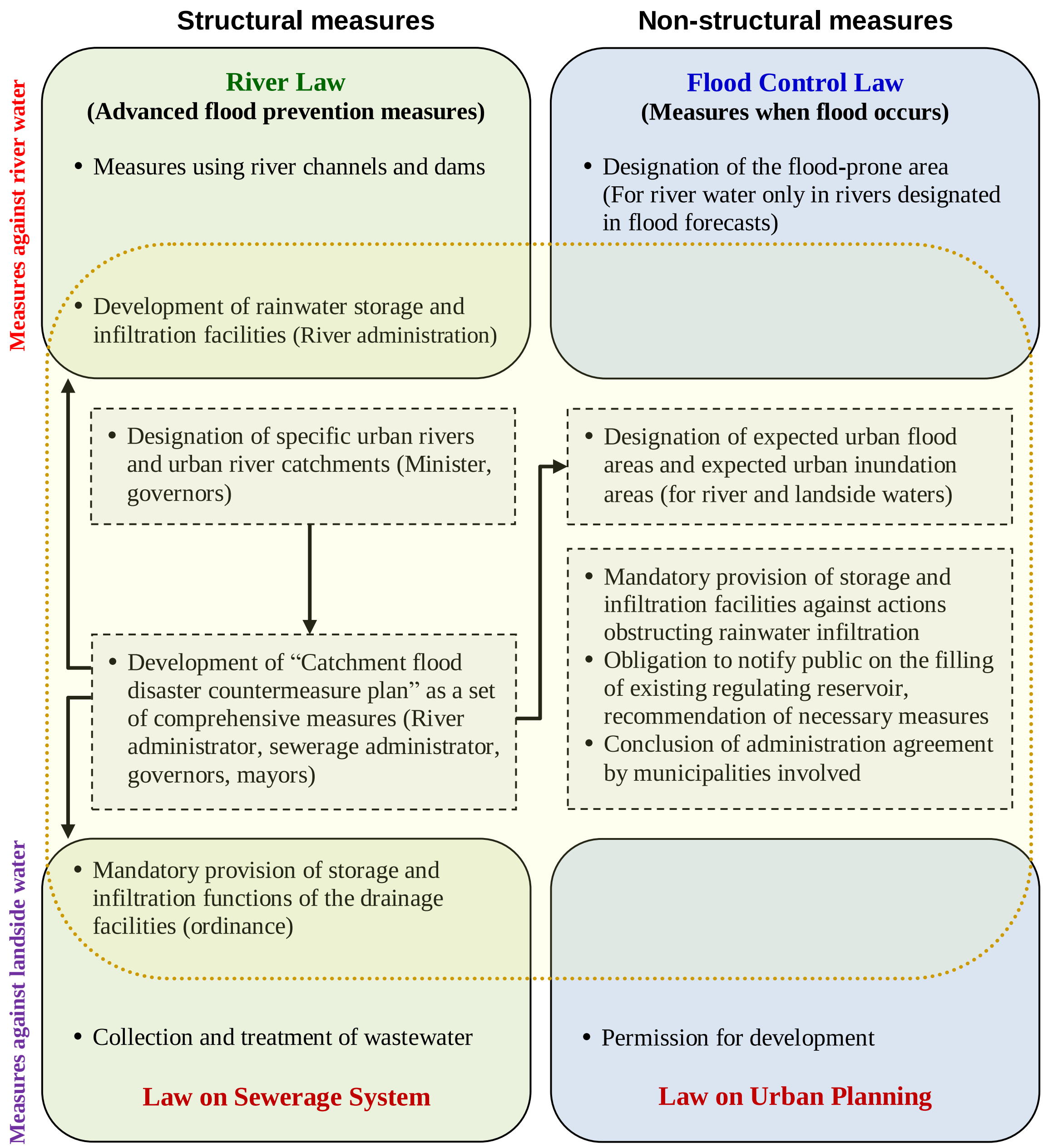

Figure 1.7 Structural and non-structural measures implemented in Japan (*Source: MLIT, Japan)*

In order to reduce the inundation damages, it is common to couple structural and non-structural preventive measures. Figure 1.7 shows the comprehensive measures against urban flood disaster coupling structural and non-structural preventive measures implemented in Japan.

The structural measures such as dam and levee have their limit of the reduction of flood disasters. Therefore, consideration of non-structural measures to minimize the flood damages is certainly necessary. Establishing non-structural measures which can be helpful for evacuation activity by making precise flood hazard map is very important.

The main aim of this study is to develop a most effective and reliable numerical method to predict inundation flow disasters. In that aim, this study focuses on flood flow in a river channel and inundation flow on a floodplain connected with a river channel. And, the variations of water level caused by hydraulic structures in river channel are also investigated in this study.

1.2 Types of inundation flows

The typical inundation disasters are divided into two classes which occurred by insufficient drainage capacity and by river water flooding. Figure 1.8 shows the Tokai disaster by heavy rainfall which occurred in the Shin river of Nagoya City, Aichi Prefecture, Japan in September, 2000. This is the representative photo showing both of the above mentioned two inundation disasters. In the photo, the left side and the right side show inundations by insufficient drainage capacity and by river water flooding, respectively. Those different types of inundations also can be recognized by the difference of water color in the left and right sides in the photo.

Figure 1.8 Typical inundation disasters *(at Shin River, Nagoya City, Aichi Pref., Japan, 2000)*
(Photo Courtesy: MLIT, Japan)

The inundation flows basically occur by unexpected amount of rainfall when localized heavy rainfall occurs. If inundation disasters happen because it is impossible to drain all the rainfall in an urban area and a river channel, it is called inundation by insufficient drainage capacity and by river water flooding, respectively. This study will focus on the inundation by river water flooding of those inundation disasters. The inundation by river water flooding is divided into the inundation by dyke failure and by overflow from a river channel. Most of the researches related to the inundation by river water flooding have been conducted about the inundation by dyke failure. In this study, however, the inundation by overflow from a river channel without dyke failure will be investigated. Furthermore, the effects of hydraulic structures in a river channel are also considered.

1.3 Flood flow disasters and their countermeasures in practice

Many people in the world suffer from many flood disasters. The protection systems that guarantee complete safety from those disasters are almost impossible. But, some measures could reduce the extent of damage if planned and implemented effectively. Flood flows are one of the most dangerous disasters that affect humans and properties, which are common in urban areas connected with river channel throughout the world. Figure 1.9 and 1.10 show the inundation flow disaster which occurred in August, 2002 in German, Europe. In August 2002, a severe flooding by heavy rainfall from storms attacked Europe. This event resulted in 22 thousand people evacuation, 15 people dead and about 3.0 billion euro damage in Czech Republic, 12,000 people evacuation, 4 people dead and about 9.2 billion euro damage in German and 8 people dead and 2.5-3.0 billion Euro damage in Austria.

Figure 1.9 Inundated Semper Opera House at Dresden, German
(Photo Courtesy: MLIT, Japan)

Figure 1.10 Family waiting for help from the air at Saxony, Germany
(Photo Courtesy: MLIT, Japan)

In Germany, the following five important projects were carried out after experiencing the 2002 European floods.

- Implementation of nationwide (consistent throughout the federal and state governments) protection plan against floods (expansion of river channel space by securing floodplain, division of flood control function, control of new development of land, reduction of damage potential)
- Preparation of action plan across the border
- Cooperation of all over Europe
- Reconsideration of river maintenance･Transportation using the ship which is good for environment
- Urgent countermeasure for reinforcement of flood control system

To apply those projects, the case studies were conducted on the Rhine river, which is one of the longest and most important rivers in Europe, and Elbe river, which is one of the major rivers of Central Europe.

In the end of May 2004, Record-breaking heavy rainfall struck Haiti and Dominican Republic located in the Caribbean Sea. Severe damages were reported about 2,000 people dead and about 5,000 house collapsed in both countries by large-scale sediment disaster and flood. In the western region of Dominican Republic, the flood disaster by river water flooding resulted in 393 people dead and 274 people missing. 414 people died in all over the Dominican Republic. The damages of Haiti were bigger than Dominican Republic and at least 1,660 people died by sediment and flood disaster. At least 237 people died by sediment and flood disaster at village near the border.

Figure 1.11 Inundation disaster at Santo Domingo, Dominican Republic
(Photo Courtesy: AFP, France)

Haiti is the poorest country in the Americas and GDP of Dominica is the lowest in Eastern Caribbean states. In particular, Haiti is the state receiving a lot of aid from other countries when flood disaster occurs. Therefore, it is judged that measures against flood disaster are insufficient because of their economic situations.

The New Orleans of the United States suffered from a major disaster by hurricane Katrina in August 2005. More than 1,200 people died, 80% of the city were inundated and 40% of the inhabitants were not able to return to their houses by failure of the dyke protecting the downtown. Figures 1.12 and 1.13 show the inundation situations of New Orleans. Judging from the fact that large-scale inundations actually occurred the countermeasures against flood disaster did not work effectively.

Figure 1.12 Inundation disaster of downtown at New Orleans, United States
(Photo Courtesy: MLIT, Japan)

Figure 1.13 Inundation disaster by dyke failure at New Orleans, United States

(Photo Courtesy: MLIT, Japan)

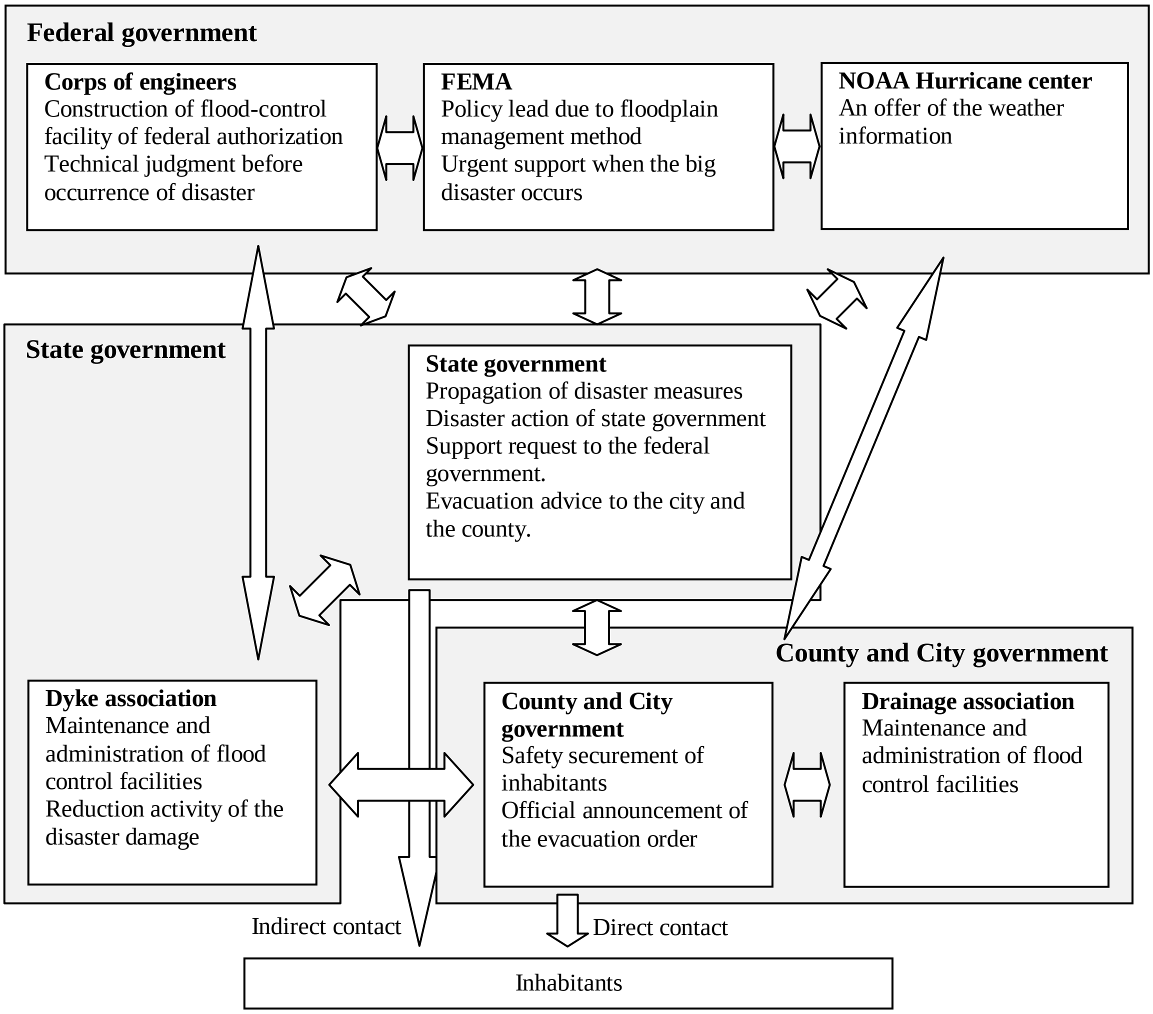

Figure 1.14 Organization and function about flood prevention of America

(Source: MLIT, Japan)

Figure 1.15 Inundation disaster at Mumbai, India
(Photo Courtesy: International Centre of Excellence in Water Resources Management)

In the United States, the federal government carries out the construction of the dyke and the local government manages the dyke. The dyke association carries out the maintenance and administration including flood control activities. The organization and function of the United States are shown in Figure 1.14. United States had such countermeasures and function, but it was not operated well by insufficiency of education and the training

In India, a severe flooding occurred in the monsoon season, in 2005. More than 1,000 people were dead or missing after weeks of incessant rainfall. The city of Mumbai was inundated with 93.98 cm of rain in 24 hours. 25 million people were impacted by the flooding. Figure 1.15 shows the inundation situation at Mumbai, India.

400 large dams have been built in India along with 16,000 km of river embankments, but the inundation areas has expanded from 2 million to 9 million hectares due to insufficient drainage and deforestation. The damage increased because a lot of people were living in low-lying area and the Mumbai drainage system was old. After the disaster, the central and state governments made efforts for the reduction of disaster and coordinated with NGOs, UN bodies, etc.

In the United Kingdom in 2007, a deluge occurred across central and southern regions. Many places recorded one month's rainfall or more in a day. England was affected by floods in June and July, 2007. 350 thousand households were inundated by this flood. In Gloucester, about 1.5 times precipitation of the average precipitation on July was observed in one day. And, 350 thousand people could not drink the water because a water station was inundated. In Oxford, a

Figure 1.16 Inundation disaster at Worcestershire, United Kingdom
(Photo Courtesy: Risk Management Solutions Inc.)

deluge occurred by a collapse of an embankment in the Thames River. By this dyke breach, 140 thousand households and over 350 thousand people suffered from the flood damages.

After that, the government announced the increase of the spending on risk management and flood prevention by 2010-11. In April 2010, the government passed the Flood and Water Management Act 2010.

In summer of 2007, flood disasters frequently occurred in Asia. Figure 1.17 and 1.18 show the inundation disasters in China and North Korea, respectively. Both countries suffered from the large damages by heavy rainfall.

Figure 1.17 Inundation disaster at Chongqing, China
(Photo Courtesy: MLIT, Japan)

Figure 1.18 Inundation disaster at Pyongyang, North Korea
(Photo Courtesy: AFP, France)

The flood disasters which occurred in China caused 1,300 people dead or missing. In North Korea, the flood by heavy rainfall resulted in 600 people dead or missing. The measures for flood management implemented in China are divided into the structural and non-structural measures. The former one includes levees, reservoirs, flood storage and water conservation and the latter one means land use controls, development controls, emergency response planning, flood insurance and preparedness.

The latest flood disaster is the flood in Pakistan 2010. Approximately one-fifth of Pakistan's total land area was inundated by this disaster. This disaster caused 1,767 peoples dead, 2,865 peoples injured and 1,884,708 houses damaged.

Figure 1.19 Bridge damaged by the flooding at Pakistan
(Photo Courtesy: Pakistan National Disaster Management Authority)

The government action against the flood disaster faced in many difficulties because approaching to the damaged areas was impossible by inundation of land and road. And, an aid for the victim met difficulty when relief supplies were sent because of political relations between nations.

So far, the representative floods which occurred in many regions of the world except Japan have been summarized. Japan is one of the countries in the world where a lot of natural disasters occurred in the world. The disasters by heavy rainfall are one of the most serious problems among natural disasters. And the countermeasures against flood disasters also have been established well in Japan because Japan has experienced many flood disasters. Figure 1.20 shows the examples of flood disaster by heavy rainfall which occurred in Japan. Figure 1.21 shows the location and the overflow evidence by backwater in JR bridge in Asuwa river, Fukui Pref. in 2004, which one of major inundation disasters occurred in Japan. It is found that considering backwater by river structures is very important to estimate the river water flooding.

Tokai flood disaster by heavy rainfall in Aichi Pref., Japan on Sept., 2000

Inundation of Naka River by Typhoon 23 in Tokushima Pref., Japan on Sept., 2004

Inundation of Hii River by heavy rainfall in Shimane Pref., Japan on July, 2006

Flood situation of Tama River by Typhoon 9 in Tokyo, Japan on Aug. ~ Sept., 2007

Flood situation of Noudai River by Typhoon 11 in Akita Pref., Japan on Sept., 2007

Figure 1.20 Flood disasters which occurred in Japan
(Photo Courtesy: MLIT, Japan)

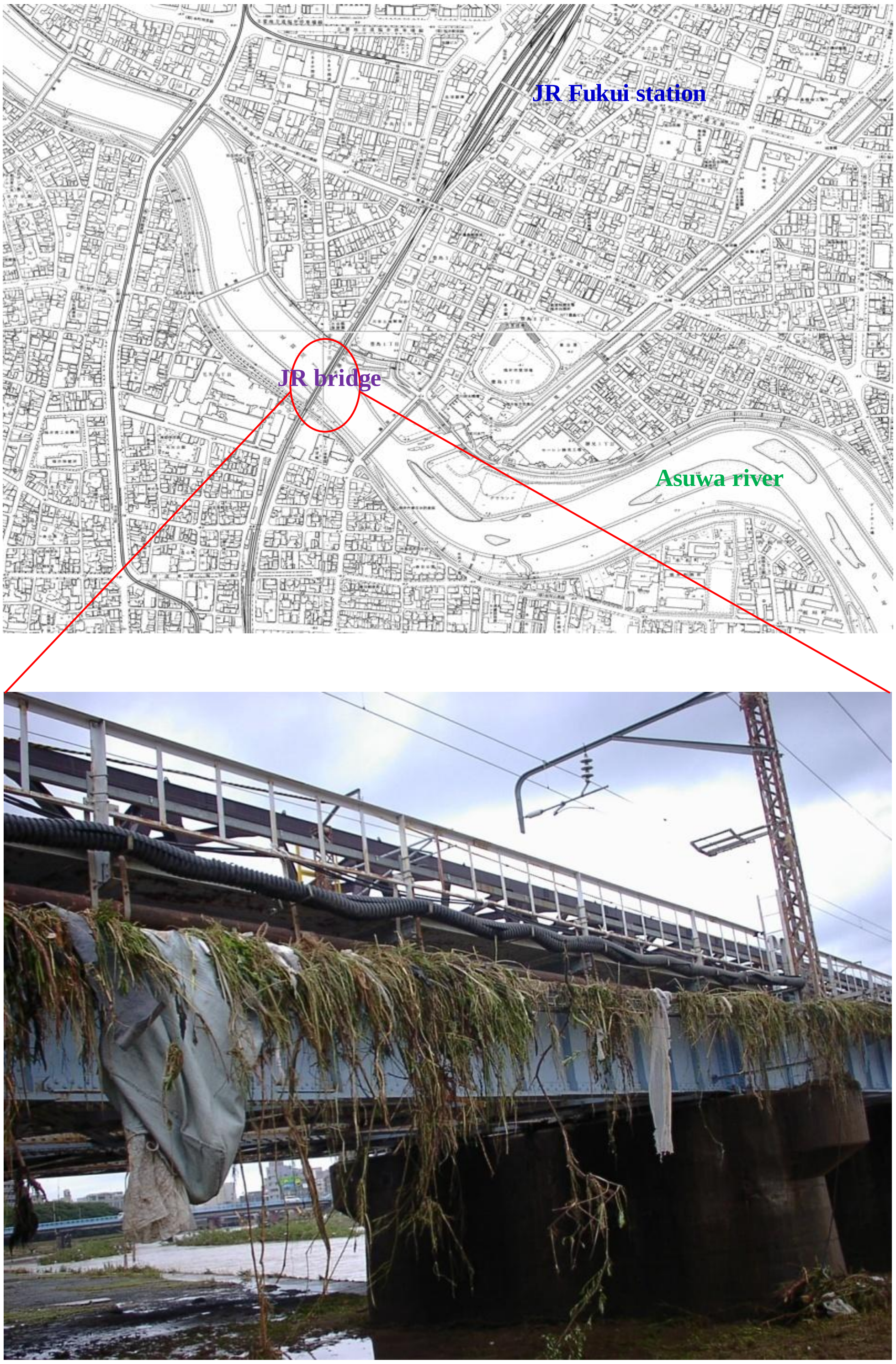

Figure 1.21 Water level rise (14cm) due to backwater by river structures in JR bridge
(Photo Courtesy: MLIT, Japan)

The countermeasures against the flood disasters in Japan are commonly coupling structural and non-structural preventive measures as shown in Figure 1.7. Many human lives and properties have been prevented from flood disasters based on appropriate consideration and judgment with those countermeasures. Figure 1.22 shows the comprehensive disaster management system and main contents of the disaster countermeasures in Japan.

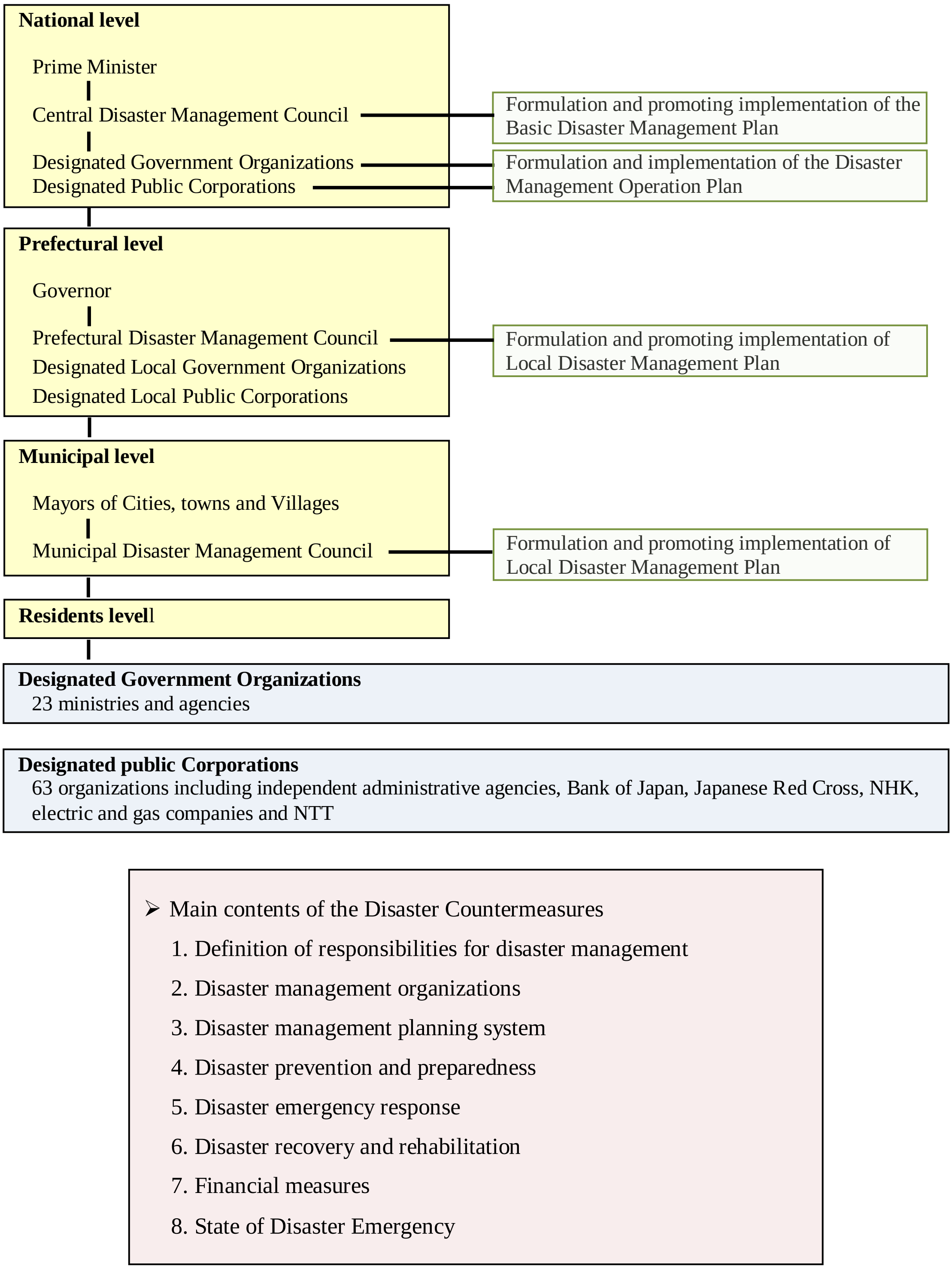

Figure 1.22 Outline and main contents of the Disaster Management System of Japan
(Source: Cabinet Office, Government of Japan)

In summary, preventive measures designed to reduce the inundation flow disasters can be classified as structural or non-structural measures. The former include dams, levees and river channel works, while the latter include hazard map, disaster warning, evacuation systems, emergency communication systems, proper land use and preparedness. The combination of structural and non-structural countermeasures is commonly used to reduce the inundation flow disasters effectively. Comprehensive analyses considering the both countermeasures to prevent the inundation flow disasters are very important. The accurate numerical simulation can be helpful for the establishment of countermeasures.

1.4 Objectives of the research

The aim of this study is to develop a numerical model as a most effective and reliable method to predict inundation flow disasters considering overflow from river channel. The main objectives of this study are summarized as follows.

(a) to develop a numerical model for computing the flood flow considering water level rise by hydraulic structures,
(b) to develop a 2D-3D numerical coupling model for computing the inundation flow analysis by coupling 2D flow field in floodplain and 3D flow field in river channel with hydraulic structures,
(c) to investigate the inundation flow considering overflow from a river channel into a floodplain with effects of river structures,
(d) to investigate and estimate actual inundation flow disaster through the application to actual area by using developed 2D-3D numerical coupling model.

1.5 Previous researches: a brief overview

Many researches have been conducted to predict the behavior of inundation flow. So far, inundation models used are divided into two types, which the dynamic inundation model and the integrated inundation model. The former one is to carry out the inundation analysis on the incorporated domain with a floodplain and a river channel, whilst the latter one is to carry out the inundation analysis separately on the domain with each flow field for a floodplain and a river channel. The previous researches about the flood inundation analysis are summarized and described below.

Shigeeda et al. (2002) carried out the numerical simulations by the horizontal two-dimensional model using the finite volume method. And, a levee failure and inundation experiment considering the structures in a floodplain were executed for the verification of the numerical model. Shigeeda and Akiyama (2003) also conducted the horizontal two-dimensional simulations and the laboratory experiments on the conditions with and without structures. Shigeeda and Akiyama (2005) carried out the numerical calculations to predict the overflow from a river channel by using the horizontal two-dimensional numerical model and the numerical results were compared and verified with the experimental results. Kawaguchi et al. (2005) developed a numerical model to estimate abrupt flooding flow and washout of houses and applied to flood of Karayata river in Niigata Pref., which occurred in 2004. Akiyama et al. (2007) estimated the overflow discharge by comprehensive analysis of a river channel and a floodplain and compared with the results obtained from a laboratory experiment. The inundation analysis in a meandering channel was carried out to estimate the overflow discharge by Akiyama et al. (2008). Nakagawa et al. (2003) simulated the inundation damage of the Kamo River, which occurred in 1935, by using the experimental setup for the large scale inundation analysis and compared with the numerical results by the horizontal two-dimensional numerical model. Mignot et al. (2004) compared with the experimental results simplifying the characteristic of the urban area to verify the application of the two-dimensional numerical model on the urban area. Han et al. (1998) performed the research for one- and two-dimensional hydrodynamic models for the simulation of flood wave due to the levee failure. Kawaike et al. (2002) simulated the inundation flow in the urban area by using different numerical models, which Cartesian coordinate, Generalized curvilinear coordinate, Unstructured meshes and Street network model. And, Kawaike et al. (2004) simulated the inundation flow by heavy rainfall in low-lying basin by using the integrated inundation analysis model. One dimensional unsteady flow analysis based on St. Venant equation as the governing equation was conducted to analyze the flow of river channel. In a floodplain, the horizontal two-dimensional inundation analysis using Leap-Frog method was carried out. Connell et al. (2001) developed a two-dimensional inundation model, and then considered friction loss and boundary condition of grid by land nature and plant condition in a floodplain. The results obtained from the model were compared with one-dimensional numerical model to verify stability and accuracy of the numerical model. From the results, it was found that accuracy of two-dimensional model is better than one-dimensional model because complicated topography and structures in a floodplain can be expressed. Kamrath et al. (2006) developed and verified simplified two-dimensional numerical model to predict the inundation flows in real time.

The above mentioned previous studies are shown in Table 1.1. As seen in the summary of previous studies, most of the researches were related with the horizontal two-dimensional numerical calculation. In those models, a river channel was considered as incorporated domain or separated domain from a floodplain. In the integrated inundation model, the simulations for a river channel have been carried out by the one-dimensional unsteady flow analysis. And, most of previous researches have been related to the inundation by levee failure of river water flooding.

Table 1.1 Summary of previous studies

Researcher	Main content	Condition	Applied model
Han et al. (1998)	Flood inundation analysis by levee failure	Levee failure occurred in 1990	1D unsteady flow model on river channel Horizontal 2D inundation model
Connell et al. (2001)	Application of two-dimensional model on floodplain	Inundation disaster occurred in 1986 and 1994	Horizontal 2D inundation model
Shigeeda et al. (2002)	Numerical simulation on propagation of flood wave considering structures in floodplain	Simulation by arrangement of structures	Horizontal 2D numerical model
Kawaike et al. (2002)	Application of inundation model to urban area	Comparison of different numerical model	Cartesian coordinate model, Generalized curvilinear coordinate model, Unstructured meshes model, Street network model
Shigeeda et al. (2003)	Numerical simulation and laboratory experiment on the cases with or without structures in floodplain	Consideration on the effects of structures in floodplain	Horizontal 2D numerical model

Nakagawa et al. (2003)	Flood inundation analysis in urban area using large scale inundation facility	Imaginary flooding	Horizontal 2D inundation model
Mignot et al. (2004)	Development of two-dimensional model for inundation simulation in urban area	Simulation by arrangement of structures in floodplain	Horizontal 2D numerical model
Kawaike et al. (2004)	Simulation of inundation flow due to heavy rainfall	Inundation in low-lying river basin	Integrated inundation model (1D unsteady flow model in river channel and horizontal 2D inundation model)
Kawaguchi et al. (2005)	Flood analysis of Kariyata river in Niigata Pref.	Flooding flow due to levee break in July, 2004	Horizontal 2D numerical model
Shigeeda et al. (2005)	Estimation of overflow discharge from the river channel	Cases with or without levee	Horizontal 2D numerical model
Kamrath et al. (2006)	Simulation of flood wave propagation and assessment of discharge by levee failure for real time prediction	Hazard mapping	1D river channel model Horizontal 2D model
Akiyama et al. (2007)	Predictions of overflow discharges by a dynamic inundation model and analysis of an urban inundation process due to dike breach	Levee failure occurred in July, 1986	Horizontal 2D numerical model
Akiyama et al. (2008)	Estimation of overflow discharge in a meandering channel	Cases with or without retarding plantations	Horizontal 2D numerical model

As seen in the previous studies, most of the researches for the inundation flow analysis mainly have conducted the inundation study by levee failure and most of them have considered the numerical analysis using the horizontal two-dimensional model. In the analysis of a river flow, the horizontal two-dimensional calculations have been carried out on the incorporated domain with a floodplain or the one-dimensional unsteady flow analysis has been executed. In the latter cases, the inundation analysis coupling one-dimensional river channel model and two-dimensional inundation model has been considered. However, there are very few or no estimation of overflow discharge by three-dimensional model in a river channel and the inundation analysis in floodplain by two-dimensional model using those. For accurate estimation of inundation flow, it is judged that assessment of overflow discharge by three-dimensional calculation in a river channel and inundation analysis by two-dimensional calculation in a floodplain is certainly necessary.

1.6 Outlines of the dissertation

The dissertation concerns the development of a most effective and reliable numerical model to predict the inundation flow disasters considering overflow from a river channel with hydraulic structures. It consists of six chapters.

Chapter 1 presents brief background of the work, objectives of the study and previous literature reviews.

Chapter 2 presents a three-dimensional numerical model with free-surface to calculate the flood flow considering the water level rise in a river channel with hydraulic structures. The proposed models are compared and verified with different cases of experimental results.

Chapter 3 presents a two- and three- dimensional numerical coupling model for computing the behavior of inundation flow considering overflow from a river channel with hydraulic structures. The two- and three-dimensional numerical model are coupled and calculated by simultaneous grid method. The simulated results are compared and verified with the results obtained from the hydraulic model experiments.

Chapter 4 presents an application to actual area of developed 2D-3D numerical coupling model. The validity and reproducibility of the numerical model are estimated through comparisons of the results of previous study.

Chapter 5 summarizes the conclusions of the study and recommendations for the future researches.

Chapter 2

Flood flow analysis

2.1 Introduction

Flood inundation disaster is one of the most critical natural hazards that affect lives and properties. Inundation by river water flooding is caused by water level rise due to increase of discharge in a river channel during heavy rainfall. Therefore, the understanding of behaviour and mechanism of flood flow in a river channel is very important in order to estimate the inundation flow in a floodplain by overflow from a river channel. It is also necessary to investigate the flood flow considering water level rise by effect of river structures. Figure 2.1 shows the variations of water surface by with and without river structures.

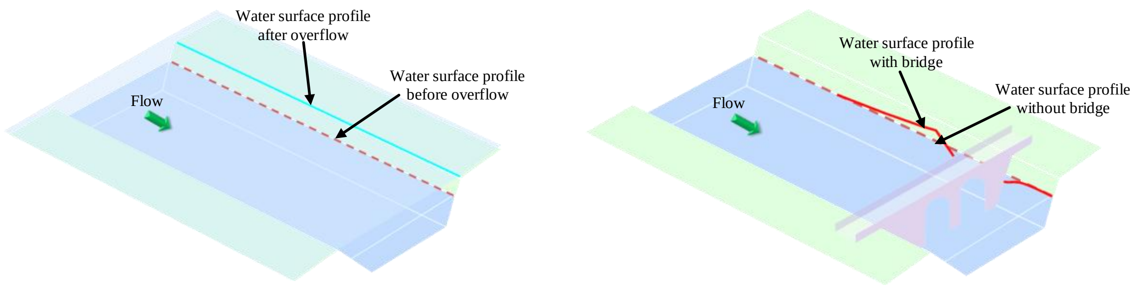

(a) without (b) with

Figure 2.1 Water surface profiles with and without river structure

A three-dimensional numerical model for the estimation of flow considering water level rise by hydraulic structures in a river channel is proposed and the results are compared with the experimental results in this chapter. 3D RANS (Reynolds Averaged Naiver-Stokes) equations are employed as governing equations for this study. The numerical simulations are carried out on the unstructured meshes with the finite volume method. The VOF (volume of fluid) method is used to reproduce the flow with the free surface and the standard k-ε model is also employed to simulate the turbulent flow. The numerical simulations and the laboratory experiments are conducted about considering the bridge pier and girder which are the representative hydraulic structures in a river channel. The validity of the developed numerical model is estimated through the results obtained from the simulations and experiments. The effects of water level rise by river structures are also evaluated in this chapter.

2.2 Three-dimensional flow modeling

2.2.1 Introduction

3D turbulence models

The mathematical modeling of the turbulent flow is one of the most difficult problems in the hydraulic engineering. The methods solving the turbulent flow are three types: DNS (Direct Numerical Simulation), RANS (Reynolds-Averaged Navier-Stokes) and LES (Large Eddy Simulation). First, DNS is the method solving the Navier-Stokes equations directly, but it leads to an extreme consumption of computer resources. Two alternatives then have been proposed: time-averaged and space-filtered. To achieve the turbulent closure, these methods introduce additional unknown terms. The former and latter ones lead to RANS and LES model, respectively. LES employs very fine grid to solve the larger eddies and uses turbulence model only for the smaller scales. LES is relatively easier to construct a universal model. However, the use of LES has still the computational burden in the engineering practice. On the other hand, RANS model is relatively simple and may greatly reduce the computational burden because this represents transport equations only for the mean flow quantities. RANS model is divided into many subcategories such as zero-equation, one-equation, two-equation and ARS (Algebraic Reynolds Stress) models. The k-ε model of those models is the most well-developed and successful one. This has been confirmed to be able to predict a fairly large variation of hydraulic flow phenomena with the same empirical parameter and can be used with some confidence (Rodi, 1980). In this study, standard k-ε model is employed for turbulence closure.

Free-surface models

Hydraulic structures such as bridge pier and girder in river channel cause water level rise during flood situations, which is of great interests in engineering practices. The simulation of these flood flows is related to three-dimensional flow with the free-surface. In numerical simulations of open channel flow, the free surface has been usually replaced by a rigid lid. This approach is suitable only if the free surface is non-complex. If the free-surface rapidly changes, this approximation will introduce nonphysical errors. There are many capturing methods available to simulate the free surface. One of the most successful methods has been the volume of fluid method proposed by Hirt and Nichols (1981). This method's popularity is based on ease of implementation, accuracy and computational efficiency. The method has been used by several researchers to capture the free surface on structured meshes. The method is a powerful approach, but there has been no example of the method to be implemented on unstructured meshes as far as the author knows. Also, instances of non-physical deformation of the interface shape have been reported (Ashgriz and Poo, 1991; Lafauie et al., 1994; Ubbink, 1997). In this study, a high resolution scheme proposed by Ubbink and Issa (1999) is used to capture the free surface. This scheme treats the volume fraction of each fluid which is used as the weighting factor to get the fluid properties. Particularly the method is adaptive to arbitrary unstructured meshes. The proposed numerical methodology is carried out to estimate flow considering hydraulic structures in river channel.

2.2.2 Governing equations

RANS equations with the *k-ε* model based on the eddy viscosity hypothesis are employed as governing equations in this study.

Fluid flow model

The governing equations for continuity and momentum expressed in a Cartesian coordinate system with the tensor notation are as follows:

Continutiy equation:

$$\frac{\partial \rho}{\partial t}+\frac{\partial \rho u_i}{\partial x_i}=0 \tag{2.1}$$

Momentum equation:

$$\frac{\partial \rho u_i}{\partial t}+u_j\frac{\partial \rho u_i}{\partial x_j}=\rho g_i-\frac{\partial p}{\partial x_i}+\mu\frac{\partial^2 u_i}{\partial x_j \partial x_j}+\frac{\partial \tau_{ij}}{\partial x_j} \tag{2.2}$$

where *t* is the time, u_i is the time-averaged velocity, x_i is the Cartesian coordinate component, *p* is the time-averaged pressure, ν is molecular kinematic viscosity, $\tau_{ij}=-\rho\overline{u_i^` u_j^`}$ are the Reynolds stress tensors, $u_i^`$ is the fluctuating velocity component. The above equations are not closed because of the unknown Reynolds stress tensors.

Turbulence model

For turbulence closure, the standard *k*-*ε* model is employed. The Reynolds tensors are acquired through the linear constitutive equation:

$$-\overline{u_i^{`}u_j^{`}} = 2\nu_t S_{ij} - \frac{2}{3}k\delta_{ij} \tag{2.3}$$

where *k* is the turbulent kinetic energy, δ_{ij} is the Kronecker delta, ν_t is the eddy viscosity and S_{ij} is the strain rate tensor defined as:

$$\delta_{ij} = \begin{cases} 1 & \text{if} \quad \mathrm{i = j} \\ 0 & \text{if} \quad \mathrm{i \neq j} \end{cases} \tag{2.4}$$

$$\nu_t = C_\mu \frac{k^2}{\varepsilon} \tag{2.5}$$

$$S_{ij} = \frac{1}{2}\left(\frac{\partial u_i}{\partial x_j} + \frac{\partial u_j}{\partial x_i} \right) \tag{2.6}$$

where *ε* is the turbulent energy dissipation rate of the turbulence kinetic energy *k*. Two transport equations are employed to estimate *k* and *ε*:

$$\frac{\partial k}{\partial t} + u_j \frac{\partial k}{\partial x_j} = \frac{\partial}{\partial x_j}\left[\left(\nu + \frac{\nu_t}{\sigma_k} \right) \frac{\partial k}{\partial x_j} \right] + G - \varepsilon \tag{2.7}$$

$$\frac{\partial \varepsilon}{\partial t} + u_j \frac{\partial \varepsilon}{\partial x_j} = \frac{\partial}{\partial x_j}\left[\left(\nu + \frac{\nu_t}{\sigma_\varepsilon} \right) \frac{\partial \varepsilon}{\partial x_j} \right] + (C_{1\varepsilon} G - C_{2\varepsilon}\varepsilon)\frac{\varepsilon}{k} \tag{2.8}$$

where *G* is the production rate of the turbulent kinetic energy *k* and is defined as:

$$G = -\overline{u_i^{'}u_j^{'}} \frac{\partial u_i}{\partial x_j} \tag{2.9}$$

The constants in equations (2.5), (2.7) and (2.8) take the values suggested by Rodi (1980) and generally the universal values are as follows:

$$C_\mu = 0.09 \quad C_{1\varepsilon} = 1.44 \quad C_{2\varepsilon} = 1.92 \quad \sigma_k = 1.00 \quad \sigma_\varepsilon = 1.30 \tag{2.10}$$

The standard k-ε model is the simplest model which is suitable for flow with complex geometry (Rodi, 1980) although it had reported some deficiencies (Speziale, 1991) as follows: the inability to properly account for the streamline curvature, rotational strains and other body-force effects, and the neglect of the non-local and histroical effects of the Reynolds stress anisotropies.

2.2.3 Discretization methods

FVM (Finite Volume Method)

The FVM is one of the most widely used numerical methods. In this method, the study domain has a number of continuous CV (Control Volume). The governing equations with the FVM have the generic conservation equation in integral form as follows:

$$\frac{\partial}{\partial t}\int_V \rho dV + \int_S \rho u \cdot n dS = 0 \tag{2.11}$$

$$\frac{\partial}{\partial t}\int_V \rho \phi dV + \int_S \rho \phi u \cdot n dS = \int_S \Gamma \nabla \phi \cdot n dS + \int_V b dV \tag{2.12}$$

where ϕ is the general conserved quantity representing either scalars or vector and tensor field components; u is the fluid velocity vector; V is the volume of the CV; S is the face of the CV with a unit normal vector n directing outwards; Γ is the diffusion coefficient; b is the volumetric source of the quantity ϕ. The above equations are valid for arbitrary polyhedral CVs. The FVM procedure is able to take full advantages of arbitrary meshes to approximate complex geometries.

Unstructured mesh

Unstructured mesh offers great flexibility in treating complicated geometries. The CVs of arbitrary shape usually can be used. In general, triangles or quadrilaterals in 2D and tetrahedral or hexahedra in 3D are used in engineering practices. Tetrahedra, prisms and pyramids are considered in special cases of hexahedra. Figure 2.2 shows the examples of CVs by eight vertices. It is possible to be considered as a nominally hexahedral mesh including CVs with less than six faces. The data structure can be simplified by this consideration.

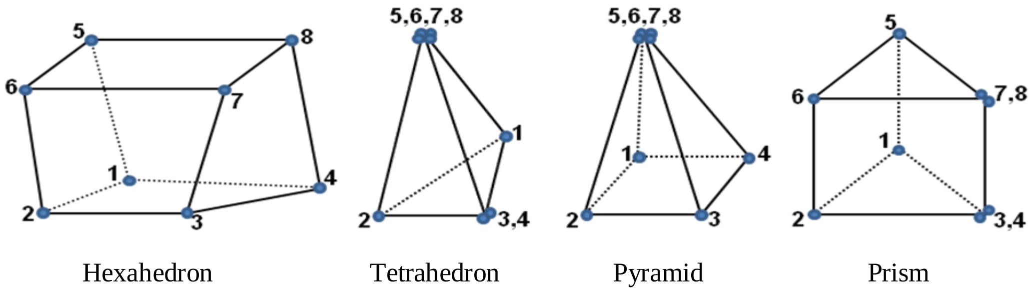

Figure 2.2 CVs by eight vertices

In 3D unstructured meshes, the most common data structure has all the information of the CVs defined by six faces. The CVs also contain the edges by the lists of associated vertices and the faces by the edges. A simplified data structure recommended by Ferziger and Perić (2002) is introduced in this study. As seen in Figure 2.2, the vertices of a CV are defined in a counter-clockwise order. The input of a mesh system used in this study includes data of nodal coordinates, vertices of the CVs and the neighboring CVs. And, a co-located variable arrangement taking advantages of unstructured meshes is also employed in this study. All variables are defined at the center of the CVs.

The data structure of the mesh system is limited to quadrilaterals in 2D and hexahedra in 3D.

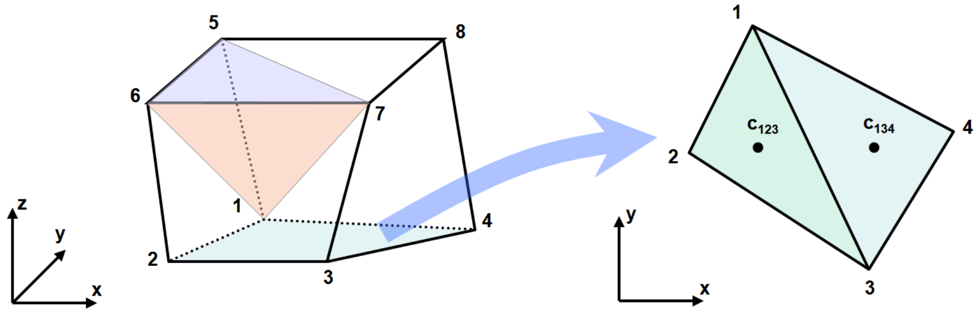

Figure 2.3 Schematic representation of mesh system

The vector area and the center of the surface of the quadrilateral in the above figure is calculated as:

$$\mathrm{r}_i = x_i \mathrm{i} + y_i \mathrm{j} + z_i \mathrm{k} \tag{2.13}$$

$$\mathrm{S}_{1234} = \mathrm{S}_{123} + \mathrm{S}_{134} = \frac{1}{2}\left[(\mathrm{r}_2 - \mathrm{r}_1)\times(\mathrm{r}_3 - \mathrm{r}_1) + (\mathrm{r}_3 - \mathrm{r}_1)\times(\mathrm{r}_4 - \mathrm{r}_1)\right] \tag{2.14}$$

$$\mathrm{c}_{1234} = \frac{\mathrm{S}_{123} c_{123} + \mathrm{S}_{134} c_{134}}{\mathrm{S}_{1234}} \tag{2.15}$$

where r_i is the ith vertex of the CV; i, j and k are unit vectors in the x, y, z coordinate directions; S_{123} and S_{134} are vector areas of the sub triangles Δ_{123} and Δ_{134}, respectively; S_{1234} is vector area of the quadrilateral surface (1,2,3,4); c is the center of the surface.

A hexahedron in 3D is divided into six tetrahedral. The volume of a tetrahedron (1,5,6,7) in Figure 2.3 is a dot product of two vectors as follows:

$$V_{1567} = \frac{1}{3}(\mathrm{r}_5 - \mathrm{r}_1)\cdot \mathrm{S}_{567} \tag{2.16}$$

$$c_V = \frac{\sum V_i c_i}{V} \tag{2.17}$$

where V_{1567} is the volume of tetrahedron (1,5,6,7); c_V is the centroid of the CV; V_i is the volume of sub tetrahedron i (i ranges from 1 to 6); c_i is the centroid of sub tetrahedron i.

Spatial discretization

The midpoint rule approximation of the mass flux is obtained in space:

$$\frac{\partial}{\partial t}\int_V \rho\phi dV + \sum_f \rho_f \phi_f (u_{f\perp} S_f) = \sum_f \Gamma_f \left.\frac{\partial \phi}{\partial n}\right|_f S_f + b_P - s_P\phi_P \tag{2.18}$$

where subscript f is the face of the CV ; subscript $\perp$ is the component of the quantity normal to the surface; subscript P is the present CV; S_f is the area of the CV surface; b_p is the part of the source term containing all the contributions excluding unknown variables; $-s_P\phi_P$ is the part of the source term including the unknown variables which can be treated implicitly. The value on the surface is calculated from the values at the center of the CV on either side:

$$\phi_f = \alpha_f \phi_P + (1-\alpha_f)\phi_A \tag{2.19}$$

where

$$\alpha_f = \frac{d_{Af}}{d_{Af} + d_{fP}} \tag{2.20}$$

where the subscript A is the adjacent CV; d_{Af} and d_{fP} are the distances from the surface to the adjacent CV and to the present CV, respectively. Using the power law scheme, Equation (2.18) can be finally reduced to:

$$\sum_f \left\{ \left[D_f A(|P_f|) + \max(-F_f, 0)\right](\phi_P - \phi_A) + F_f\phi_P \right\} = b_P - s_P\phi_P \tag{2.21}$$

where

$$F_f = \rho_f u_{f\perp} S_f \tag{2.22}$$

$$D_f = \frac{\Gamma_f S_f}{d_{AP}} \tag{2.23}$$

$$P_f = \frac{F_f}{D_f} \tag{2.24}$$

$$A(|P_f|) = \max\left[0, (1-0.1|P_f|)^5\right] \tag{2.25}$$

$$\Gamma_f = \frac{\Gamma_A \Gamma_P}{\alpha_f \Gamma_P + (1-\alpha_f)\Gamma_A} \tag{2.26}$$

where F_f is the strength of the convection; D_f is the diffusion conductance. The interpolation method proposed by Rhie and Chow (1983) is employed to cure the checkerboard variable distribution.

Mesh skewness is divided into two kinds: non-conjunctionality and non-orthogonality. The former one shows that the intersection is not the middle of the surface. The latter one means a poor perpendicularity. The method proposed by Ferziger and Perić (2002) is employed to maintain the discretization accuracy. If a non-conjunctional mesh occurs, the value at the center of the surface is estimated as:

$$\phi_f = \phi_{f'} + (\nabla\phi)_{f'} \cdot (\mathrm{r}_f - \mathrm{r}_{f'}) \tag{2.27}$$

where *f'* is the intersection of the surface and the line connecting the two neighboring CVs. For a non-orthogonal mesh, the approximation dividing the diffusive term into a normal diffusion and a cross diffusion is proposed as follows:

$$\left.\frac{\partial\phi}{\partial n}\right|_f = \frac{\phi_A - \phi_P}{d_{AP}} + (\nabla\phi)_f^{\exp} \cdot (n - l) \tag{2.28}$$

where

$$l = \frac{\mathrm{r}_A - \mathrm{r}_P}{|\mathrm{r}_A - \mathrm{r}_P|} \tag{2.29}$$

where l is the unit vector in the direction of the line connecting the center of the present mesh and its neighboring mesh.

Temporal discretization

The temporal discretization of the discretised form of the momentum equations can get the following equation:

$$\frac{\partial}{\partial t}\int_V \rho\phi dV = F \tag{2.30}$$

where

$$F = \sum_{nb} a_{nb}\phi_{nb} + b_P - a_P\phi_P \tag{2.31}$$

where subscript *nb* stands for the neighboring CVs. The second order implicit Crank-Nicolson scheme is applied as follows:

$$\frac{\phi^{m+1}-\phi^{m}}{\Delta t}\rho V=\frac{F^{m+1}+F^{m}}{2} \tag{2.32}$$

where the superscript $m+1$ and m mean the previous and the present time step, respectively. The final algebraic equation can be obtained as:

$$a_P\phi_P^{m+1}=\sum_{nb}a_{nb}\phi^{m+1}+b_p \tag{2.33}$$

in which

$$a_P=a_P^{m+1}+\frac{2\rho V}{\Delta t} \tag{2.34}$$

$$a_P^{m+1}=\sum_{nb}a_{nb}\phi^{m+1}+\sum_{f}F_f+s_P^{m+1} \tag{2.35}$$

$$b_P=b_P^{m+1}+\frac{2\rho V}{\Delta t}\phi_P^{m}+\left(\sum_{nb}a_{nb}\phi_{nb}+b_P-a_P\phi_P\right)^{m} \tag{2.36}$$

Pressure-velocity coupling

The widely used SIMPLE (Semi-Implicit Method for Pressure-Linked Equations) algorithm is used for the pressure-velocity coupling. This method is to guess a pressure distribution firstly and then get a pressure correction with the continuity equation. The corrected values are as follows:

$$u_i=u_i^{*}+u_i^{'} \tag{2.37}$$

$$p_i=p^{*}+p^{'} \tag{2.38}$$

where the index * stands for the guessed pressure distribution and the velocity field not satisfying the continuity equation; the index ’ is the corrections of the variables. The velocity component in the x-direction extracting the pressure term from the source term in the discretised momentum equation has the following form:

$$a_Pu_P^{*}=\sum_{nb}a_{nb}u_{nb}^{*}-\sum_{f}S_{fx}p_f^{*}+b_p \tag{2.39}$$

The same discretised momentum equation based on the corrected velocity component as follows:

$$a_Pu_P=\sum_{nb}a_{nb}u_{nb}-\sum_{f}S_{fx}p_f+b_p \tag{2.40}$$

If Equation (2.39) is subtracted from Equation (2.40) and is taken into account Equation (2.37) and (2.38), the correction of the velocity for u is obtained as:

$$u_P^{'} = -\frac{\sum S_{fx} p_f^{'}}{a_P} \tag{2.41}$$

The correction of the other velocity components can be derived in the same way. An obtained equation for the pressure correction as follows:

$$a_P^p p_P^{'} = \sum_{nb} a_{nb}^p p_{nb}^{'} + b_P^p \tag{2.42}$$

in which

$$a_P^p = \sum_{nb} a_{nb}^p \tag{2.43}$$

$$a_{nb}^p = \frac{S_{fx}^2}{a_{Px}} + \frac{S_{fy}^2}{a_{Py}} + \frac{S_{fz}^2}{a_{Pz}} \tag{2.44}$$

$$b_P^p = \sum_f \left(u_f^* S_{fx} + v_f^* S_{fy} + w_f^* S_{fz} \right) \tag{2.45}$$

where a_{Px} a_{Py} and a_{Pz} are the coefficients for the calculation of variables u, v and w, respectively. The velocity field is renewed with Equation (2.37) and (2.38).

2.2.4 Free-surface modeling

Previous researches to calculate free-surface flows can be classified into two major groups (Ferziger & Perić, 2002): interface-tracking methods and interface-capturing methods. The former one is tracked by making marker points or attaching to a mesh surface. The latter one is captured by an indicator function. Figure 2.4 shows a schematic expression of those methods and details of the two methods will be followed next.

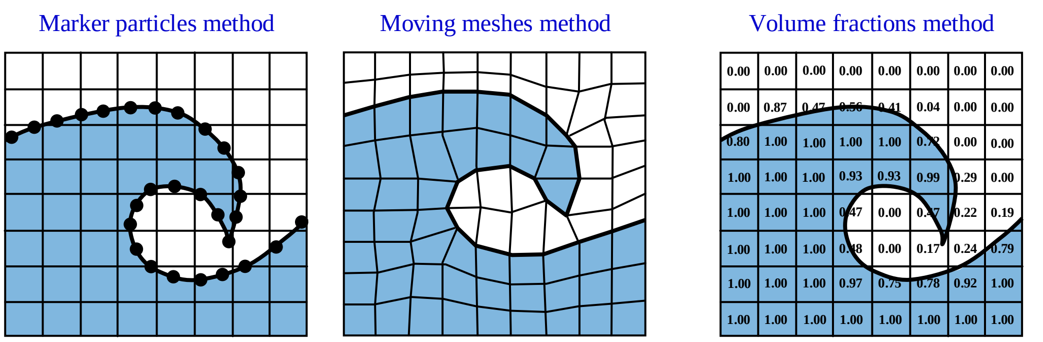

(a) Interface-tracking method (b) Interface-capturing method

Figure 2.4 Methods for free-surface modeling

Interface-tracking methods

In these methods, the free-surface on interface is represented by marker points. The positions of points are approximated by interpolation such as piecewise polynomial (Hyman, 1984). This approach has the advantages that position of interface is known throughout the calculation and it eases the effort for the calculation of the interface curvature. Several researches using this approach have been reported: particles on interface (Daly, 1969), height functions (Nichols & Hirt, 1973; Soulis, 1992; Lai & Yen, 1993; Farmer et al., 1994; Muzaferija et al., 1995), level set method (Osher & Sethian, 1988; Li, 1993; Sussman et al., 1994; Zhou, 1995; Sethian, 1996) and surface fitted methods (Dervieux & Thomasset, 1979; Glimm et al., 1986; Takizawa et al., 1992; Li & Zhan, 1993; Clarke & Issa, 1995). These methods are limited to interfaces without large deformations because it leads to significant distortion on interfaces.

Interface-capturing methods

This marks the volume of fluid on interface. In this approach, scalar indicator functions between zero and one are used to discriminate between water and air. A value of zero indicates the air and a value of unity indicates the water in Figure 2.2. The volume fraction values between water and air indicate the free-surface. The values of free-surface are given by the relative proportions occupying the cell volume. These methods require special techniques to capture a well-defined interface. Several researches have proposed the methods to maintain a well-defined interface: line techniques (Noh & Woodward, 1976; Chorin, 1980; Youngs, 1982; Ashgriz & Poo, 1991), donor-acceptor scheme (Ramshaw & Trapp, 1976; Hirt & Nichols, 1981; Torrey et al., 1987; Lafaurie et al., 1994) and higher order differencing schemes (Van Leer, 1977; Ghobadian, 1991; Darwish, 1993; Pericleous & Chan, 1994; Ubbink & Issa, 1999). Hirt and Nichols (1981) improved the donor-acceptor scheme with VOF (Volume of Fluid) method by including information on the slope of the interface. One of most successful methods has been VOF method proposed by Hirt and Nichols (1981). This method’s popularity is based on ease of implementation, accuracy and computational efficiency. VOF method is a powerful approach than any others, but there has been no example of VOF method to be implemented on unstructured meshes and instances of non-physical deformation of the interface shape have been reported (Ashgriz & Poo, 1991; Lafauie & Nardone, 1994; Ubbink, 1997). To improve these problems a high resolution scheme proposed by Ubbink and Issa (1999) is employed in this study. This scheme treats volume fractions of each fluid which is used as the weighting factor to get the fluid properties. In particular, this method has the advantage adaptive to arbitrary unstructured meshes. The method to capture the free-surface is discussed below.

The momentum equation of Equation (2.2) is closed with the constitutive relations for the density and dynamic viscosity as follows:

$$\rho = \alpha\rho_1 + (1-\alpha)\rho_2 \tag{2.46}$$

$$\mu = \alpha\mu_1 + (1-\alpha)\mu_2 \tag{2.47}$$

where the subscripts 1 and 2 show the water and the air, respectively. The volume fraction α is given by the initial distribution and defined as:

$$\alpha(x,y,z,t) = \begin{cases} 1 & \text{for the point(x,y,z,t) inside water} \\ 0 & \text{for the point(x,y,z,t) inside air} \\ 0 < \alpha < 1 & \text{for the point(x,y,z,t) inside transitional area} \end{cases} \tag{2.48}$$

It is assumed that both fluids are incompressible in this study. The conservative form of the scalar convection equation for the volume fraction α is (Hirt & Nichols, 1981):

$$\frac{\partial \alpha}{\partial t} + \frac{\partial \alpha u_i}{\partial x_i} = 0 \tag{2.49}$$

After discretising Equation (2.14), the discretised equation for volume fraction α is obtained as:

$$\alpha_P^{t+\delta t} = \alpha_P^t + \frac{\delta t}{V_P}\sum_{f=1}^{n} \alpha_f^* F_t \tag{2.50}$$

where F_t is the volumetric flux at the cell face. To compute accurately the above equation, it is necessary that advection algorithm needs to avoid the values of non-physical volume fraction and to compute correct α_f^*. In other words, a differencing scheme which guarantees a bounded solution while maintaining the sharpness of the interface is needed.

CICSAM method

The existing differencing schemes have some problems and limitations to capture the interface. They create too diffusive or a non-physical deformation of the interface, and besides they are limited to structured meshes. Therefore, in this study, CICSAM (Compressive Interface Capturing Scheme for Arbitrary Meshes) (Ubbink, 1997) is employed to overcome those problems. This is a high resolution differencing scheme based on the normalized variable diagram (Leonard, 1991). The volume fraction values at the cell face and the donor cell expressed as normalized variable are defined as:

$$\tilde{\alpha}_D = \frac{\alpha_D - \alpha_U}{\alpha_A - \alpha_U} = 1 + \frac{\alpha_D - \alpha_A}{2(\nabla\alpha)_D \cdot \underline{d}} \tag{2.51}$$

$$\tilde{\alpha}_f = \frac{\alpha_f - \alpha_U}{\alpha_A - \alpha_U} = 1 + \frac{\alpha_f - \alpha_A}{2(\nabla\alpha)_D \cdot \underline{d}} \tag{2.52}$$

where $\underline{d}$ is the vector between the cell centres of the donor and acceptor cells; subscripts U, D and A show the upwind, donor, acceptor cells, respectively. Figure 2.5 shows a schematic expression with an arbitrary arrangement.

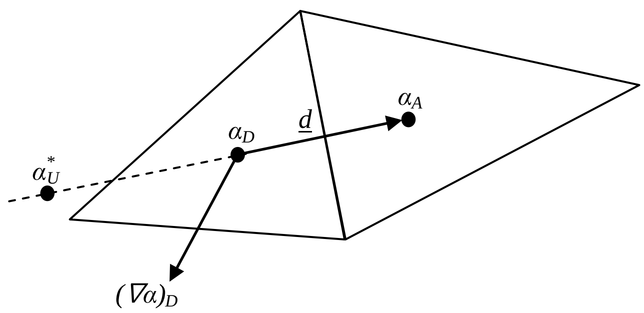

Figure 2.5 Prediction of the upwind value for an arbitrary cell

The value of α_f at the cell face can be obtained from Equation (2.51) and (2.52) as follows:

$$\alpha_f = (1 - \beta_f)\alpha_D + \beta_f \alpha_A \tag{2.53}$$

where β_f is the weighting factor which contains the upwind, the donor and the acceptor values:

$$\beta_f = \frac{\tilde{\alpha}_f - \tilde{\alpha}_D}{1 - \tilde{\alpha}_D} \tag{2.54}$$

In the donor-acceptor scheme used in VOF method, deformation of interface shape has been mentioned because it does not comply with the local boundedness criteria (Versteeg & Malalasekera, 1995). In this study, the Hyper-C scheme (Gaskell & Lau, 1988) following the upper bound of the CBC (Convective Boundedness Criteria) is employed and defined as:

$$\tilde{\alpha}_{fCBC} = \begin{cases} \max\left\{\tilde{\alpha}_D, \min\left\{1, \dfrac{\tilde{\alpha}_D}{c_D}\right\}\right\} & \text{if} \quad 0 \le \tilde{\alpha}_D \le 1 \\ \tilde{\alpha}_D & \text{if} \quad \tilde{\alpha}_D < 0,\ \tilde{\alpha}_D > 1 \end{cases} \tag{2.55}$$

where c_D is the Courant number as:

$$c_D = \sum_{f=1}^{n} \max\left\{\frac{F_f \delta t}{V_D}, 0\right\} \tag{2.56}$$

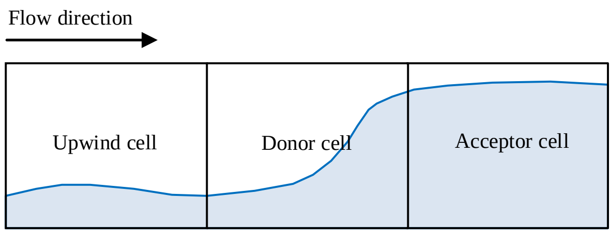

(a) Original fluid distribution

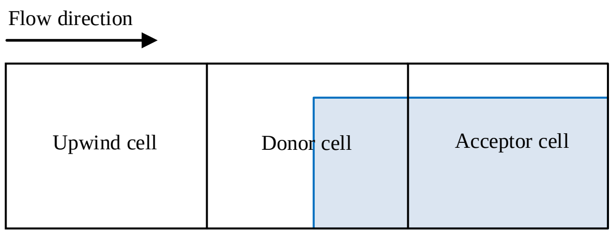

(b) Donor-acceptor scheme

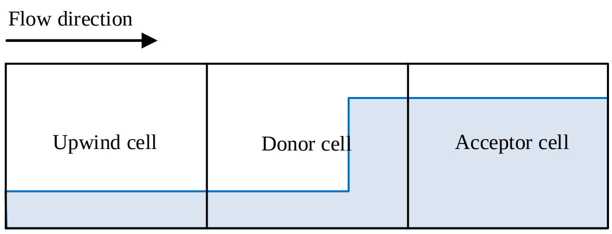

(c) Hyper-C scheme

Figure 2.6 Comparison between the donor-acceptor and the Hyper-C scheme

Figure 2.6(b) and (c) is the fluid distribution represented by the donor-acceptor scheme and by the Hyper-C scheme following the upper bound of the CBC. The Hyper-C scheme reproduces more realistic fluid distribution than the donor-acceptor scheme because it considers the value of the upwind cell. Equation (2.55) shows the optimum differencing scheme with the local boundedness criteria, but this scheme does not preserve the interface shape which lies almost tangentially to the flow direction. In case of multidimensional flows, the wrinkle phenomenon occurs at the interface. This problem can be solved by the method which switches to another high resolution scheme. Therefore, in this study, UQ (Ultimate-Quickest) scheme proposed by Leonard (1991) is employed for that purpose:

$$\tilde{\alpha}_{fUQ} = \begin{cases} \min\left\{ \dfrac{8c_f \tilde{\alpha}_D + (1-c_f)(6\tilde{\alpha}_D + 3)}{8}, \tilde{\alpha}_{fCBC} \right\} & \text{if} \quad 0 \le \tilde{\alpha}_D \le 1 \\ \tilde{\alpha}_D & \text{if} \quad \tilde{\alpha}_D < 0,\ \tilde{\alpha}_D > 1 \end{cases} \tag{2.57}$$

A weighting factor γ_f based on the angle between the interface and the direction is also employed to predict the value at the normalized cell face. The equation using the weighting factor to switch linearly gives:

$$\tilde{\alpha}_f = \gamma_f \tilde{\alpha}_{fCBC} + (1-\gamma_f)\tilde{\alpha}_{fUQ} \tag{2.58}$$

where

$$\gamma_f = \min\left\{k_\gamma \frac{\cos(2\theta_f)+1}{2},\ 1\right\} \tag{2.59}$$

where θ_f is the angle between the vector normal to the interface $(\nabla\alpha)_D$ and the vector $\underline{d}$ as follows:

$$\theta_f = \arccos\left|\frac{(\nabla\alpha)_D \cdot \underline{d}}{|(\nabla\alpha)_D|\,|\underline{d}|}\right| \tag{2.60}$$

where k_γ is a constant used to control each scheme. The value recommended by Ubbink (1997) is k_γ=1. Equation (2.57) means that if the CBC cannot preserve the gradient at the interface, the equation reduces to UQ, and if UQ cannot maintain a sharp gradient at the interface, the equation reduces to CBC.

Meanwhile, the existing VOF method uses the split operator technique limited in the structured meshes. Thus, the sum of the volumetric rate passing through arbitrary special cell-face has difference by sweep procedure according to directions of coordinate axis. In the CICSAM method, the values of α_f^* at the cell face are represented by the Crank-Nicolson scheme with the second order accuracy represented as:

$$\alpha_f^* = \frac{1}{2}(\alpha_f^t + \alpha_f^{t+\delta t}) \tag{2.61}$$

If the time step is small enough, a variation of the angle between the orientation of motion and the interface slope is small. Thus, it is reasonable to assume that the weighting factors of the new time can be replaced by the old weighting factors. Equation (2.53) is substituted into Equation (2.61) and the final expression for the face value reduces to:

$$\alpha_f^* = (1-\beta_f)\frac{\alpha_D^t + \alpha_D^{t+\delta t}}{2} + \beta_f \frac{\alpha_A^t + \alpha_A^{t+\delta t}}{2} \tag{2.62}$$

However, Equation (2.27) does not always satisfy all boundary criteria. In some cases, the volume fraction α can represent the values less than 0 or larger than 1. To correct this problem, the donor-acceptor scheme replaces the non-physical values as 0 or 1 by force. Since modifing the non-physical values by force causes the conservation error by affecting the momentum equation, in the CICSAM scheme, the problem is solved by introducing a predictor-corrector solution procedure. A predictor solution precedure means the method mentioned above and a corrector solution procedure is carried out only when the non-physical values occur for the reduction of computational effort. The procedure is briefly summarized below.

Corrector solution procedure

If the values of the volume fraction have non-physical values, a corrector solution procedure is proceeded with setting $\beta_f^*=\beta_f$. First, the negative values of the volume fractions are discussed. The new values at the face is represented with a new approximation for the weighting factor:

$$\alpha_f^{**} = (1-\beta_f^{**})\frac{\alpha_D^t + (\alpha_D^{t+\delta t} + E^-)}{2} + \beta_f^{**}\frac{\alpha_A^t + (\alpha_A^{t+\delta t} - E^-)}{2} \tag{2.63}$$

where β_f^{**} is the corrected weighting factor and it should always be less or equal to the previous weighting factor; E^- is the magnitude of the unbounded volume fraction value, defined as:

$$\beta_f^{**} = \beta_f^* - \beta_f^{'} \tag{2.64}$$

$$E^- = \max\left\{-\alpha_D^{t+\delta t}, 0\right\} \tag{2.65}$$

From the bound of the corrected weighting factor, one is obtained:

$$0 \le \beta_f^{'} \le \beta_f^* \tag{2.66}$$

where

- Case when the volume fractions have the negative values:

$$\beta^{'} = \begin{cases} \min\left\{\dfrac{E^-(2+c_f-2c_f\beta_f^*)}{2c_f(\Delta\alpha^* - E^-)}, \beta_f^*\right\} & \text{if} \quad \Delta\alpha^* > E^- \\ 0 & \text{if} \quad \Delta\alpha^* \le E^- \end{cases} \tag{2.67}$$

- Case when the values of the volume fractions exceed unity:

$$\beta^{'} = \begin{cases} \min\left\{\dfrac{E^+(2+c_f-2c_f\beta_f^*)}{2c_f(-\Delta\alpha^* - E^+)}, \beta_f^*\right\} & \text{if} \quad \Delta\alpha^* < -E^+ \\ 0 & \text{if} \quad \Delta\alpha^* \ge -E^+ \end{cases} \tag{2.68}$$

where

$$\Delta\alpha^* = \frac{\alpha_A^t + \alpha_A^{t+\delta t}}{2} - \frac{\alpha_D^t + \alpha_D^{t+\delta t}}{2} \tag{2.69}$$

$$E^+ = \max\left\{\alpha_D^{t+\delta t} - 1,\ 0\right\} \tag{2.70}$$

The above equations are used for the new corrected values of the volume fractions. If the non-physical values still exist, the corrector solution procedure is repeated.

2.2.5 Boundary conditions

It is necessary to define the boundary conditions as well as the initial conditions to completely specify the model. There are two kinds of boundary conditions, namely Dirichlet boundary (fixed value) conditions and Von Neuman boundary (fixed gradient) conditions. It is necessary to define an appropriate condition for the different types of boundaries.

Inlet

An inlet boundary has a specified velocity distribution. The pressure is unknown and a value in a boundary is extrapolated from the interior of the flow domain. However, if the gradient of the pressure at the inlet boundary is small, it is sufficient to apply a zero gradient boundary condition. And, the inlet condition for the function of the volume fractions is fixed.

Outlet

The outlet boundary is positioned at downstream where there are small variations in the flow. The boundary condition at the outlet should be considered to satisfy the overall mass continuity for the computational domain. There are two approaches to ensure this condition as follows: extrapolation of all the flow quantities and fixed pressure boundary condition. The former one shows that velocity distribution of the first row of cells next to the boundary is used for the construction of a velocity distribution. Then, the velocities at the boundary are given according to the velocity profile satisfying the overall continuity. The latter one means that pressure at the boundary is fixed and a zero gradient condition is applied to the velocities (Versteeg & Malalasekera, 1995). This allows a fluid to enter the flow domain. It is sufficient to consider a zero gradient condition to the function of the volume fractions.

Impermeable wall

In order to avoid the possible integration through the viscous sub layer and implement the wall roughness more flexibly, the wall function approach is preferred in this study. In the wall function approach, the dimensionless distance y^+ and the dimensionless velocity u^+ are as follows:

$$y^+ = \frac{u_* y_\perp}{\nu} \tag{2.71}$$

$$u^+ = \frac{u_{//}}{u_*} \tag{2.72}$$

where u_* is the friction velocity near the bed; $y_\perp$ is the normal distance from the center of the near wall CV to the wall surface. The universal wall function is written as:

$$u^+ = \frac{1}{\kappa}\ln(E_r y^+) \tag{2.73}$$

where κ is the van Karman constant (=0.41); E_r is the roughness parameter of the wall. If flow is locally equilibrium, the production and the dissipation of the turbulence are nearly equal. Thus, one is obtained as:

$$u_* = C_\mu^{1/4} k_P^{1/2} \tag{2.74}$$

And, the wall shear stress is as follows:

$$\tau_w = \rho u_*^2 = \frac{\rho C_\mu^{1/4} k_p^{1/2} u_{//}}{u^+} \tag{2.75}$$

The coupling with the wall in the momentum equations is suppressed by setting it to zero and adding the wall force from Equation (2.75) as a source term. The normal derivative of k at the wall boundary is set to zero in the k-ε equation. And the production and ε in the wall boundary is offered from:

$$G_P = \frac{\tau_w}{\rho}\frac{\partial u_{//}}{\partial n} = \frac{\tau_w}{\rho}\frac{u_{//}}{y_\perp} \tag{2.76}$$

$$\varepsilon_P = \frac{u_*^3}{\kappa y_\perp} = \frac{C_\mu^{3/4} k_P^{3/2}}{\kappa y_\perp} \tag{2.77}$$

2.2.6 Solution methods

The final algebraic equation system is under-relaxed before submitted to the linear equation solver by the method proposed by Patankar (1980). The final algebraic equation systems resulted from the discretization process are characterized by sparse and non-symmetry of coefficient matrices. Two solvers are used in this study: a Bi-CGSTAB (Bi-conjugate gradient stabilized method) solver and a preconditioned GMRES (Generalized minimal residual method) solver incorporated with an ILUTP (Incomplete LU factorization with threshold and pivoting) preconditioner proposed by Saad (2003).

The calculation sequence is:

(a) Initialize all the variables used in the computation.

(b) If it is necessary, calculate the Courant number and adjust the time step.

(c) Solve the volume fraction equation by using the old volumetric fluxes.

(d) Estimate the new viscosity, density and the face density.

(e) Predict a momentum by using the above values.

(f) Stop the computation if the final time has been reached or advance to the next time and return to step (b)

2.3 Laboratory experiments

2.3.1 Introduction

The objective of the laboratory experiments is to compare with the results obtained from the numerical simulations. The variations of flow according to a kind of river structures under the same hydraulic conditions are also estimated.

2.3.2 Laboratory flume

The experimental flume used in this study is located at Ujigawa Open Laboratory, DPRI (Disaster Prevention Research Institute), Kyoto University in Japan.

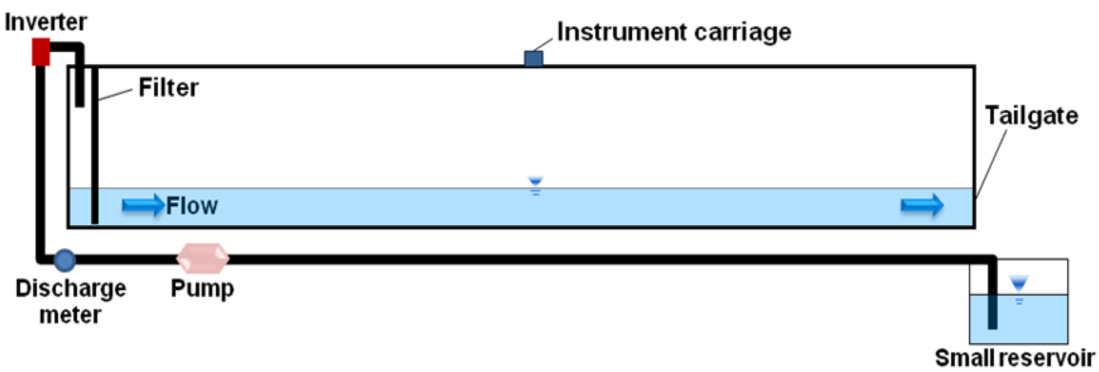

Figure 2.7 Longitudinal cross-section of experimental flume

The real size of flume is straight channel with width 40cm, depth 23cm, and length 14.6m. Figure 2.7 shows the longitudinal cross-section of flume used in the experiments. Figure 2.8

shows a schematic representation for the position of hydraulic structures and the coordinate axis for the study domain focused in whole experimental flume.

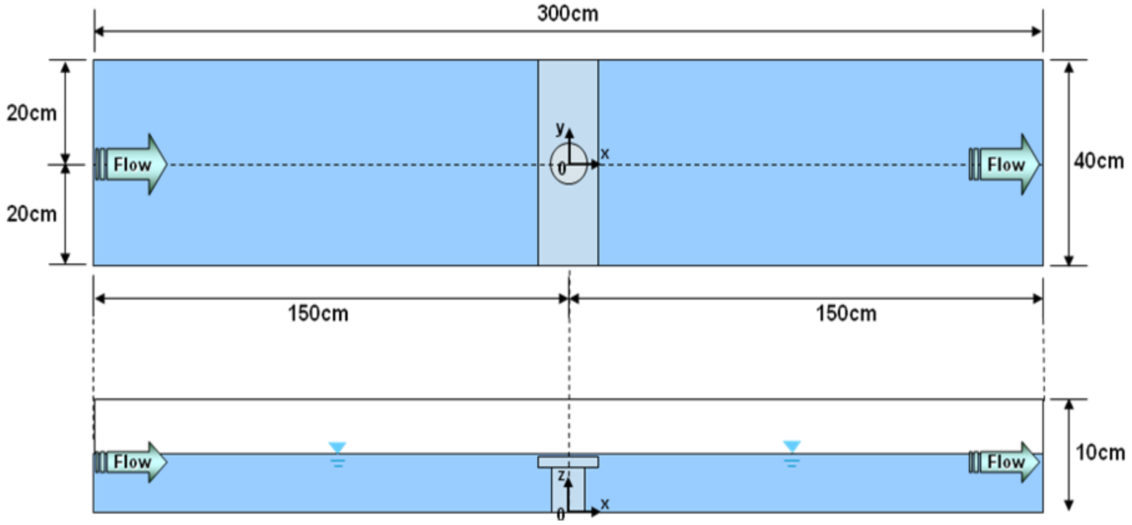

Figure 2.8 Study domain focused in whole experimental flume

The discharge is controlled by the inverter controlling the rotative velocity of the pump and the discharge meter measuring the discharge. The weir controlling the water stage located in the downstream is used for maintaining the uniform flow. The hydraulic structures are located at 6.5m from the upstream end of the actual channel. The channel slope is about 1/1000.

2.3.3 Model hydraulic structures

The bridge which means the representative hydraulic structures in a river is considered as model in this study. The structures were selected to carry out the experiments in the case considering overtopping flow or not. The details of the structures are shown in Figure 2.9. Case-1 does not consider hydraulic structures. The kinds of the structures employed in the experiments are pier (Case-2), girder (Case-3) and pier+girder (Case-4). The pier in Case 2 is circular shaped and uses a brass material with diameter 5cm and height 7cm. The girder in Case 3 uses a wooden material with length 40cm, width 8cm and thickness 1.4cm. And, the girder is placed at the position where the top of the girder is 4.7cm from the channel bottom. In Case 4, the conditions of girder are the same as those of Case 3 and the pier is consisted of a wooden material with diameter 5cm and height 3.3cm. All structures are located at the center of the channel.

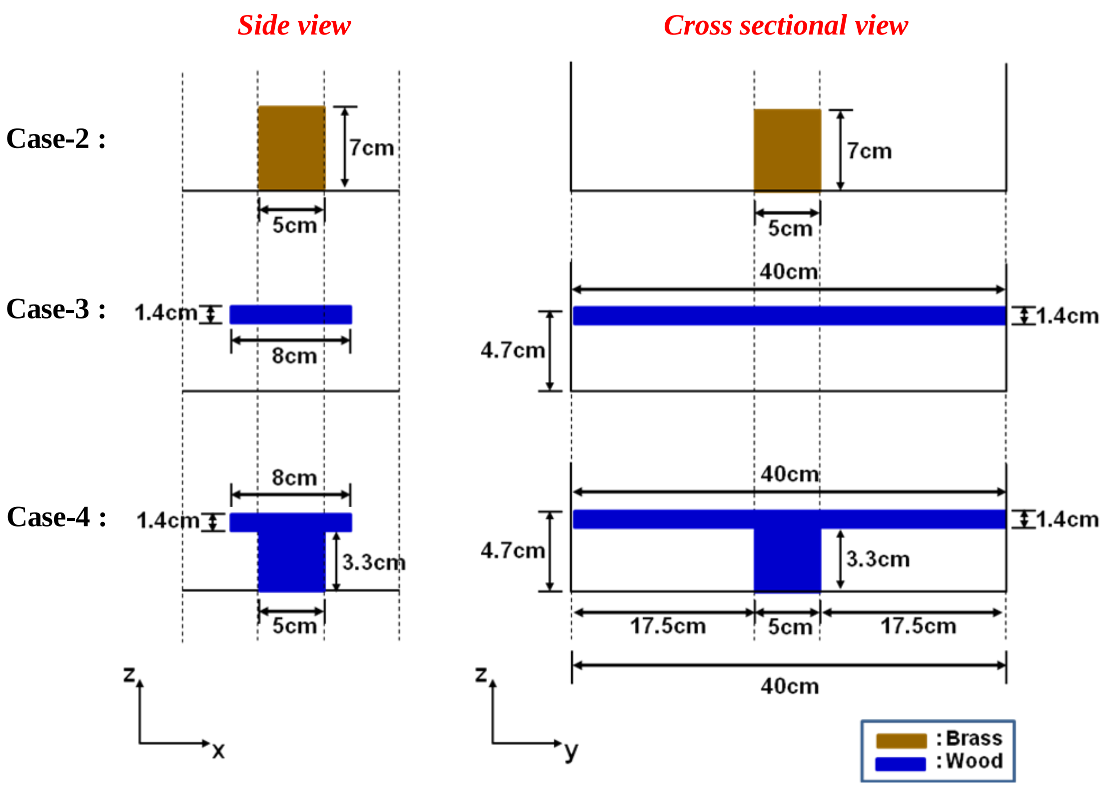

Figure 2.9 Details of hydraulic structures

2.3.4 Measurement apparatus

In this experiment, the measured data are the water stage, the velocity at z=2cm from the channel bottom and the velocity at the free-surface. In order to measure the water stage, the servo type water level meter with the resolution capability of 50μm is used. In the measurement of the velocity at z=2cm from the channel bottom, the electromagnetic velocity meter of L type with the resolution capability of 0.1cm/s is used for the measurement. Each velocity of u, v, and w is obtained by changing the direction of the electromagnetic velocity meter. The data are collected by converting the output voltage to digital signal of AD converter from each measurement device. The sampling frequency is 20Hz and the measuring time is 37.5s. And, 750 data are obtained on each measuring point. As shown in Figure 2.10, the measuring zone is total 300cm which is each 150cm in upstream and downstream side in location of 650cm from upstream of channel. The measuring interval is from 1cm to 10cm. The measurement around hydraulic structure is carried out as in detail as possible. The velocity at free-surface is measured by PIV (Particle Image Velocimetry) analysis proposed by Fujita et al. (1998). The PIV analysis is a method to determine the free-surface velocity by demanding a mean transferring distance of tracer for each measuring point based on a similarity of tracer shape between continuous pictures on the inspection domain. PVC (Polyvinyl Chloride) powder with mean diameter of 50μm is used as the tracer in the experiments.

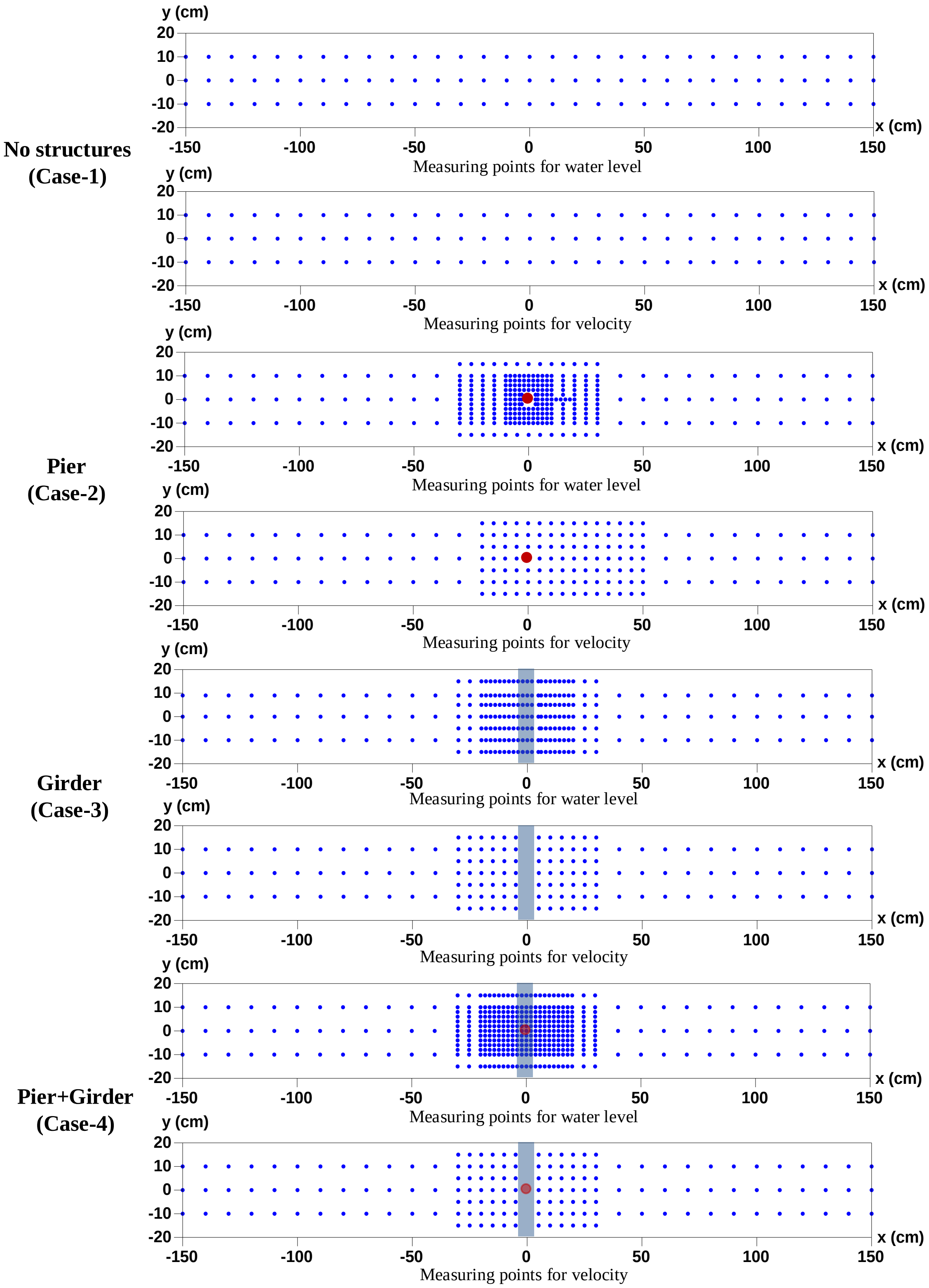

Figure 2.10 Measuring points for water level and velocity at z=2cm

The PIV analysis is conducted by taking a picture using the video camera positioned at the downstream of the channel. The measuring domain is the range of each 50cm in the upstream and downstream side from the center of the hydraulic structures. The spatial interval of measurement is 2cm. The mean velocity was obtained by preparing the 450 images for minimum 15*s*.

2.3.5 Experimental procedures

The measurements for the channel slope and the correction of warp of rail before the experiments are carried out. After that, the uniform depth is measured under the condition without hydraulic structure with flow discharge. Then, the experiments are conducted by changing only the condition of hydraulic structure under the same discharge condition. The results obtained from the measurement for the rail is used as the corrected values for the experimental results.

2.3.6 Experimental conditions

Table 2.1 shows the hydraulic conditions. The experiments are conducted under steady flow.

Table 2.1 Hydraulic conditions (uniform flow)

<table>
<tr><th>Parameters</th><th>Symbols(unit)</th><th colspan="2">Values</th></tr>
<tr><td>Flow discharge</td><td>Q (l/s)</td><td colspan="2">7.00</td></tr>
<tr><td>Water depth</td><td>h_0 (cm)</td><td colspan="2">4.76</td></tr>
<tr><td>Slope</td><td>I</td><td colspan="2">1/987</td></tr>
<tr><td>Mean velocity</td><td>u_m (cm/s)</td><td colspan="2">36.80</td></tr>
<tr><td rowspan="4">Water temperature</td><td rowspan="4">T (°C)</td><td>Case-1</td><td>6.2</td></tr>
<tr><td>Case-2</td><td>6.2</td></tr>
<tr><td>Case-3</td><td>10.4</td></tr>
<tr><td>Case-4</td><td>9.1</td></tr>
<tr><td rowspan="4">Reynolds number</td><td rowspan="4">Re</td><td>Case-1</td><td>11200</td></tr>
<tr><td>Case-2</td><td>11200</td></tr>
<tr><td>Case-3</td><td>13500</td></tr>
<tr><td>Case-4</td><td>13000</td></tr>
<tr><td>Froude number</td><td>Fr</td><td colspan="2">0.54</td></tr>
</table>

In the experimental cases, Case-1 with no structures is conducted to compare with the other cases. Case-2, Case-3 and Case-4 are the experiments to consider the effect of water level rise by the cylinder pier, girder and cylinder pier+girder, respectively.

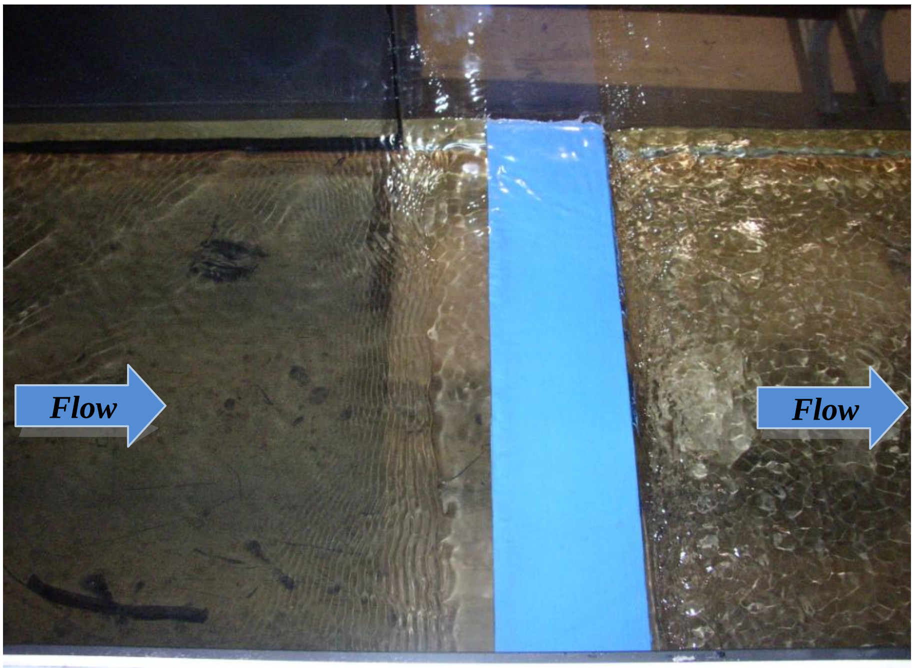

(a) Top view

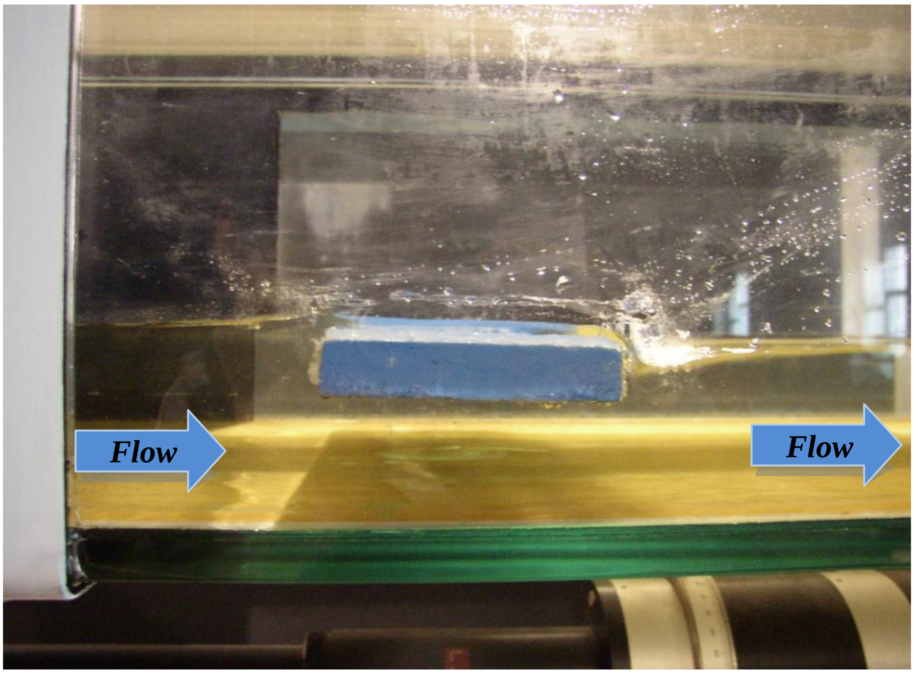

(b) Side view

Figure 2.11 Experimental photos of Case-3

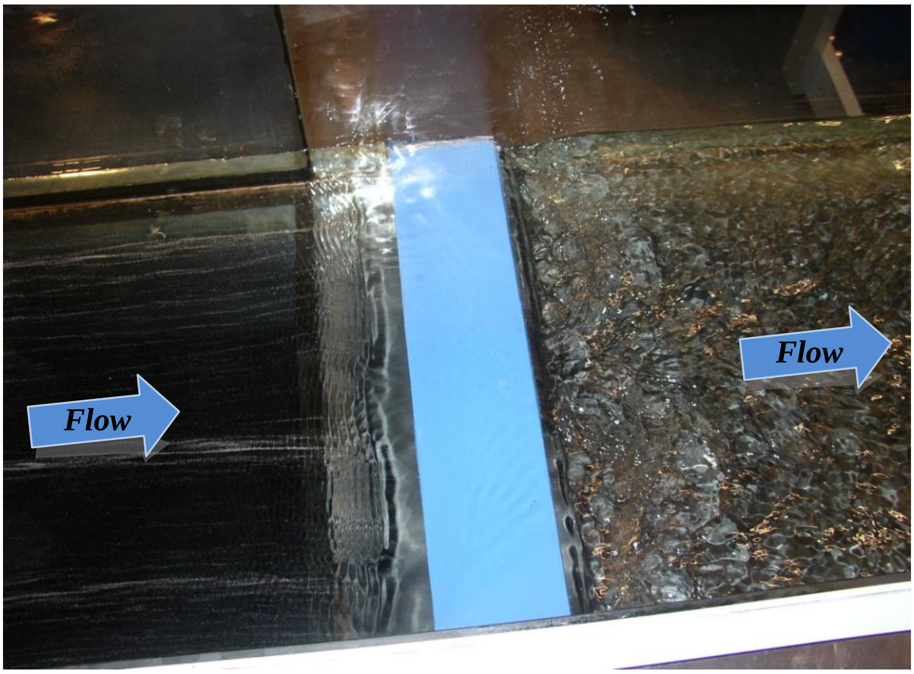

(a) Top view

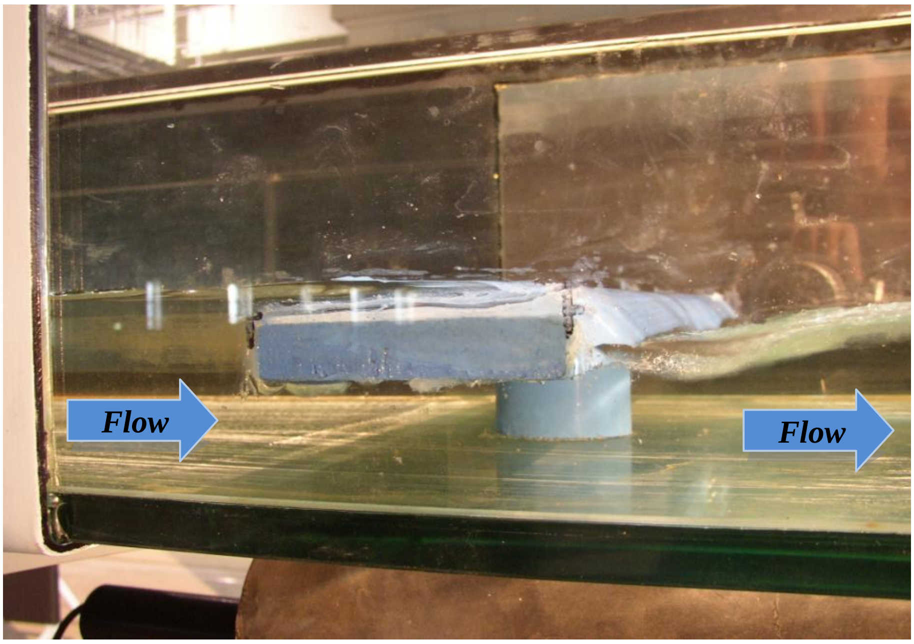

(b) Side view

Figure 2.12 Experimental photos of Case-4

Figures 2.11 and 2.12 show the actual experimental photos for Case-3 and Case-4, respectively. In Case-3 and Case-4, the overtopping flow occurs over the hydraulic structures. As shown in the figures, the backwater in the upstream area due to effect of the hydraulic structures is definitely represented.

2.4 Numerical simulations

2.4.1 Introduction

The numerical simulations are carried out to verify the developed numerical model by comparing with the experimental results. The water level rise due to effect of hydraulic structures is also computed in the numerical simulations. Estimating the applicability of numerical model is purpose of the numerical simulations

2.4.2 Computational domain

The computational domain consists of the unstructured mesh to represent the complicated geometries accurately, in particular the shape of the cylinder pier and girder. The total number of hexahedral meshes used is 24,890. And, the grid of z-direction is considered as 8 layers with 1cm interval. Figure 2.13 shows the computational domain for the comparisons of simulated and experimental results. The domain is the range of each 150cm in the upstream and the downstream side from the center of the hydraulic structures. And, the domain for comparison of the velocity at the free-surface is the range of each 50cm in the upstream and the downstream side from the center of the hydraulic structures.

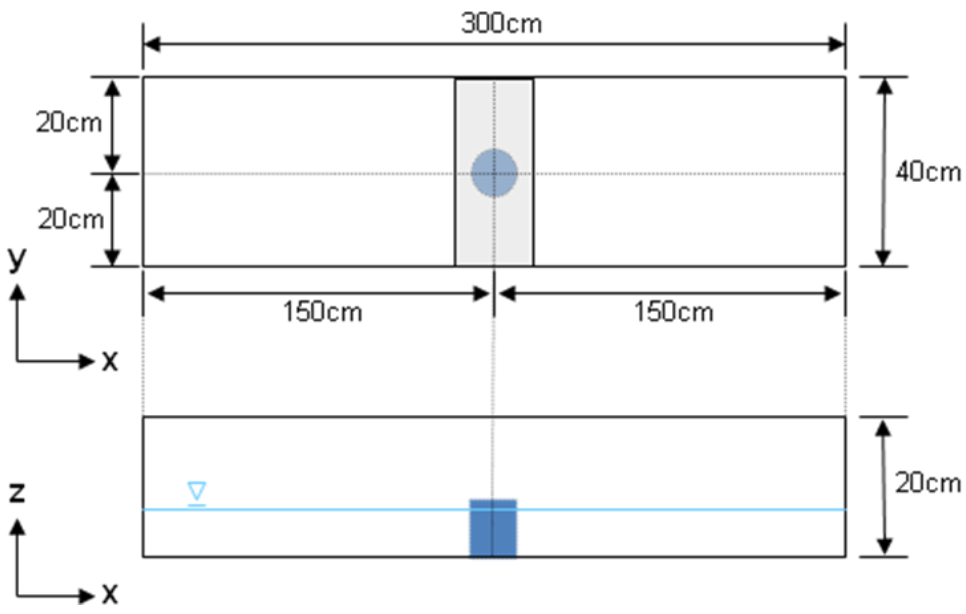

Figure 2.13 Computational domain

And, Figure 2.14 shows the computational meshes used in this simulation. As seen in Figure 2.14, the meshes around hydraulic structures consist of fine meshes and other meshes consist of coarse meshes.

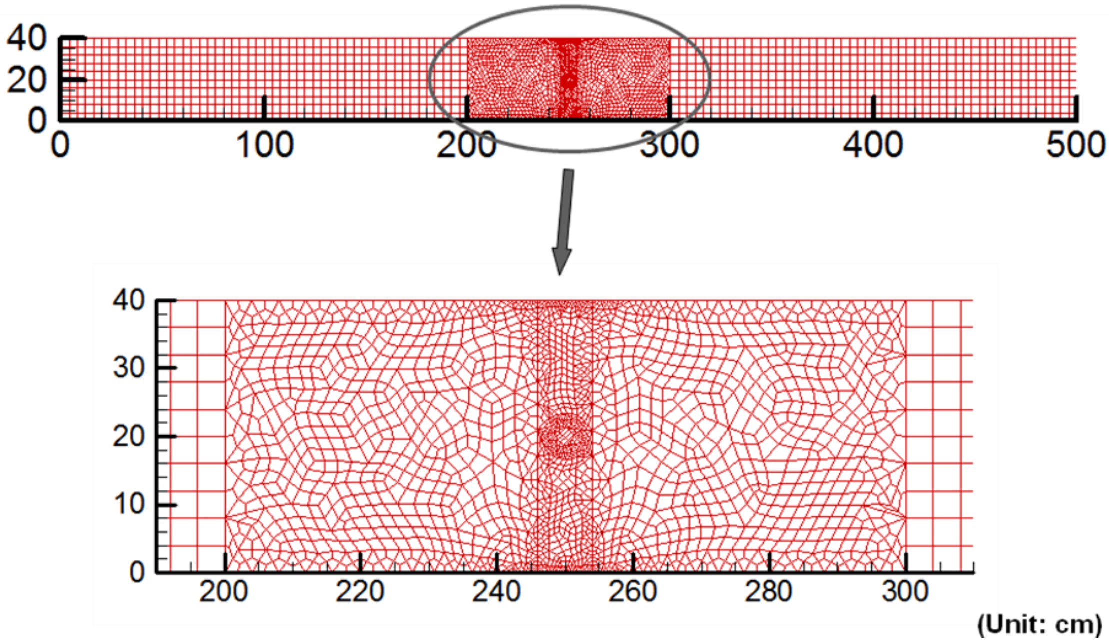

Figure 2.14 Computational meshes

2.4.3 Computational conditions

The conditions obtained from the experiment are applied as the initial conditions of computation. Initial depth is 4.76cm and applied flow discharge is 7.0*l/s*. The computational time interval is 0.001*s*. The turbulence kinetic energy k and the dissipation rate ε are specified corresponding to a viscosity ratio of 10.0 and taking the turbulence intensity 8%. And, as with the experiments, the different types of hydraulic structures are considered in the computation. The numerical results compared with the experimental results are shown in the following section.

2.5 Results and analyses

The objectives of the study in this chapter are to verify numerical model by comparing with the experimental results and estimate the water level rise due to effect of hydraulic structures. The simulated and experimental results of water level, velocity at z=2cm and velocity at free-surface are compared here. And then the applicability of numerical model will be discussed.

2.5.1 Comparisons of water level

The results of the water level obtained from the simulations and experiments are compared and discussed here.

Plane distribution of water level

The results of plane distribution of water level are compared in this section. Figure 2.15 is the results of Case-1 where there is no structure. Figures 2.16, 2.17 and 2.18 show the results of Case-2, 3 and 4, respectively.

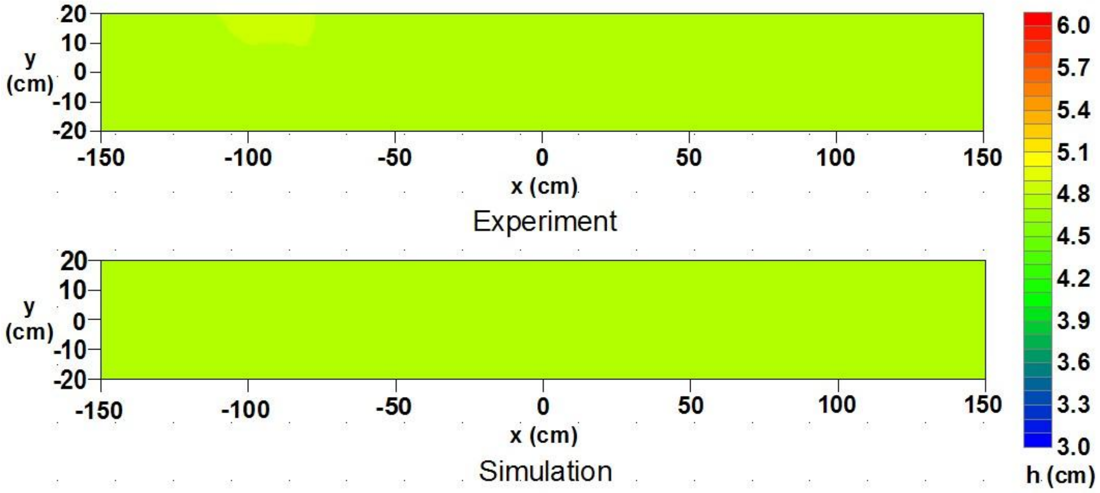

Figure 2.15 Results of water level (Case-1)

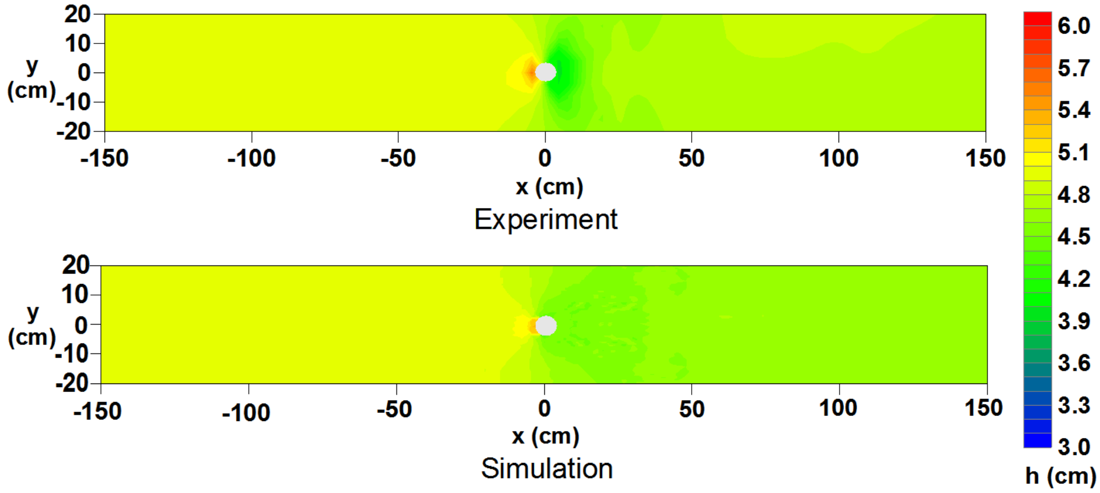

Figure 2.16 Results of water level (Case-2)

Case-2 is not considering the overtopping flow over hydraulic structures. Case-3 and Case-4 are considering the overtopping flow over hydraulic structures.

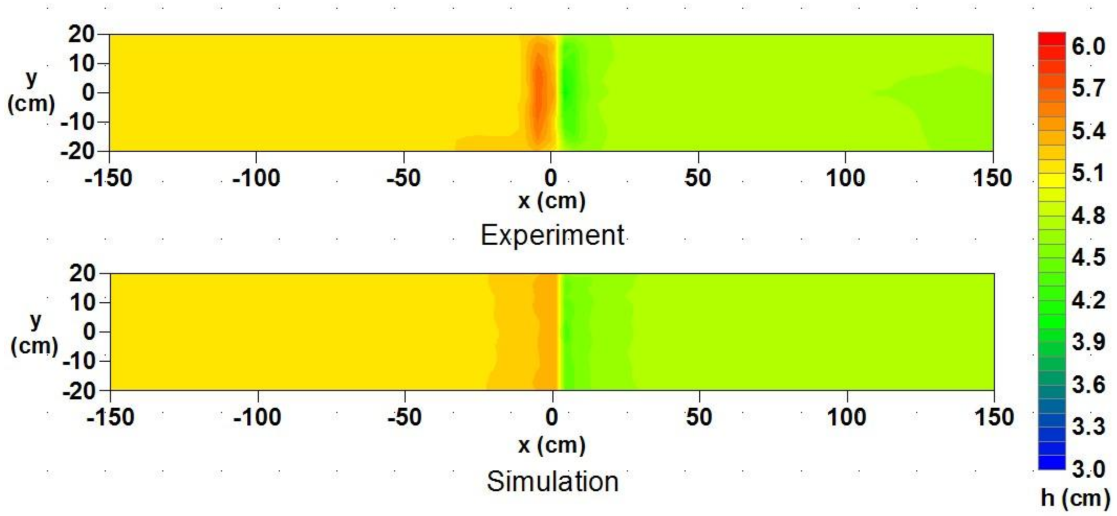

Figure 2.17 Results of water level (Case-3)

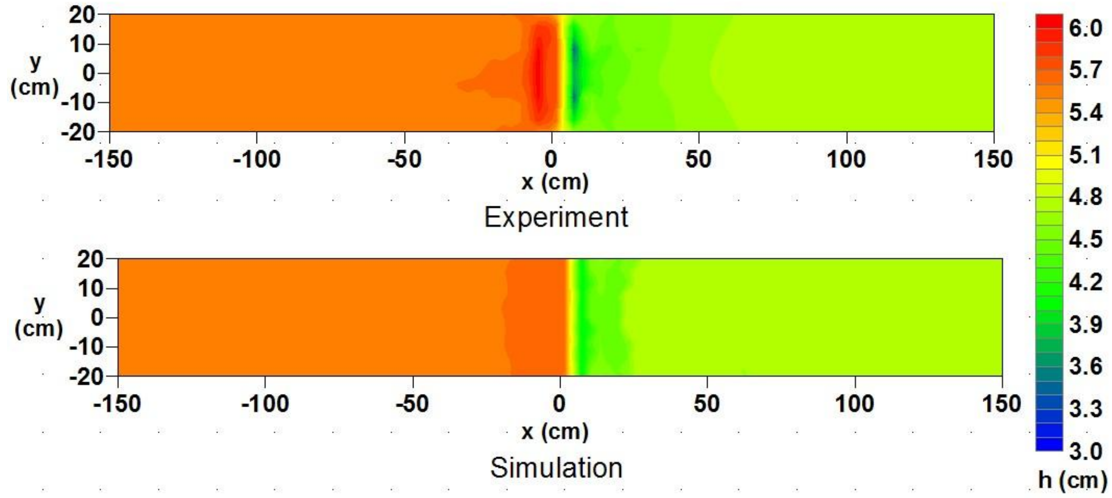

Figure 2.18 Results of water level (Case-4)

From the computational results, it is judged that the effect of backwater and water level rise by the hydraulic structures generally have good agreements with the experimental results although the simulated and experimental results have some differences. And, it is judged that effect of the girder structure is larger than the pier structures from the comparison of Case-2 and 3. From the computational results of water level, it is found that tendency of the water level profile can be expressed well around hydraulic structures.

Comparison of water level in cross-section

The results of the water level along the center line of the channel (y=0) on each case are shown in Figures 2.19, 2.20, 2.21 and 2.22.

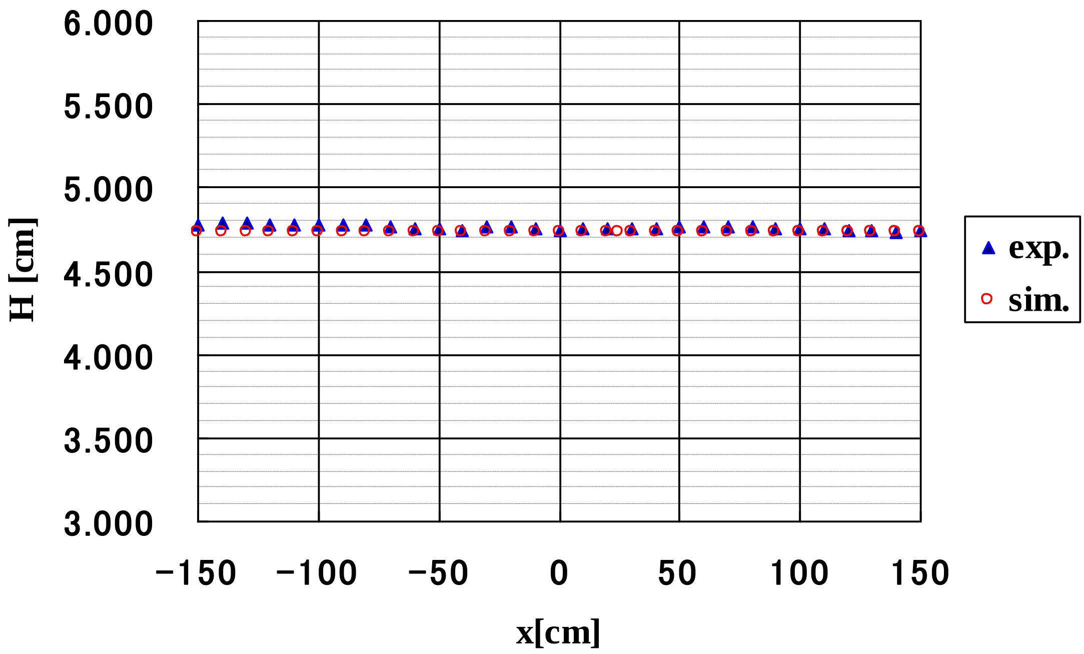

Figure 2.19 Comparison of water level (Case-1, y=0)

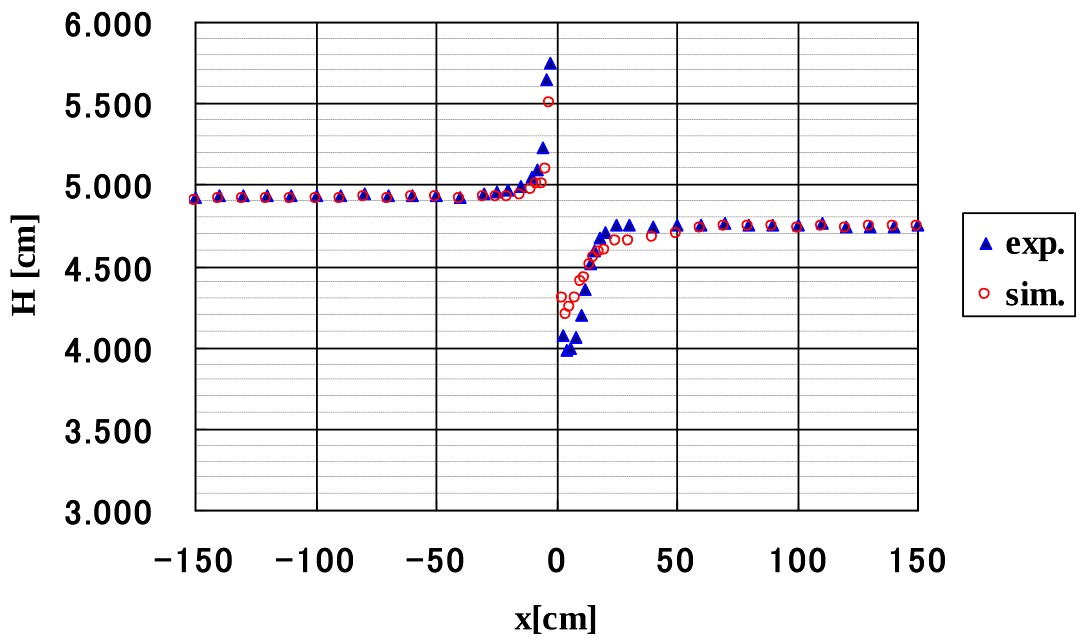

Figure 2.20 Comparison of water level (Case-2, y=0)

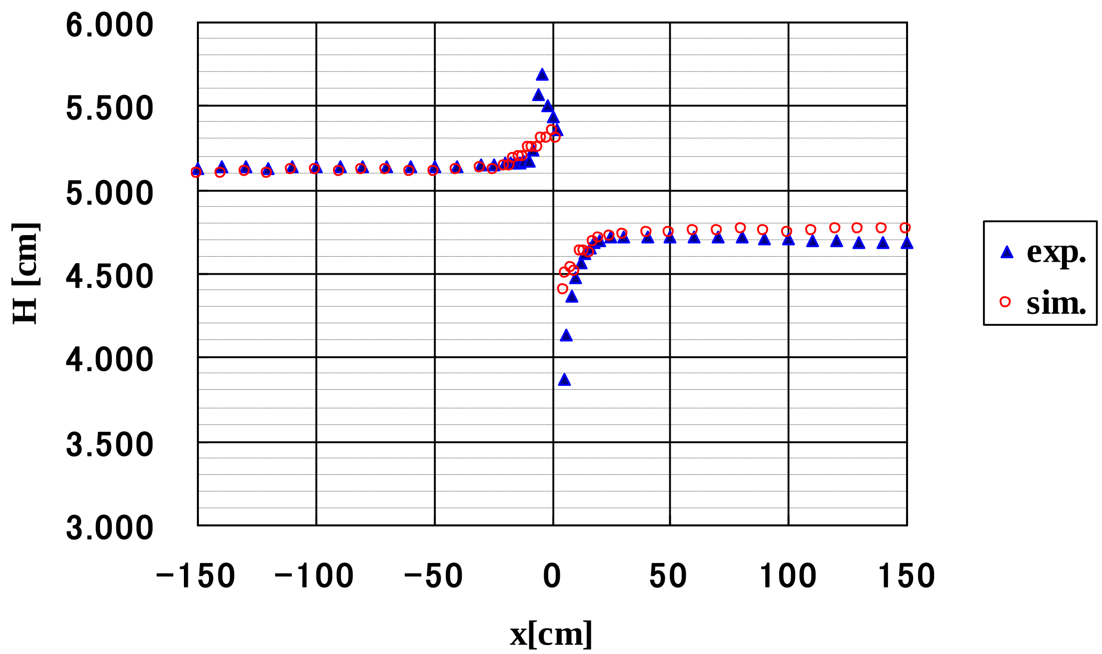

Figure 2.21 Comparison of water level (Case-3, y=0)

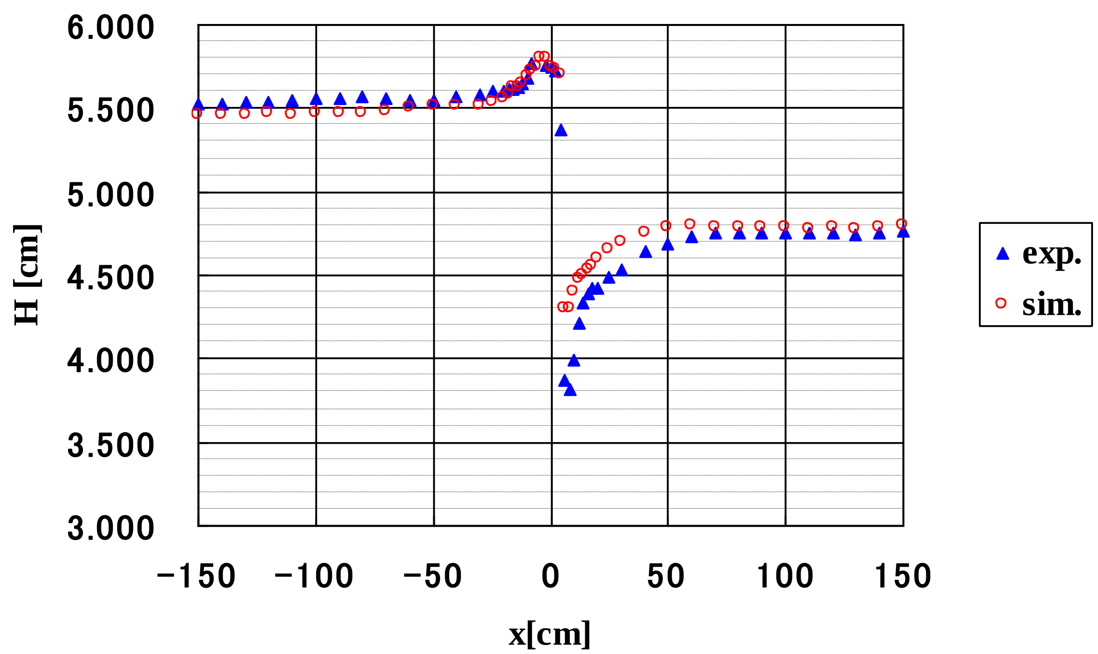

Figure 2.22 Comparison of water level (Case-4, y=0)

From the obtained results, it is found that the water levels generally have good agreements with the experimental results. And, it is judged that effect of backwater by the hydraulic structures was well represented in the simulation.

2.5.2 Comparisons of flow velocity

Plane distribution of velocity at z=2cm

The simulated and experimental results of velocity at z=2cm from the channel bottom are compared in this section. Figure 2.23 is the results of Case-1 where there is no structure. Figure 2.24, 2.25 and 2.26 show the results of Case-2, 3 and 4, respectively. As with the results of water level, the overtopping flow is considered in Case-3 and 4.

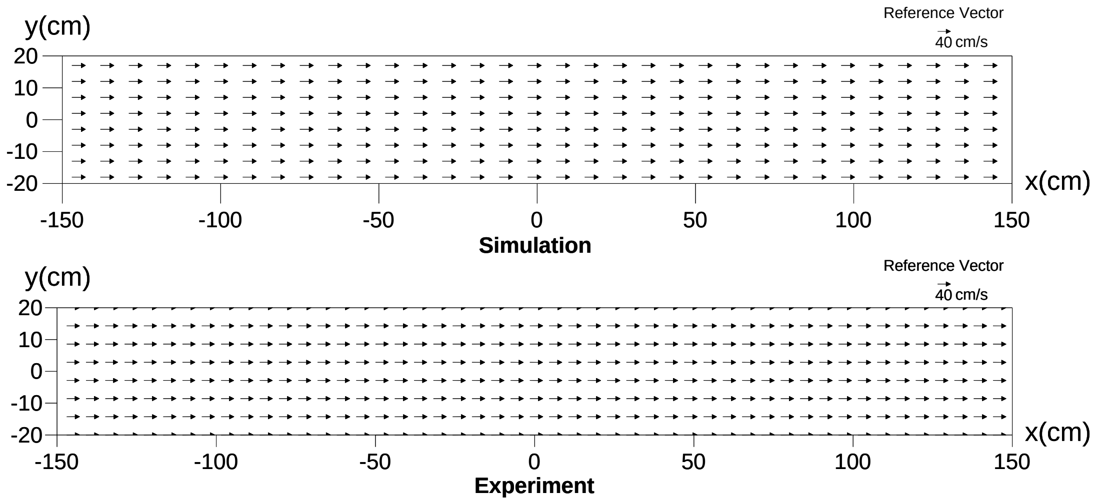

Figure 2.23 Results of velocity at z=2cm (Case-1)

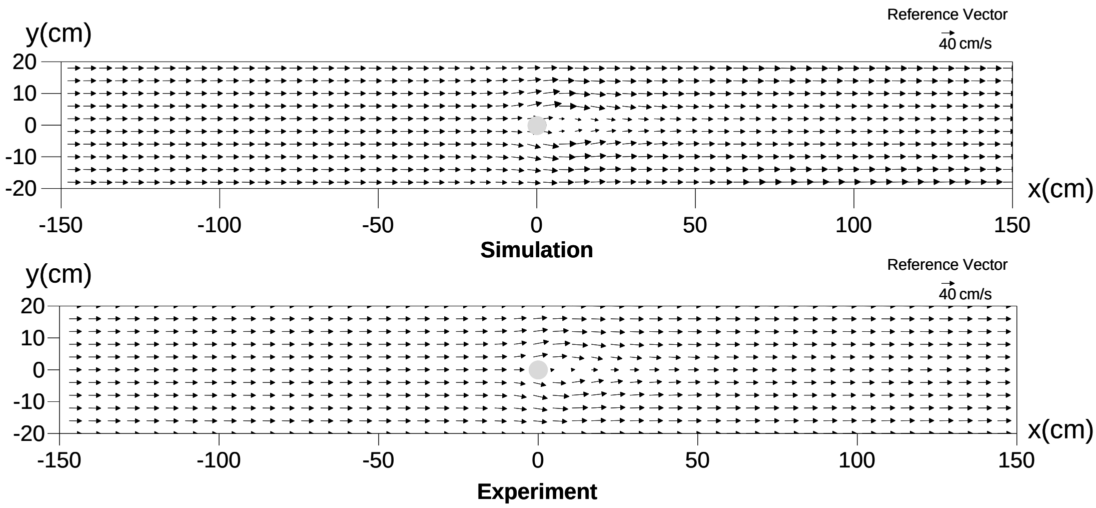

Figure 2.24 Results of velocity at z=2cm (Case-2)

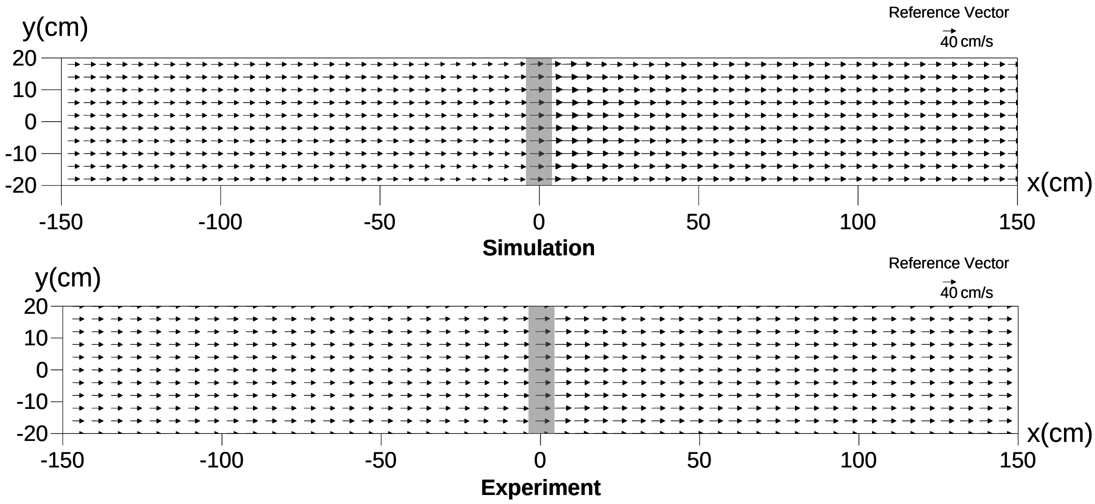

Figure 2.25 Results of velocity at z=2cm (Case-3)

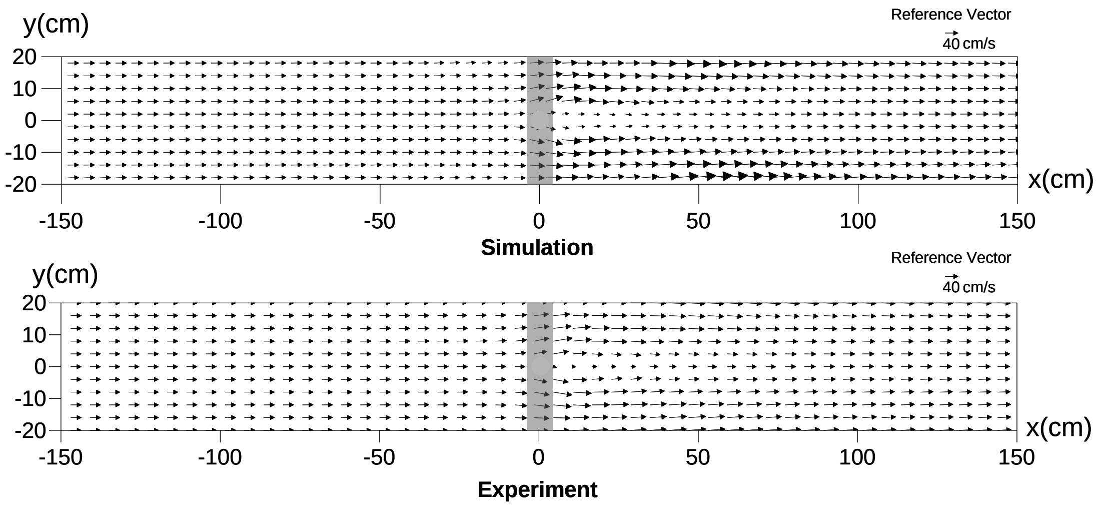

Figure 2.26 Results of velocity at z=2cm (Case-4)

From the results, it is found that the values of the numerical simulation are slightly larger than the experimental results. However, it is judged that the effects of velocity by the hydraulic structures were represented well.

Comparison of velocity in the cross-section at z=2cm

The results of simulated velocity at z=2cm from the channel bottom along the center line of the channel are compared with the experimental data in Figures 2.27 ~ 2.30. In the figures, horizontal and vertical axis show the distance in the longitudinal direction and the velocity, respectively.

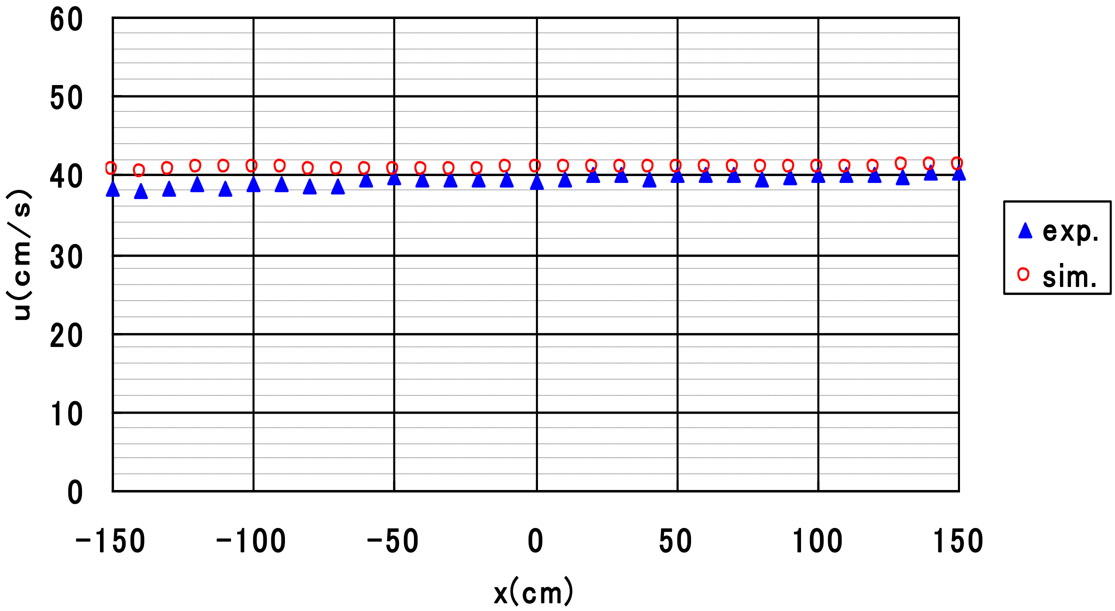

Figure 2.27 Comparison of velocity in cross-section at z=2cm (Case-1, y=0)

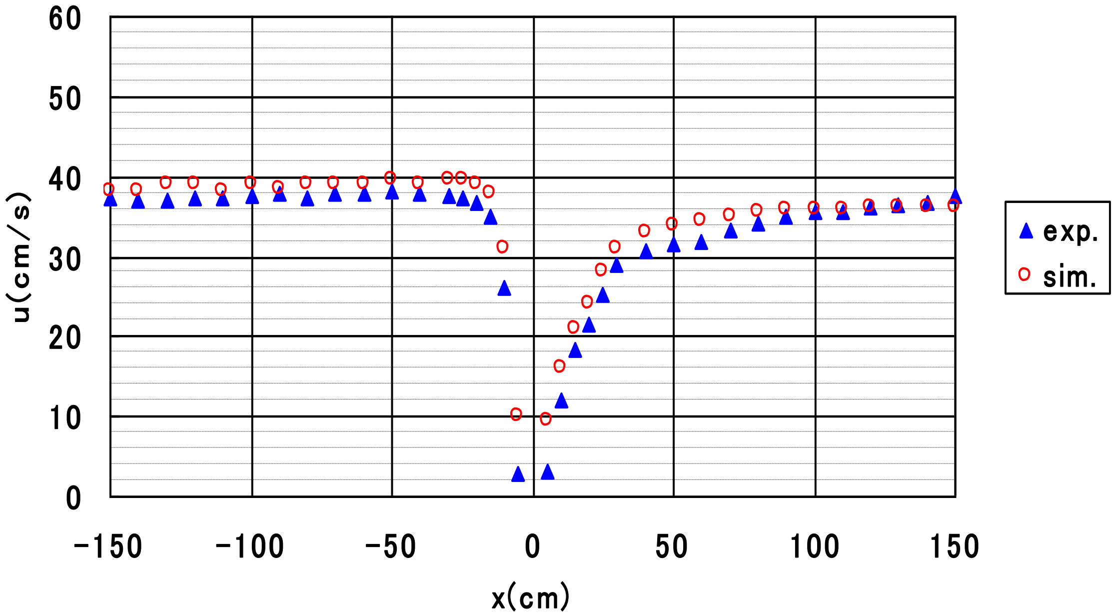

Figure 2.28 Comparison of velocity in cross-section at z=2cm (Case-2, y=0)

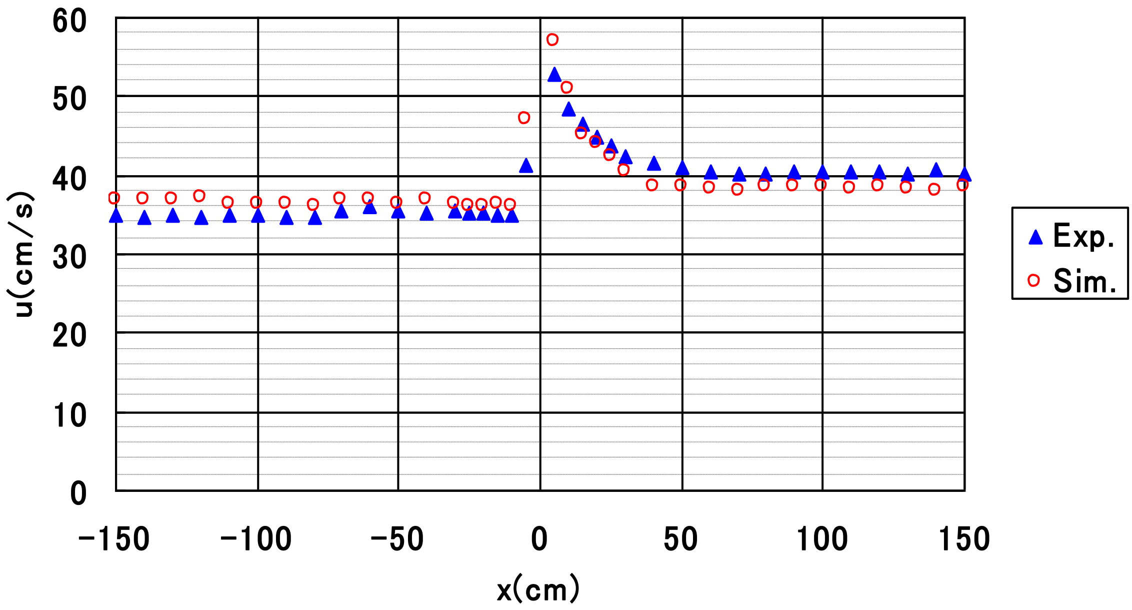

Figure 2.29 Comparison of velocity in cross-section at z=2cm (Case-3, y=0)

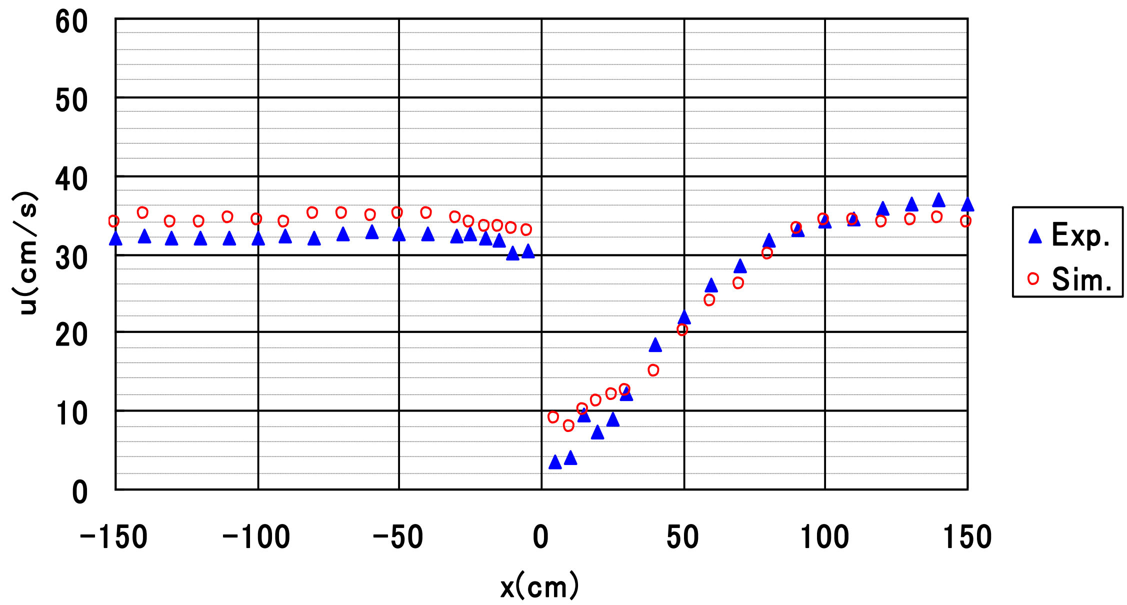

Figure 2.30 Comparison of velocity in cross-section at z=2cm (Case-4, y=0)

The above mentioned numerical results of the velocity generally have good agreements with the experimental results. In the numerical results including hydraulic structures, the variations of velocity around hydraulic structures can be seen.

Plane distribution of velocity at free-surface

The numerical results at free-surface are compared with the experimental results obtained from PIV analysis as shown in Figures 2.31 ~ 2.34.

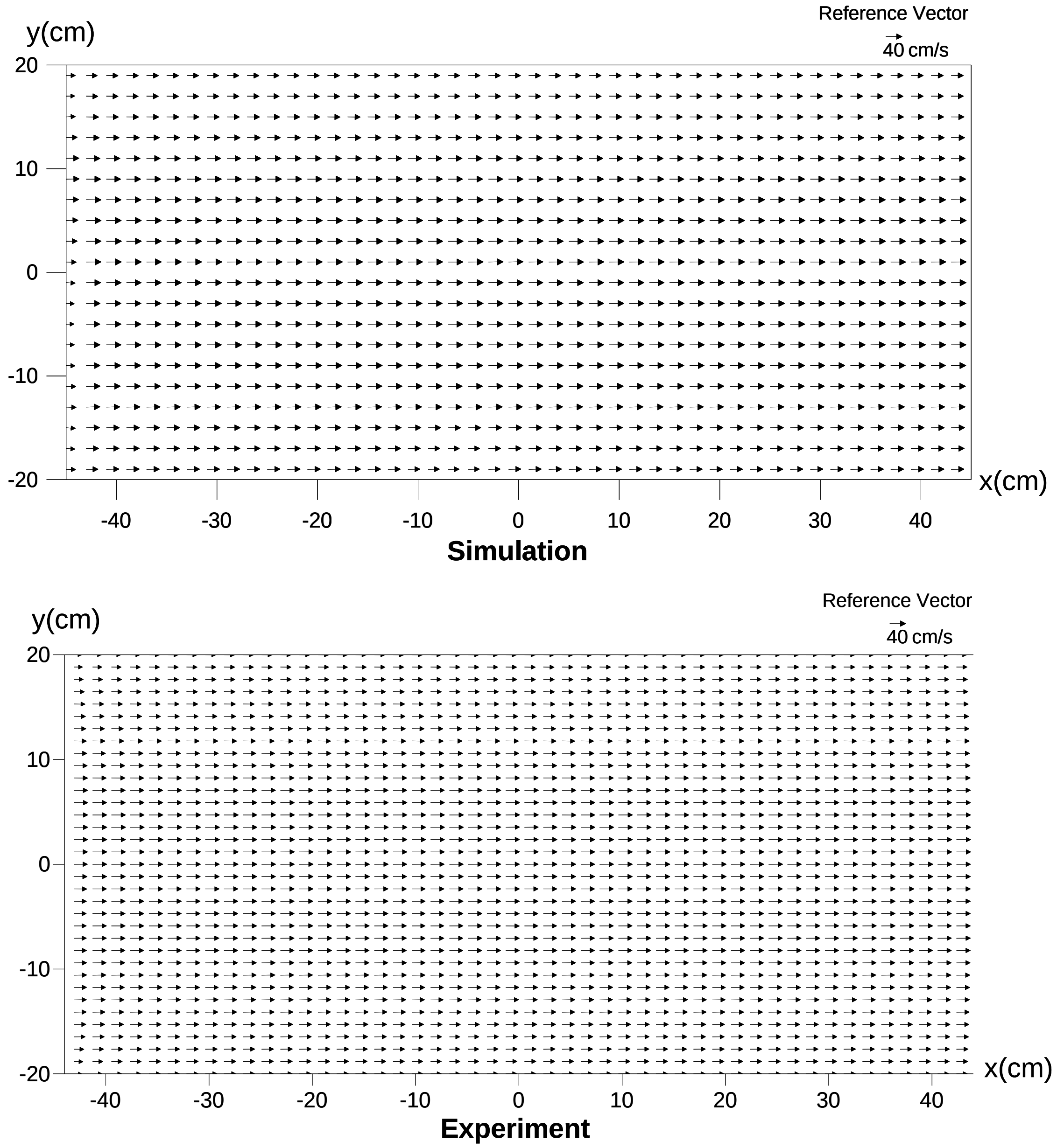

Figure 2.31 Comparison of velocity at free-surface (Case-1)

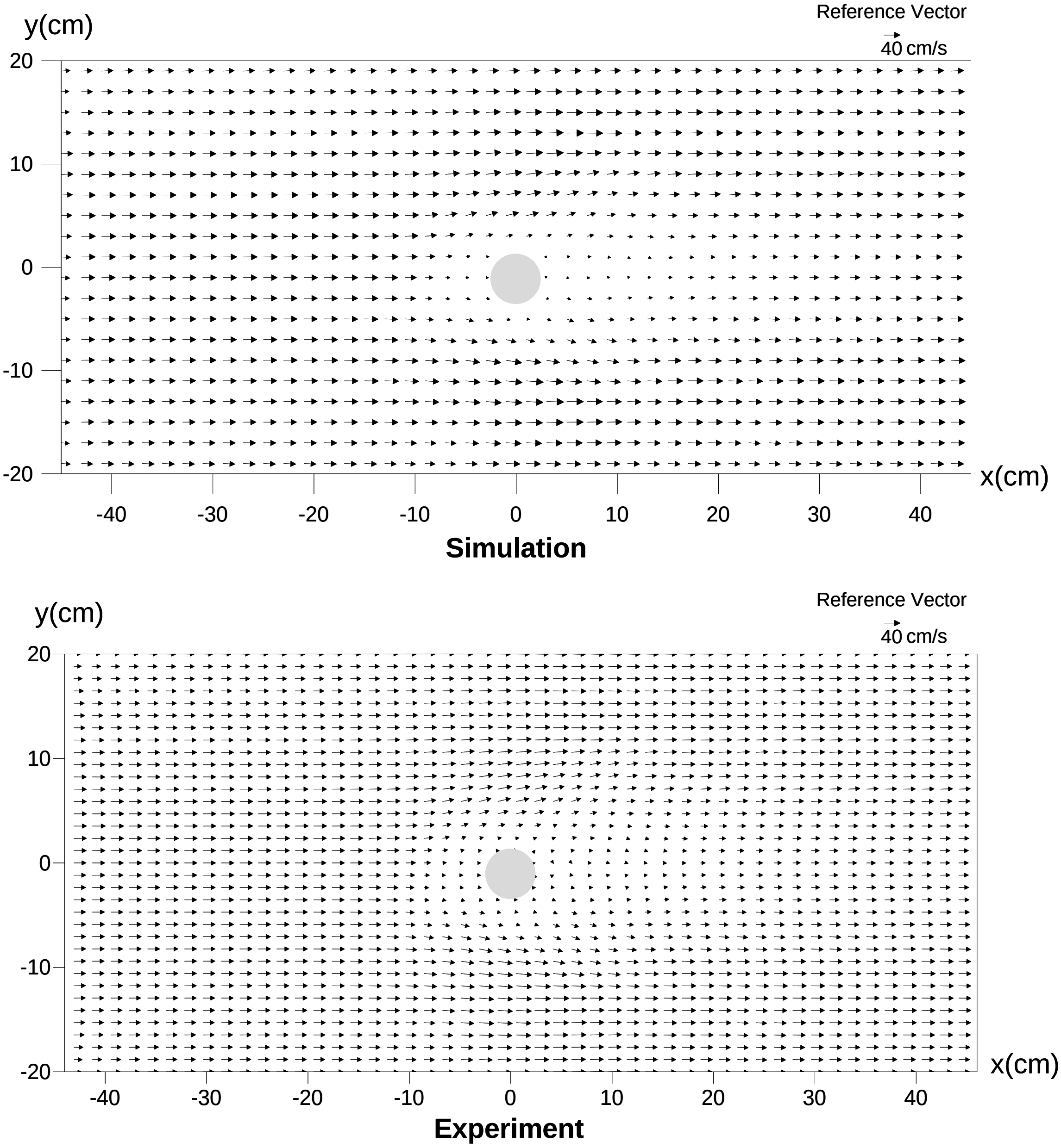

Figure 2.32 Comparison of velocity at free-surface (Case-2)

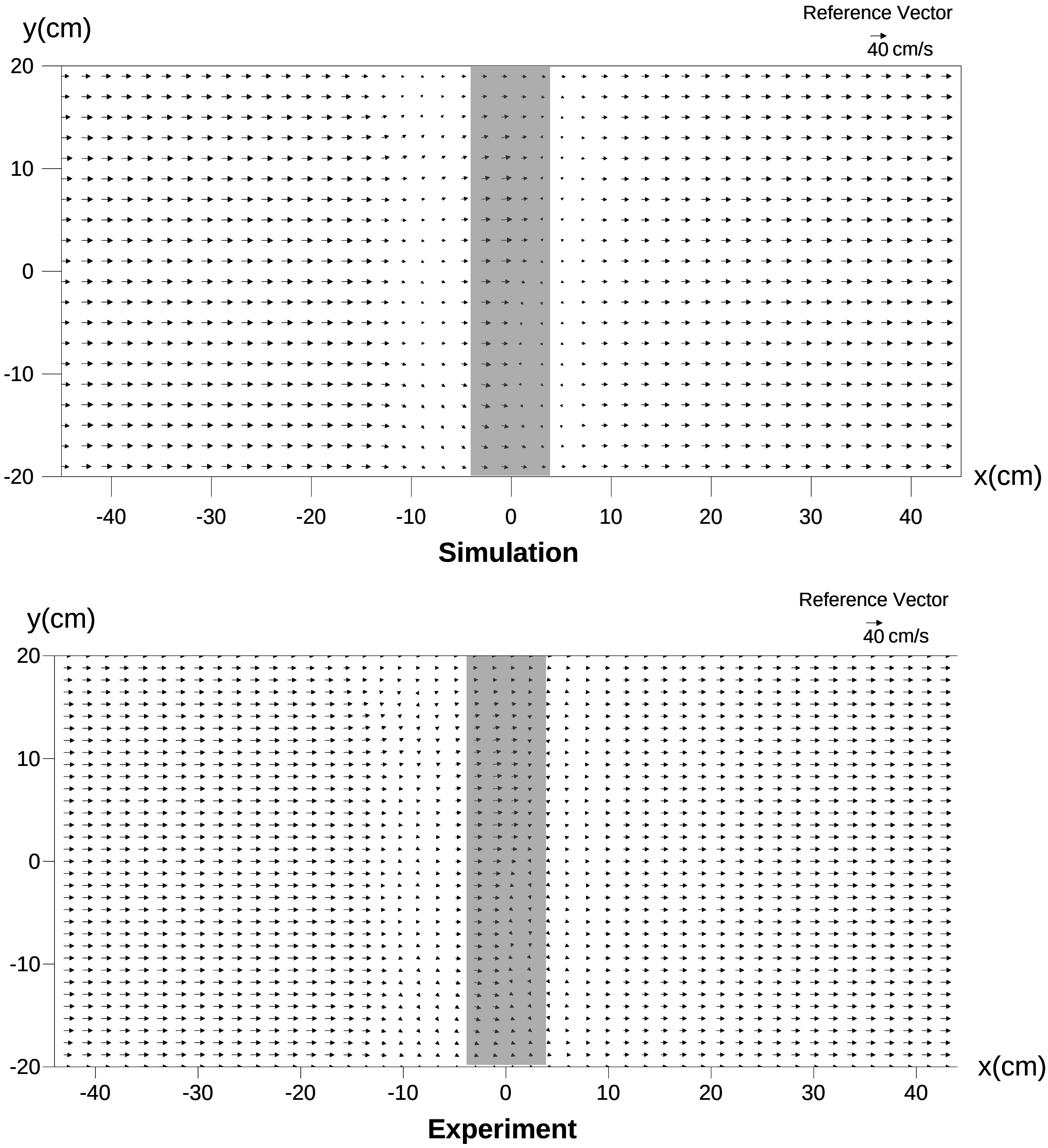

Figure 2.33 Comparison of velocity at free-surface (Case-3)

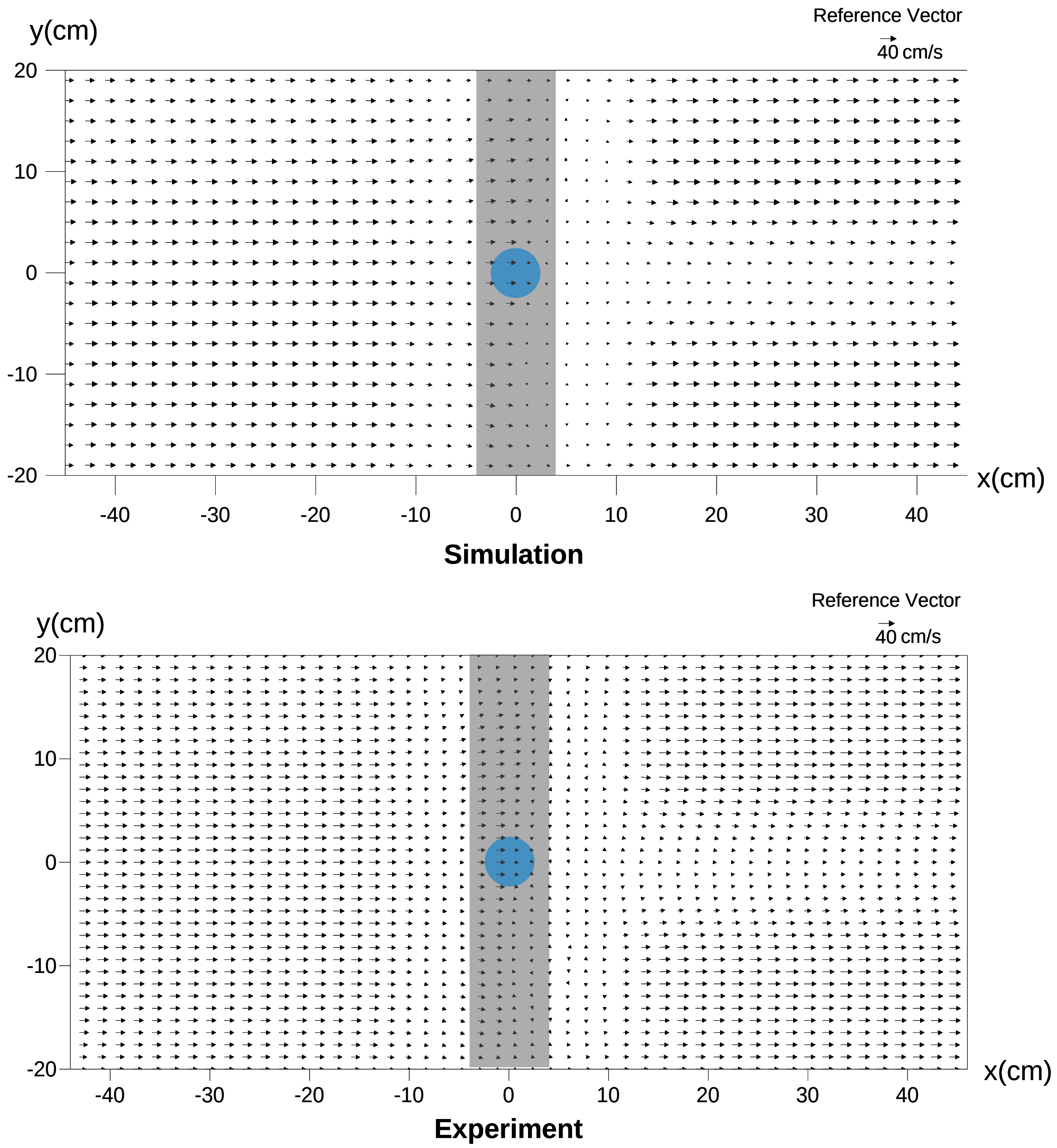

Figure 2.34 Comparison of velocity at free-surface (Case-4)

In view of the results so far achieved, it is found that all the results generally can reproduce well the effect of hydraulic structures but the numerical model slightly under-predicts the water level. The main causes of those under-predictions seem to be in the modeling of the turbulence. The turbulence model employed in this study is the standard k-ε model, which has several problems as pointed out by Speziale (1991), for example the inability to properly account for the streamline curvature, rotational strains and other body force effects and the neglect of the non-local and the effects of the Reynolds stress anisotropies. In order to correct those problems, the consideration of model by introducing non-linear constitutive relation between the mean strain rate and the turbulence stresses is required.

Summary

In this study, the three-dimensional numerical simulation was conducted to estimate the effects of water level rise by hydraulic structures within a river. The developed numerical model can treat the flow with free surface on an unstructured mesh with finite volume method. The standard k-ε model was used for turbulence model and the volume of fluid method proposed by Hirt and Nichols (1981) was used to represent the free water surface. The differencing scheme proposed by Ubbink and Issa (1999) is also employed to capture the free water surface in unstructured mesh.

The prediction of the water level rise by hydraulic structures is very important from the viewpoint of flood disasters. The present study shows that the numerical model used in this study can be used to simulate the changes of the flow field around hydraulic structures although the numerical model underestimates the water level rise around hydraulic structures. In order to improve the model developed in this study, further researches considering different turbulence models and various flow conditions are needed.

Chapter 3

Inundation flow analysis

3.1 Introduction

So far, most of the inundation studies have been carried out about the inundation flow due to insufficient drainage capacity of sewerage or levee failure (Inoue et al., 2000; Toda et al., 1999; Kawaike et al., 2004; Shigeeda and Akiyama, 2005). Besides those factors, overflow into a floodplain by water level rise in a river channel causes inundation disasters. Therefore, in this study, the inundation flow analysis is carried out to understand characteristics of the inundation flow considering overflow from a river channel. The existing inundation analysis models are divided into integrated inundation models (Kawaike et al., 2004) and dynamic inundation models (Shigeeda and Akiyama, 2005). In the former one, each flow field for a floodplain and a river channel is computed separately and connected by the overtopping formula. The latter one is conducted by the planar inundation analysis on incorporated domain with a floodplain and a river channel. In the most of those numerical models, a river channel has been considered as one-dimensional or two-dimensional flow and a floodplain or an urban area has been considered as two-dimensional flow. But, in the river channel, three-dimensional computation is required for estimation of accurate overflow discharge from a river channel because one-dimensional or two-dimensional calculations are insufficient for evaluation of complicated flow around river structures and overtopping flow into a floodplain from a river channel. Therefore, in this study, a numerical coupling model, which includes three-dimensional computation with free-surface in a river channel mentioned in the previous chapter and two-dimensional horizontal computation in a floodplain, is proposed and applied for estimation of the inundation flow in a floodplain considering overflow from a river channel. And, the laboratory experiments are carried out to compare with the numerical results and to understand those flows. In this chapter, the explanation of three-dimensional model mentioned in the previous chapter is omitted, and the description for laboratory experiments and two-dimensional model is included. For coupling of two-dimensional model and three-dimensional model, the explanation for the connection of the domains is also included here.

3.2 2D-3D numerical coupling model

3.2.1 Introduction

In general, three-dimensional calculation with the free-surface modeling and appropriate turbulence modeling is necessary for the estimation of the free-surface shape considering the effects of hydraulic structures. However, if the inundation analysis considering those effects is carried out on whole urban area by using the three-dimensional model, too much computational time and effort are required. It is not efficient. Thus, the consideration of more effective computational method is necessary. In this study, the three-dimensional model proposed in the previous chapter is applied for the computation of river channel and the two-dimensional horizontal model applied in many inundation analyses is employed for an urban area. Both models are connected and progressed by simultaneous grid method. The description of the two-dimensional model and the coupling method of 2D and 3D meshes are represented in this section.

3.2.2 Two-dimensional flow modeling

The governing equations of 2D horizontal model are obtained by integrating the equations in 3D model from the riverbed to the free-surface as follows:

Continutiy equation:

$$\frac{\partial h}{\partial t}+\frac{\partial M}{\partial x}+\frac{\partial N}{\partial y}=0 \tag{3.1}$$

Momentum equation:

$$\frac{\partial M}{\partial t}+\frac{\partial (uM)}{\partial x}+\frac{\partial (vM)}{\partial y}=-gh\frac{\partial H}{\partial x}+\frac{1}{\rho}\left[\frac{\partial h\tau_{xx}}{\partial x}+\frac{\partial h\tau_{xy}}{\partial y}\right]-\frac{\tau_{bx}}{\rho} \tag{3.2}$$

$$\frac{\partial N}{\partial t}+\frac{\partial (uN)}{\partial x}+\frac{\partial (vN)}{\partial y}=-gh\frac{\partial H}{\partial y}+\frac{1}{\rho}\left[\frac{\partial h\tau_{yx}}{\partial x}+\frac{\partial h\tau_{yy}}{\partial y}\right]-\frac{\tau_{by}}{\rho} \tag{3.3}$$

where H is water stage (i.e. $H=h+z_b$); z_b is bed elevation; h is water depth; x and y are Cartesian coordinate components; u and v are depth-averaged flow velocity components in the x and y directions, respectively; M and N are discharge flux ($M=uh$, $N=vh$); τ_{xx}, τ_{xy}, τ_{yx} and τ_{yy} are depth-averaged turbulent stresses, τ_{bx} and τ_{by} are bottom shear stresses as:

$$\tau_{bx}=\frac{\rho g n^2 u\sqrt{u^2+v^2}}{h^{1/3}} \tag{3.4}$$

$$\tau_{by} = \frac{\rho g n^2 v\sqrt{u^2 + v^2}}{h^{1/3}} \tag{3.5}$$

where ρ is density of water; g is acceleration of gravity; n is Manning's coefficient. The turbulent stresses are related to the depth-averaged eddy viscosity as:

$$\tau_{ij} = \rho \nu_t \left(\frac{\partial u_i}{\partial x_j} + \frac{\partial u_j}{\partial x_i} \right) - \frac{2}{3} k \delta_{ij} \tag{3.6}$$

where both i and j denote x and y. In the k-ε model, the eddy viscosity is given as:

$$\nu_t = C_\mu \frac{k^2}{\varepsilon} \tag{3.7}$$

The two quantities k and ε are solved from the transport equations as follows:

$$\frac{\partial k}{\partial t} + u\frac{\partial k}{\partial x} + v\frac{\partial k}{\partial y} = \frac{\partial}{\partial x}\left(\frac{\nu_t}{\sigma_k}\frac{\partial k}{\partial x} \right) + \frac{\partial}{\partial y}\left(\frac{\nu_t}{\sigma_k}\frac{\partial k}{\partial y} \right) + P_h + P_{kv} - \varepsilon \tag{3.8}$$

$$\frac{\partial \varepsilon}{\partial t} + u\frac{\partial \varepsilon}{\partial x} + v\frac{\partial \varepsilon}{\partial y} = \frac{\partial}{\partial x}\left(\frac{\nu_t}{\sigma_\varepsilon}\frac{\partial \varepsilon}{\partial x} \right) + \frac{\partial}{\partial y}\left(\frac{\nu_t}{\sigma_\varepsilon}\frac{\partial \varepsilon}{\partial y} \right) + C_{1\varepsilon}\frac{\varepsilon}{k}P_h + P_{\varepsilon v} - C_{2\varepsilon}\frac{\varepsilon^2}{k} \tag{3.9}$$

where

$$P_h = \nu_t \left[2\left(\frac{\partial u}{\partial x}\right)^2 + 2\left(\frac{\partial v}{\partial y}\right)^2 + \left(\frac{\partial u}{\partial y} + \frac{\partial v}{\partial x}\right)^2 \right] \tag{3.10}$$

$$P_{kv} = \frac{u_*^3}{h C_f^{1/2}} \tag{3.11}$$

$$P_{\varepsilon v} = \frac{C_{2\varepsilon} C_\mu^{1/2}}{(e_* \sigma_t)^{1/2} C_f^{3/4}} \frac{u_*^4}{h^2} \tag{3.12}$$

in which σ_t is Schmidt number expressing the relation between the eddy viscosity and the diffusivity for scalar transport (=1.0); e_* is dimensionless diffusivity coefficient.

The discretization methods described in the 3D model are also used for the 2D model. The governing equations with a Cartesian coordinate system may be written as follows:

$$\frac{\partial (h\phi)}{\partial t} + \frac{\partial (uh\phi)}{\partial x} + \frac{\partial (vh\phi)}{\partial y} = \frac{\partial}{\partial x}\left(\Gamma h \frac{\partial \phi}{\partial x} \right) + \frac{\partial}{\partial y}\left(\Gamma h \frac{\partial \phi}{\partial y} \right) + s_\phi \tag{3.13}$$

where $h\phi$ is transport quantity; Γ is diffusive coefficient; s_ϕ is source term. The form of the momentum equations for M and N at a CV surface are reduced to:

$$a_f M_f = \sum a_{nb} M_{nb} - \int gh \frac{\partial H}{\partial x} dl \bigg|_f + b_f \tag{3.14}$$

$$a_f N_f = \sum a_{nb} N_{nb} - \int gh \frac{\partial H}{\partial y} dl \bigg|_f + b_f \tag{3.15}$$

where subscript f is the interface between two neighboring CVs; subscript nb is the neighboring CV; a is coefficient of the final discretized equations; b is source term excluding the pressure term. The pseudo variables corresponding to M and N are as follows:

$$\hat{M}_f = \frac{\sum a_{nb} M_{nb} + b_f}{a_f} \tag{3.16}$$

$$\hat{N}_f = \frac{\sum a_{nb} N_{nb} + b_f}{a_f} \tag{3.17}$$

Thus, the following is obtained from Equations (3.14), (3.15), (3.16) and (3.17):

$$M_f = \hat{M}_f - \frac{\int gh \frac{\partial H}{\partial x} dl \Big|_f}{a_f} \tag{3.18}$$

$$N_f = \hat{N}_f - \frac{\int gh \frac{\partial H}{\partial y} dl \Big|_f}{a_f} \tag{3.19}$$

The guessed pressure and the velocity components are obtained from the momentum equation not satisfying the continuity equation.

$$M = M^* + M' \tag{3.20}$$

$$N = N^* + N' \tag{3.21}$$

$$H = H^* + H' \tag{3.22}$$

where superscript * is the variable not satisfying the continuity equation; superscript ' is the corrected variable. The Equation (3.14) and (3.15) can be expressed as:

$$a_f M_f^* = \sum a_{nb} M_{nb}^* - \int gh \frac{\partial H^*}{\partial x} dl \bigg|_f + b_f \tag{3.23}$$

$$a_f N_f^* = \sum a_{nb} N_{nb}^* - \int gh \frac{\partial H^*}{\partial y} dl \bigg|_f + b_f \tag{3.24}$$

Subtracting Equation (3.23) and (3.24) from Equation (3.14) and (3.15) with taking Equation (3.20), (3.21) and (3.22), one obtains the velocity correction as:

$$M_f^{'} = \frac{\sum a_{nb} M_{nb}^{'}}{a_f} - \frac{\int gh \frac{\partial H^{'}}{\partial x} dl \Big|_f}{a_f} \tag{3.25}$$

$$N_f^{'} = \frac{\sum a_{nb} N_{nb}^{'}}{a_f} - \frac{\int gh \frac{\partial H^{'}}{\partial y} dl \Big|_f}{a_f} \tag{3.26}$$

In those equations, if the first term on the right hand side is omitted, the velocity correction has a simple relation with the pressure correction.

$$M_f = M_f^{*} - \frac{\int gh \frac{\partial H^{'}}{\partial x} dl \Big|_f}{a_f} \tag{3.27}$$

$$N_f = N_f^{*} - \frac{\int gh \frac{\partial H^{'}}{\partial y} dl \Big|_f}{a_f} \tag{3.28}$$

In order to guarantee the mass conservation, the continuity equation for each CV should be satisfied as described below:

$$\int \frac{\partial H}{\partial t}\Big|_P + \sum \left(M_f l_x + N_f l_y \right) = 0 \tag{3.29}$$

where l_x and l_y are projected length of the dry-wet boundary, respectively.

At the dry-wet boundary, the zero velocity and water depth at the center of the dry CV bring numerical problems when calculating the velocity correction by using the pressure correction. Thus, special treatment is needed for the dry-wet boundary. First, the pressure correction is used to correct surface fluxes around dry CVs as follows:

$$M_{f,new}^{*} = M_f^{*} \frac{1}{a_f} gh\left(H_A^{'} - H_P^{'}\right) l_x \tag{3.30}$$

$$N_{f,new}^{*} = N_f^{*} \frac{1}{a_f} gh\left(H_A^{'} - H_P^{'}\right) l_y \tag{3.31}$$

where subscript A is the adjacent CV (=wet CV); subscript *new* is the corrected surface flux. A new pressure correction for the dry CV considering Equation (3.29) is obtained as:

$$H_P' = \frac{ghH_A' \sum \frac{l^2}{a_f} - \sum \left(M^*_{f,new} l_x + N^*_{f,new} l_y \right)}{ghH_A' \sum \frac{l^2}{a_f} + A_p / \Delta t} \tag{3.32}$$

where A_p is area of present CV (=dry CV). If the dry CV has a zero water depth in the old time step, the pressure correction directly gives the new water stage. All the other quantities at the center of the dry CV are estimated by linear interpolation from the surface values.

3.2.3 Necessity of continuation of domains

In the design of a numerical computation for a river flooding in an urban area, predicting accurately complicated flow in a river channel is a very important task to do. The computation of inundation flow including complicated flow around river structures needs consideration of 3D simulation, but conducting the 3D computation for a whole domain of a river channel and a floodplain is not efficient at all from the point of calculation time and capacity. Thus, in order to solve this problem, connection of domains is carried out here. In some studies, connection of domains has been conducted in study field on storm surge and tsunami to solve the restriction of the computational capacity and time for open boundary in sea side. They can be classified into two types: successive grid method and simultaneous grid method. The former one is a method that whole domain is divided into coarse meshes and the focused domain is divided into fine meshes. A solution obtained from whole domain is used as boundary condition of the focused domain. The computational domains could be narrow by this method. The latter one is a method considering overlapping meshes between large domain and small domain. Both meshes are arranged to be connected. In the overlapping meshes, a solution of large domain is given as the boundary condition of small domain, and that of small domain is given as the boundary condition of large domain. The computation is carried out by simultaneous progression on both domains. This study is focused on the latter one because large domain used in the research on storm surge and tsunami is not considered here.

3.2.4 Method for continuation of 2D and 3D meshes

The simultaneous grid method is employed in this study to solve the above mentioned problem. 2D domain (floodplain area) and 3D domain (river area) are arranged to be connected and the domain has overlapped meshes between 2D and 3D areas.

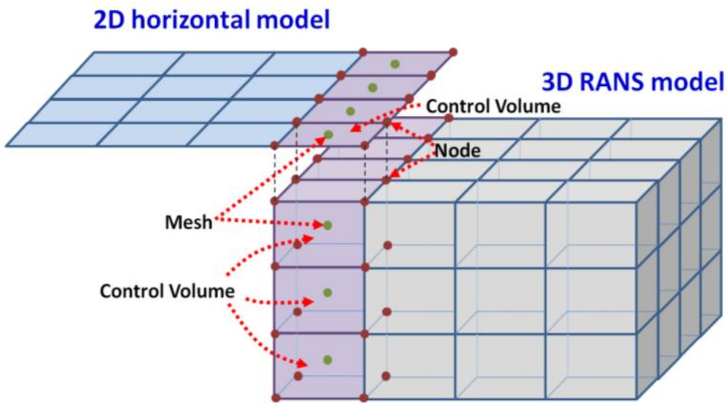

Figure 3.1 Conceptional diagram for coupling of 2D and 3D meshes

In the connected areas, the values obtained from 3D calculation are given as the boundary condition of 2D calculation and the value obtained from 2D calculation is given as the boundary condition of 3D calculation. The 3D calculation requires the vertical distribution of velocity at the interface. But, the 2D calculation has no information on the vertical velocity distribution. The velocity at the interface of 3D calculation is approximated as a vertically uniform value. In the 2D calculation, the boundary values are obtained as the depth-averaged values of the results obtained from the 3D calculation. The calculation is carried out by simultaneous progress in both domains. This method is expected to get more correct results because this can consider a complicated flow around the river structures. Figure 3.1 shows a conceptional diagram for coupling of 2D and 3D meshes. All hydraulic quantities are connected at overlapped position in space.

3.3 Laboratory experiments

3.3.1 Introduction

The laboratory experiments are carried out to understand variations of the inundation flow considering overflow from a river channel and to compare with the results obtained from the numerical simulations. The details of the experiments are described below.

3.3.2 Laboratory flume

The experimental flume used in this study is located at Ujigawa Open Laboratory of Kyoto University, Japan. The experimental flume has 20m long, 1m wide and 0.3m deep. Figure 3.2 shows a schematic diagrams of the experimental flume used in this study.

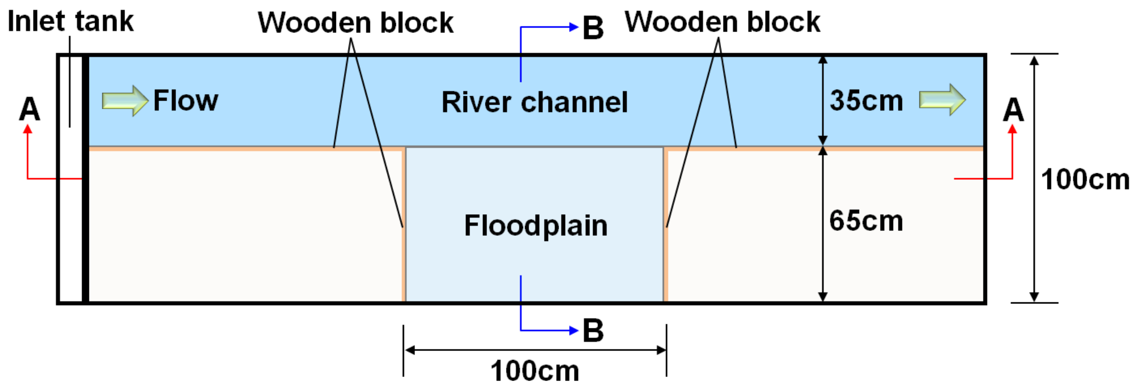

Top view of experimental flume

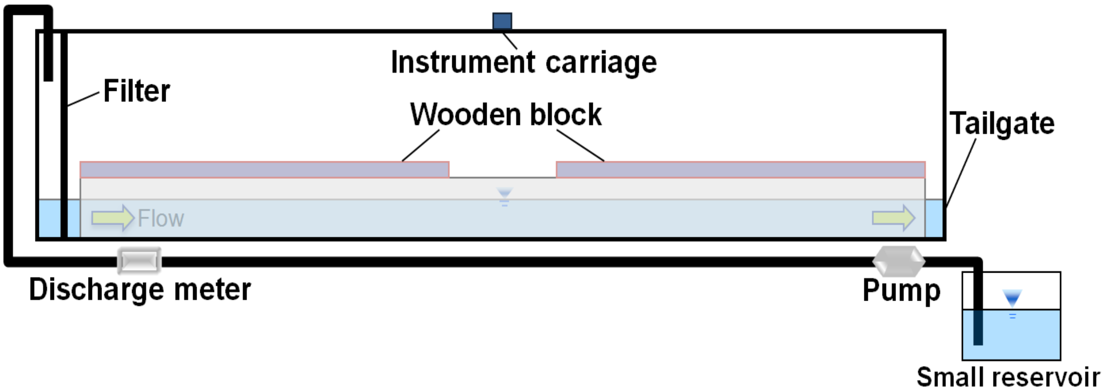

Longitudinal cross-section A-A

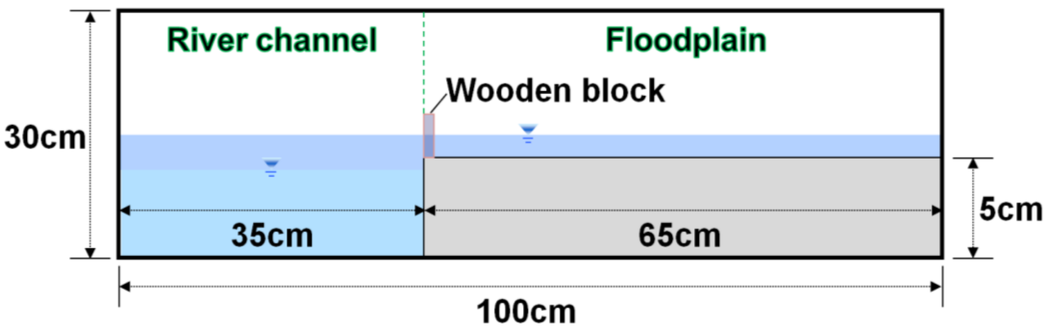

Transverse cross-section B-B

Figure 3.2 Schematic representations of experimental flume

Each cross-section of the experimental flume is represented in Figure 3.2. The experimental flume consists of parts of a river channel and a floodplain. The river channel has 35cm width and the floodplain has 100cm length, 65cm width and 5cm height. The floodplain area is made of wooden block. The water is pumped back to the laboratory system and passed through a filter.

3.3.3 Model hydraulic structures

The laboratory experiments are carried out in the cases of no structures, pier, girder and pier+girder. Those structures are made of wooden material. And, the river structures are located in the middle of the river channel. Details of the model hydraulic structures are shown in Figure 3.3. The bottom side of girder structure is located at 3cm above from the bottom of the river channel.

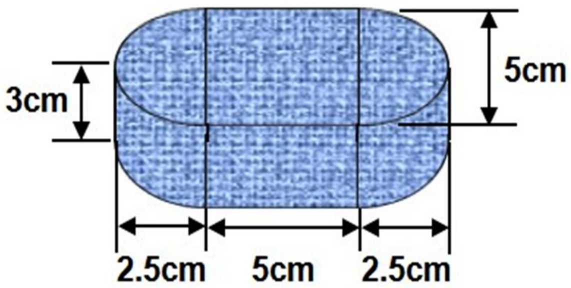

Pier structure

Girder structure

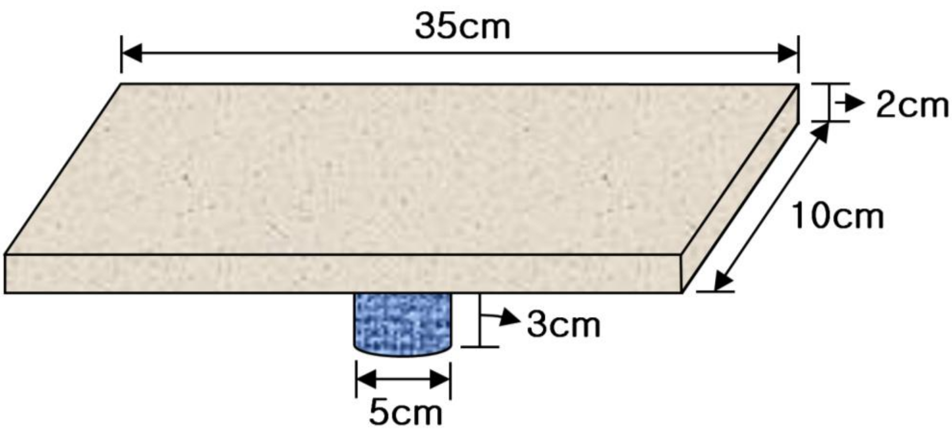

Pier+Girder structure

Figure 3.3 Details of hydraulic structures

3.3.4 Measurement apparatus

In this study, the water level and free-surface velocity are measured. The servo type water level meter mentioned in Chapter 2 is used for the measurement of water level. And, the PIV measurement is also carried out for the measurement of free-surface velocity. Figure 3.4 shows actual experimental photos for measuring the water level by the servo type water level meter (left, Case 1-4) and the free-surface velocity by the PIV measurement (right, Case 2-3).

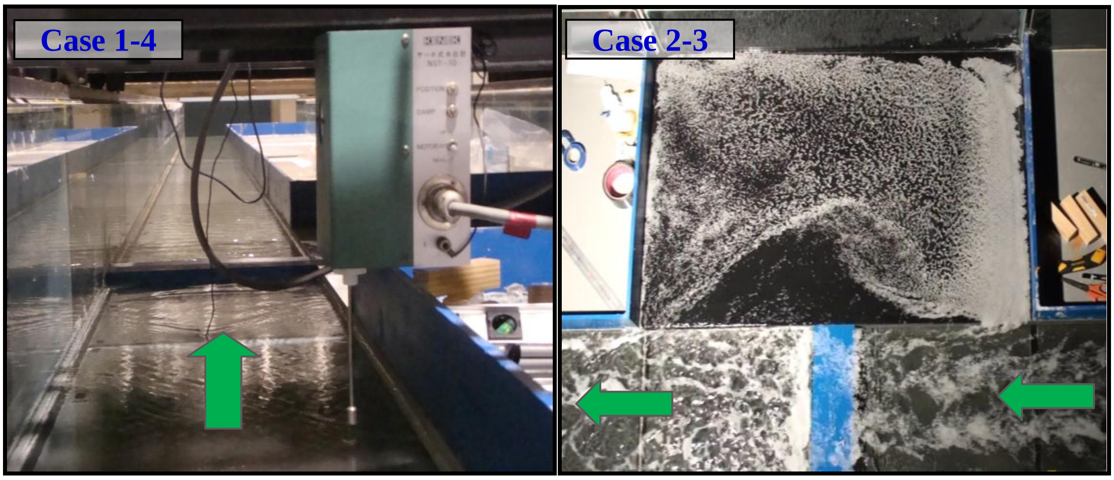

Figure 3.4 Experimental photos for measuring water level and free-surface velocity

3.3.5 Experimental procedures

Like the preceding experiments, the channel slope and the warp of rail were firstly checked. And, the elevation of floodplain was measured. Then, the uniform depth is also measured. The experiments are carried out after the preliminary works. The measurement intervals of water level are 2.0~10.0cm in x-direction and 2.5~7.0cm in y-direction. More detailed measurements are conducted around river structures. Total number of measurement points is about 250 ~300 for each case as shown in Figure 3.5. The PVC (Polyvinyl Chloride) powder of mean diameter 50μm is used as the tracer for PIV analysis. The PIV analysis is carried out by taking a picture with video camera.

3.3.6 Experimental conditions

The experiments are carried out on three different flow discharge conditions.

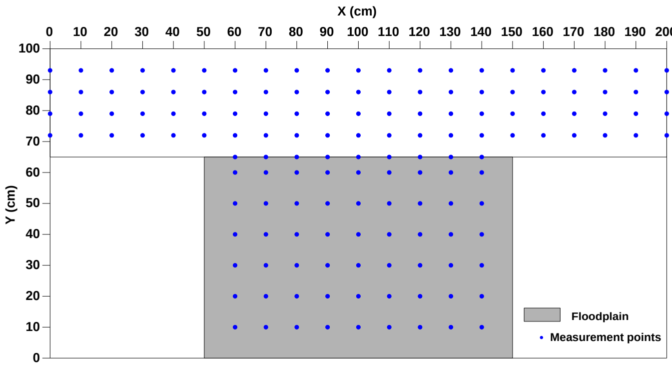

(a) No structure

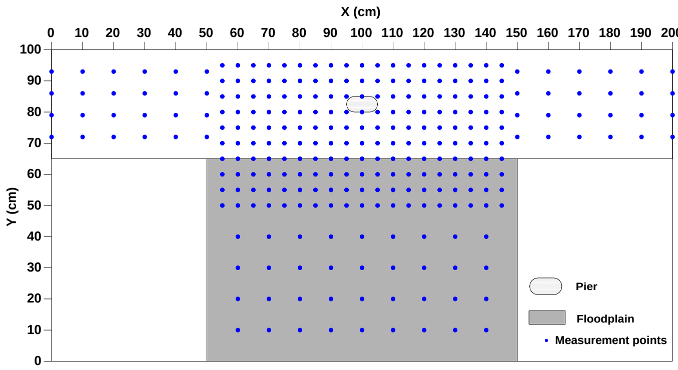

(b) Pier structure

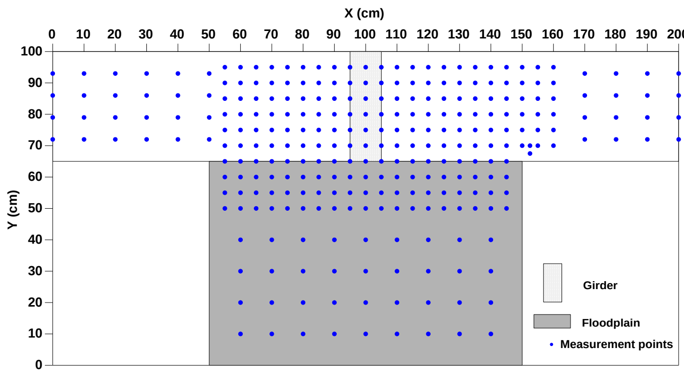

(c) Girder structure

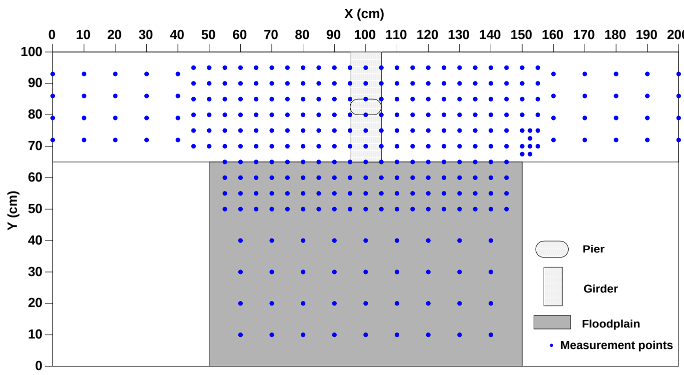

(d) Pier+Girder structure

Figure 3.5 Measuring points for water level in Case 3

Table 3.1 and 3.2 show experimental cases and hydraulic conditions, respectively. The flow discharges of experimental cases were determined by considering no inundation (Case 1-1, 1-2, 1-3, 1-4, 2-1 and 2-2), inundation due to girder structure (Case 2-3 and 2-4) and fully inundation (Case 3-1, 3-2, 3-3 and 3-4).

Table 3.1 Experimental cases

Case	1-1 2-1 3-1	1-2 2-2 3-2	1-3 2-3 3-3	1-4 2-4 3-4
Structure	No structures	Pier	Girder	Pier+Girder

Table 3.2 Hydraulic conditions (Uniform flow)

Parameters	Symbols (unit)	Case 1	Case 2	Case 3
Flow discharge	Q (l/s)	4.00	6.00	12.00
Flow depth	H (cm)	3.48	4.56	7.12
Channel slope	I	1/987	1/987	1/987
Mean velocity	u_m (cm/s)	32.84	37.59	48.15
Reynolds number	Re	11428	17141	34282
Froude number	Fr	0.56	0.56	0.57

3.4 Numerical simulations

3.4.1 Introduction

The numerical simulations are carried out under the same condition as those of experimental cases. The results obtained from the simulations are compared with the experimental results

3.4.2 Computational domain

Figure 3.6 shows the computational meshes used in this study. In the 3D mesh, the grid of z-direction is considered as 10 layers with 1cm interval. The numbers of computational meshes in 2D and 3D are 1,686 and 30,230 meshes, respectively.

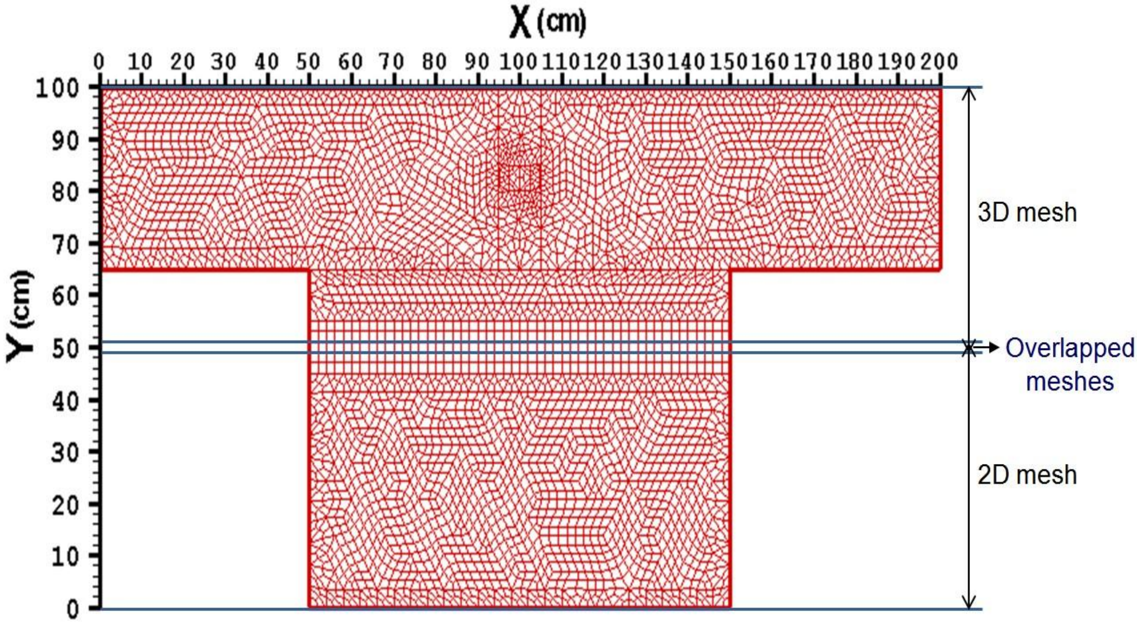

Figure 3.6 Computational mesh

3.4.3 Computational conditions

The results obtained from the experiment are given as the initial conditions of computation. And, in the same way as the experiments, the different types of hydraulic structures are considered in the each case of computation. Manning's roughness coefficient and time interval are 0.02 and 0.001s, respectively.

3.5 Results and analyses

The results of numerical simulations are verified by comparing with the experimental results. The water level rise due to effect of hydraulic structures is estimated by the simulated and experimental results. The simulated and experimental results of water level and velocity at free-surface are compared here. And then the applicability of numerical model will be discussed.

3.5.1 Comparison of water level

The results of the water level obtained from the simulations and experiments are compared. And, the effects of hydraulic structures through the comparison of plane distribution and cross-section for water level are estimated.

Plane distribution of water level

Case 1-1

Experiment

Simulation

Case 1-2

Experiment

Simulation

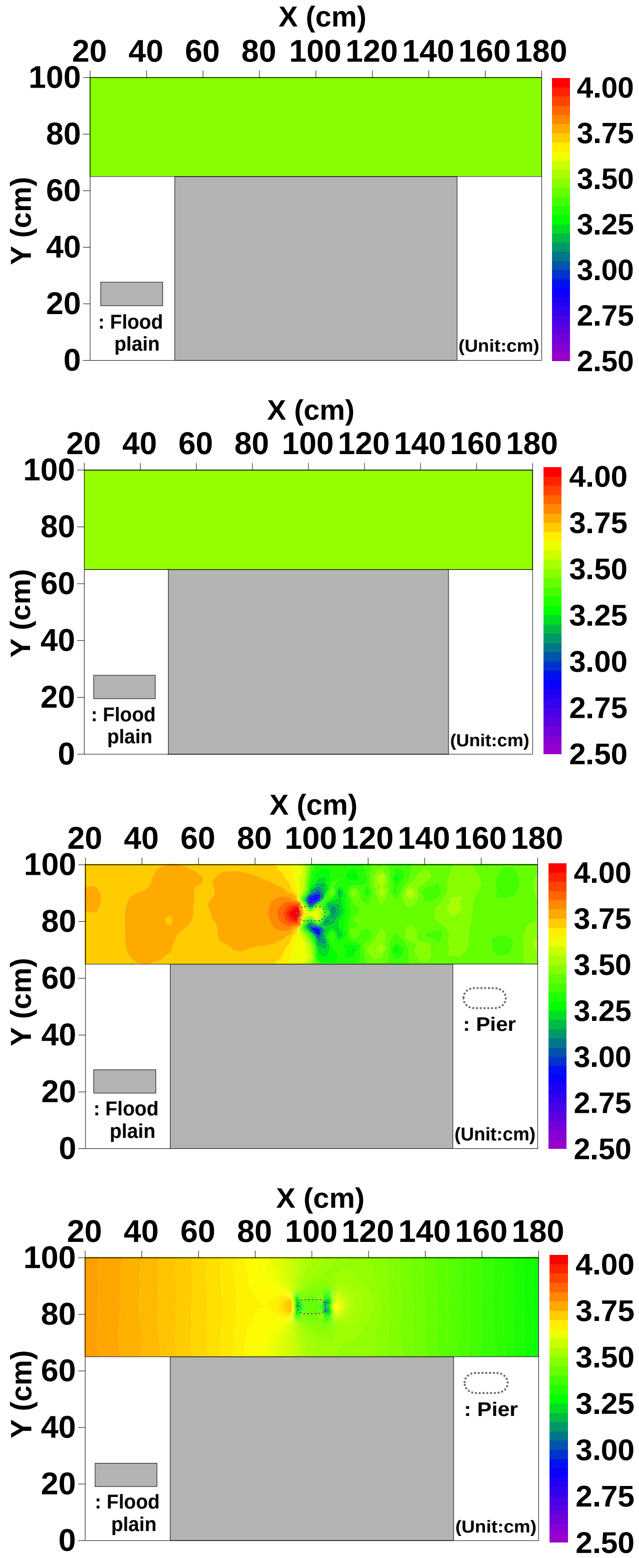

Figure 3.7 Results of water level (Case 1-1&1-2)

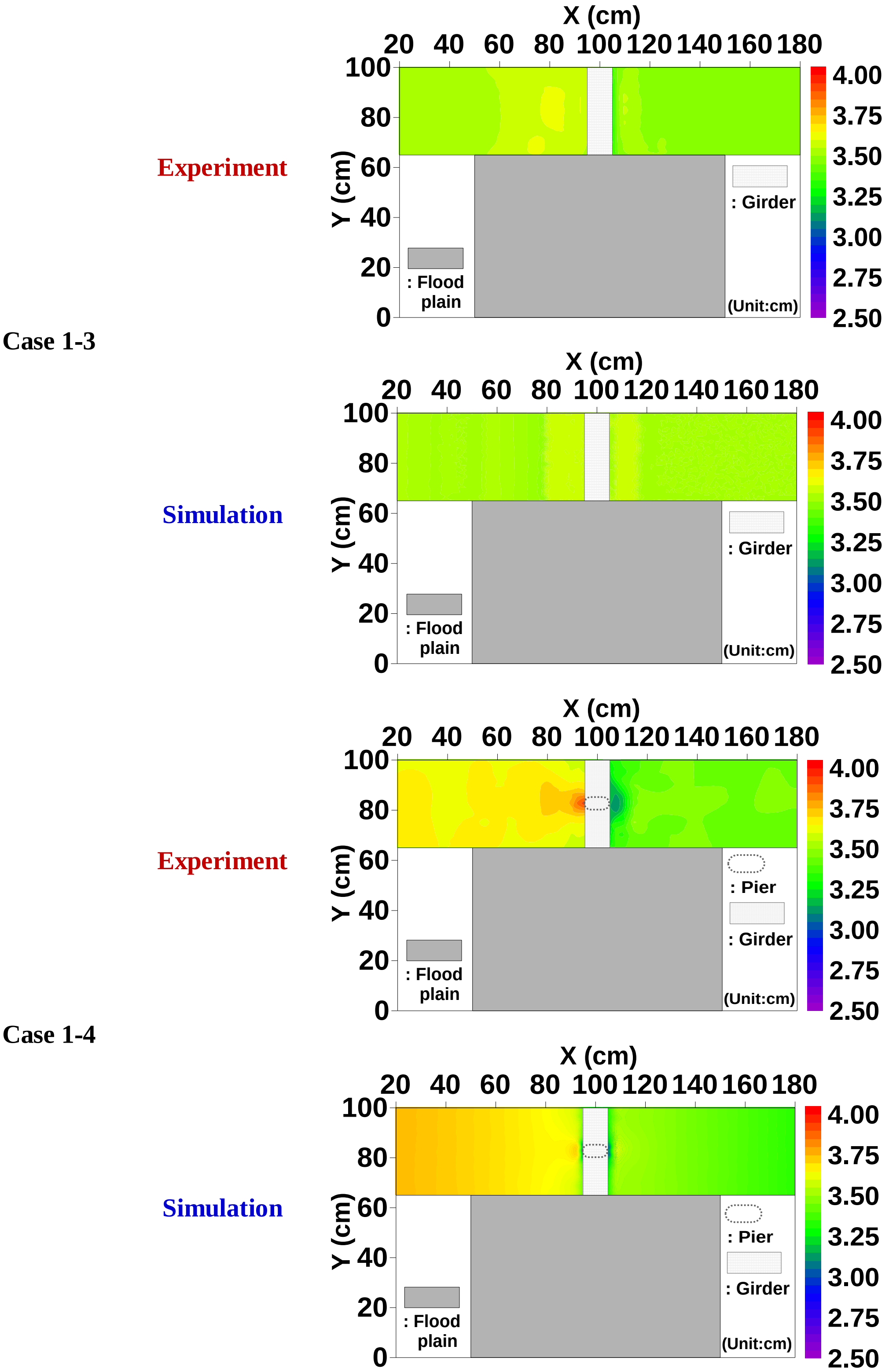

Figure 3.8 Results of water level (Case 1-3&1-4)

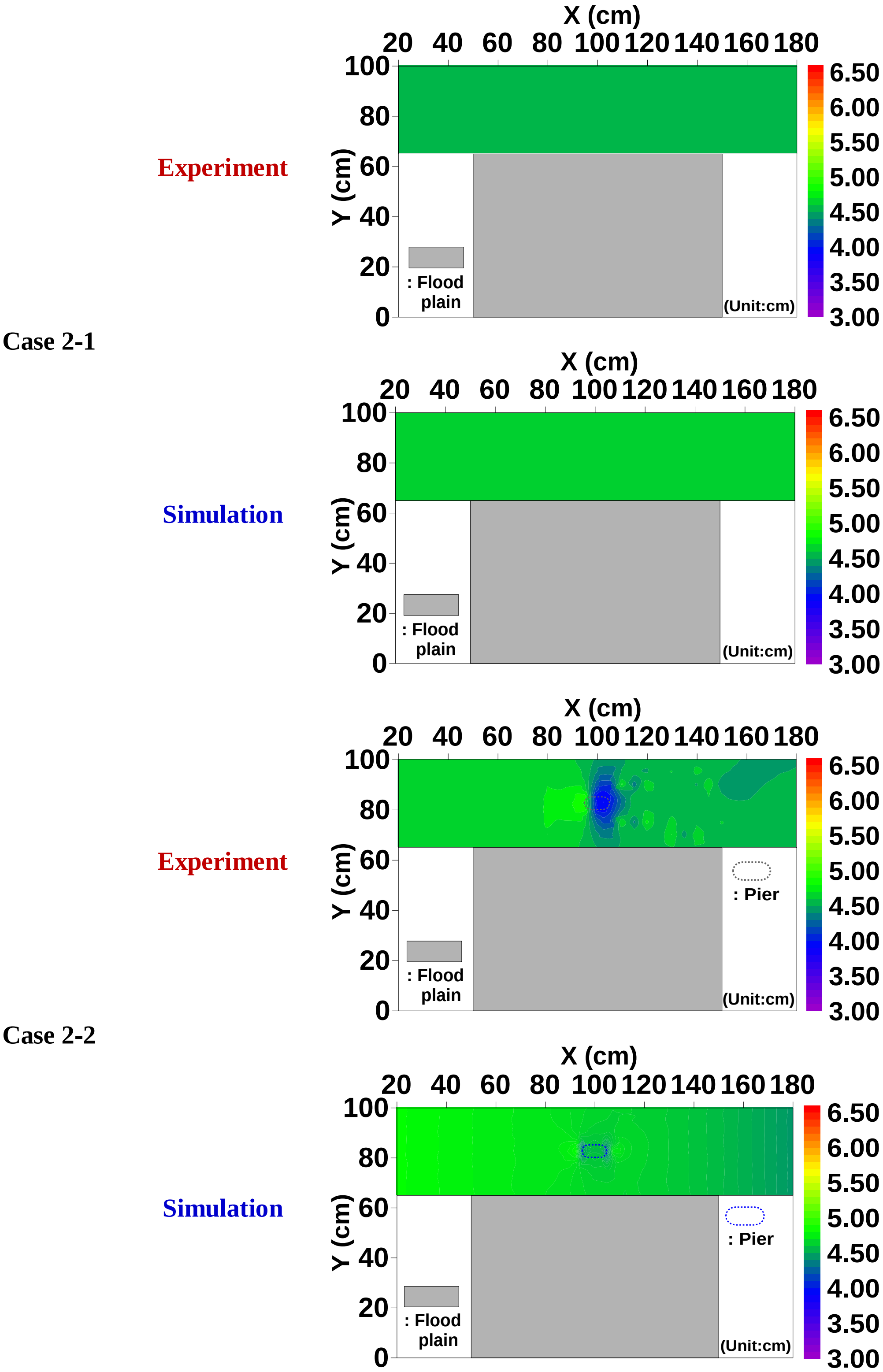

Figure 3.9 Results of water level (Case 2-1&2-2)

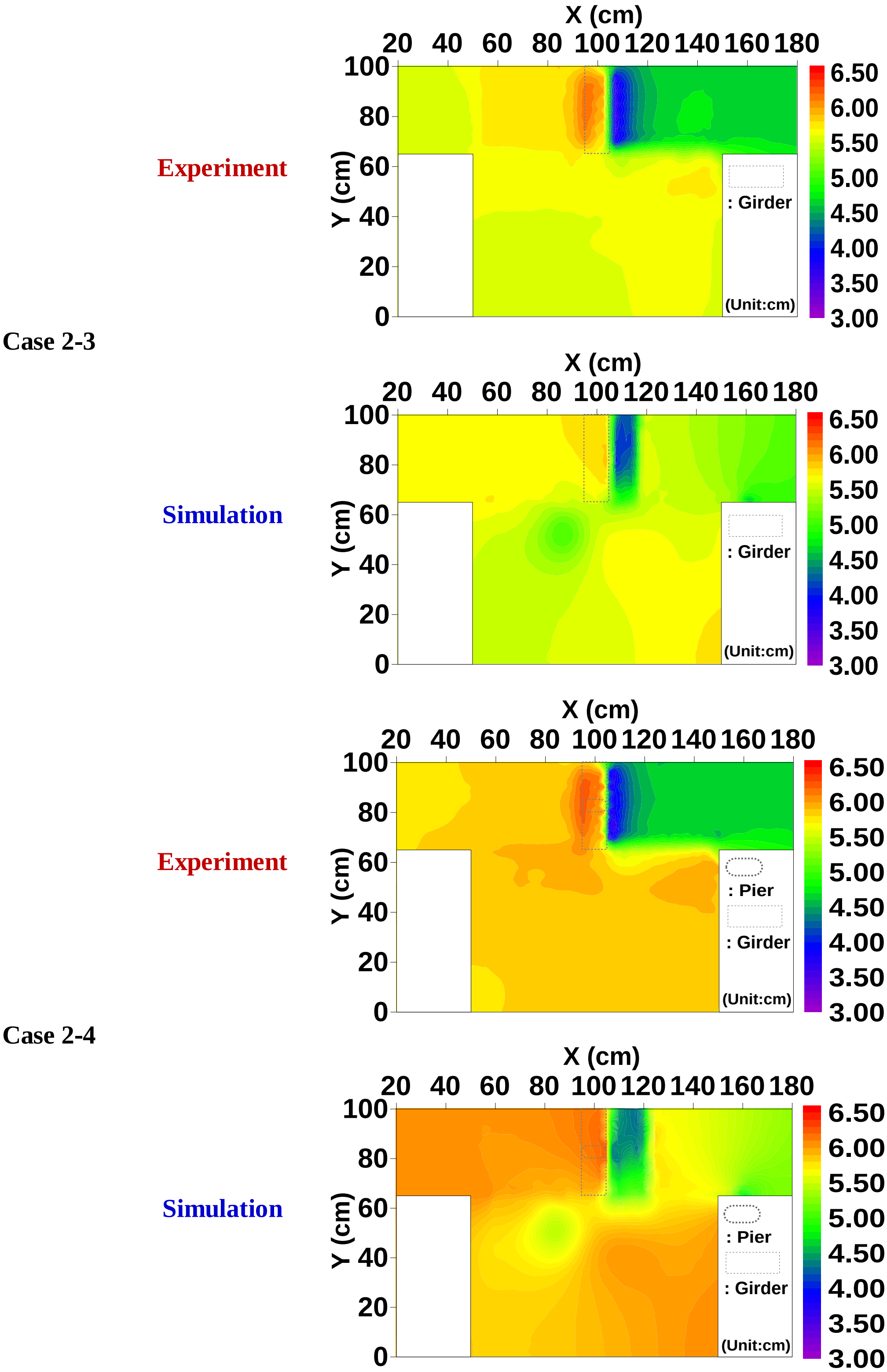

Figure 3.10 Results of water level (Case 2-3&2-4)

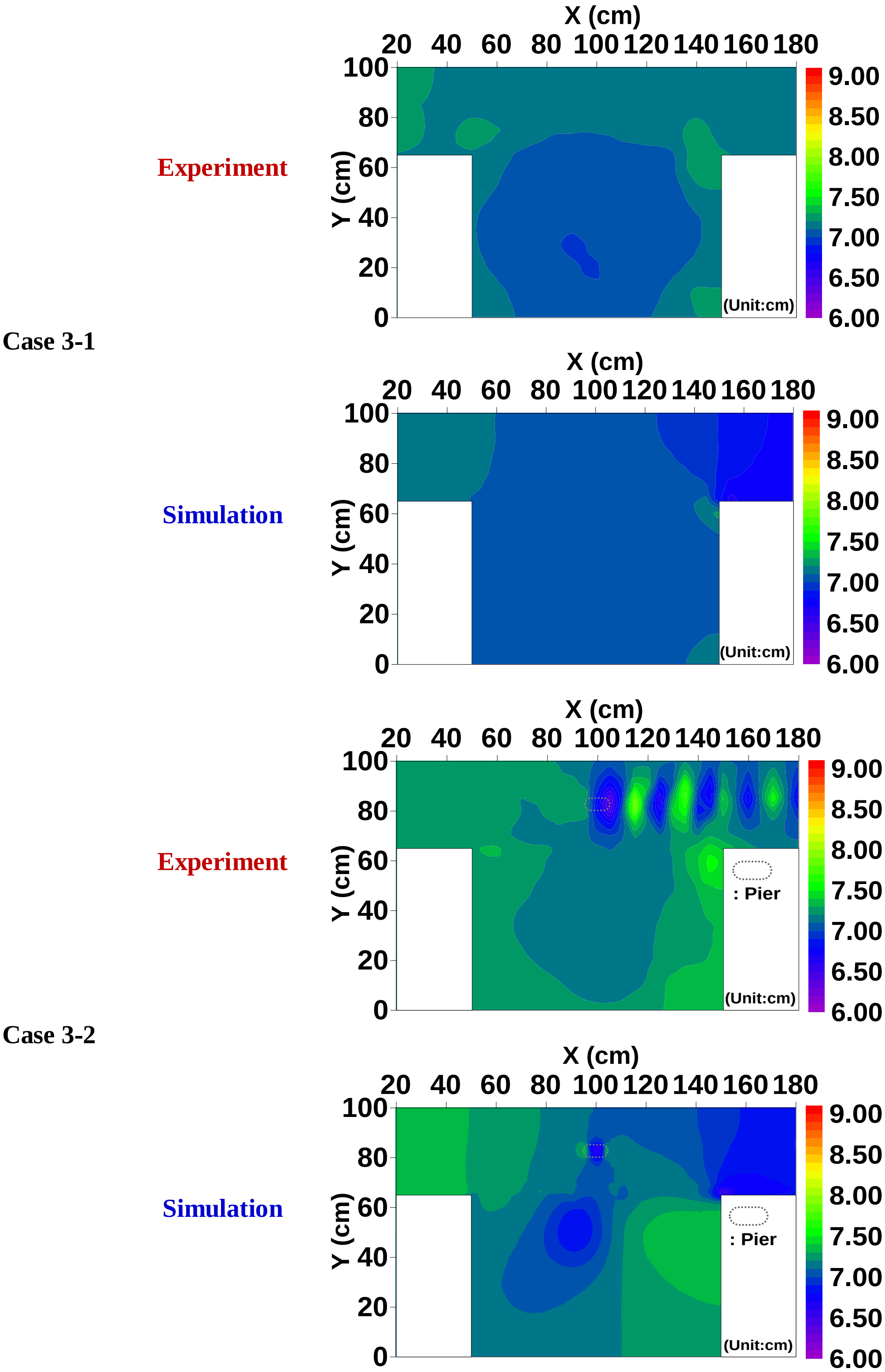

Figure 3.11 Results of water level (Case 3-1&3-2)

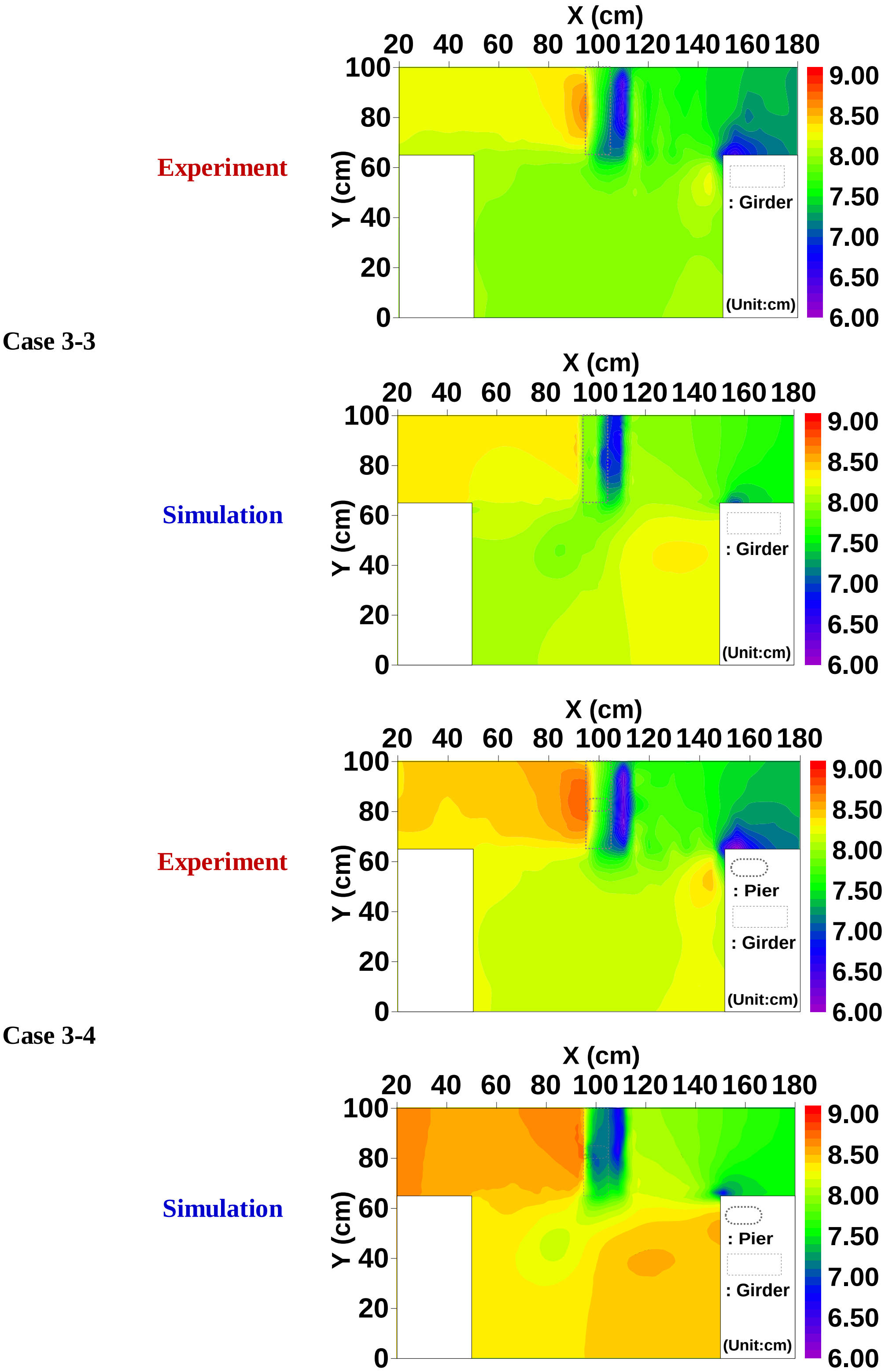

Figure 3.12 Results of water level (Case 3-3&3-4)

Figure 3.7 - 3.12 show the results of the water level obtained from the experiments and the simulations. In Case 1, 2 and 3, experimental conditions are the same except for flow discharge. In Case 1, the pier structure is submerged and the girder structure is not submerged. In Case 2 and 3, all structures are submerged. The overflow into floodplain does not occur in Case 1 and occurs in Case 3. In Case 2, overflow into floodplain does not occur in case of 2-1 and 2-2 and occurs in case of 2-3 and 2-4. As seen in the results of Case 2 and 3, it is found that the effect of the water level rise by girder structure is larger than that of pier structure. From the numerical results of the water level, changes of water level rise by river structures are appropriately reproduced. It is judged that estimation of the inundation flow into a floodplain from a river channel is possible using the proposed numerical coupling model.

Comparison of water level in the cross-section

In this section, the results of water level in the cross-section are compared. Along the center of channel and floodplain (Figure 3.13), comparison between simulation and experiment are shown in Figure 3.14 - 3.21. The results of Case 1, Case 2-1 and 2-2 are compared only for cross-section A-A because overflow into floodplain does not occur in those cases. All the other cases are compared for the cross-sections A-A and B-B.

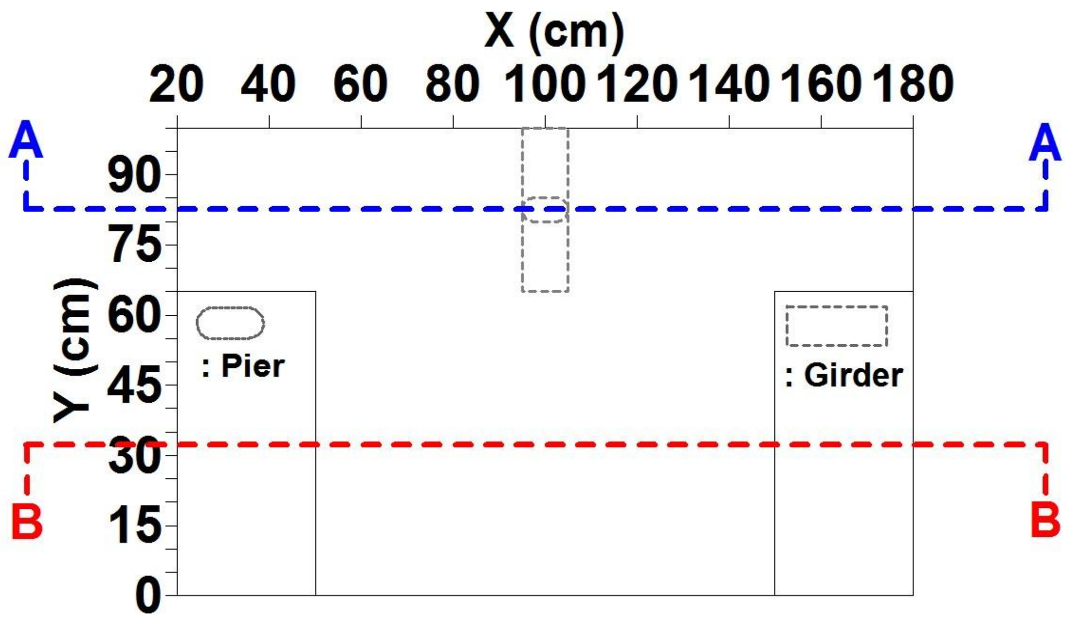

Figure 3.13 Location of cross section for comparison of water level

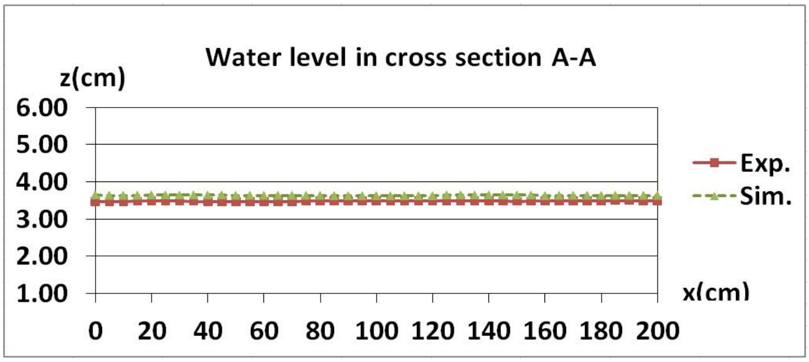

Case 1-1

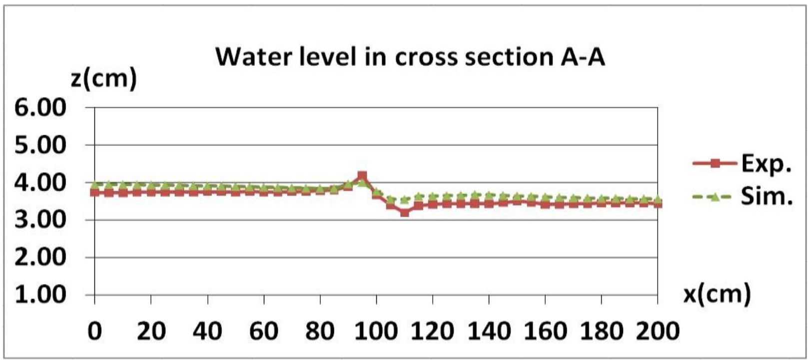

Case 1-2

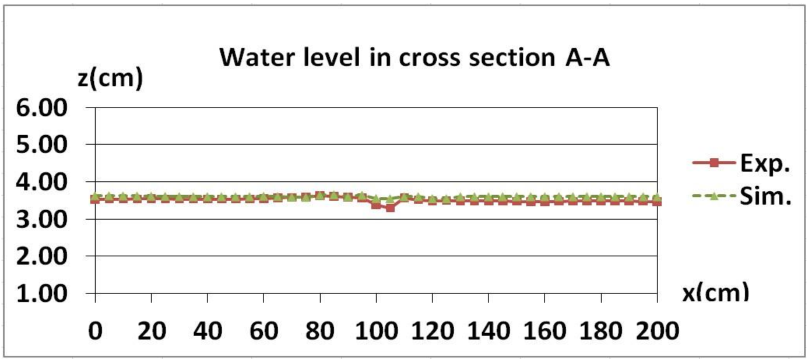

Case 1-3

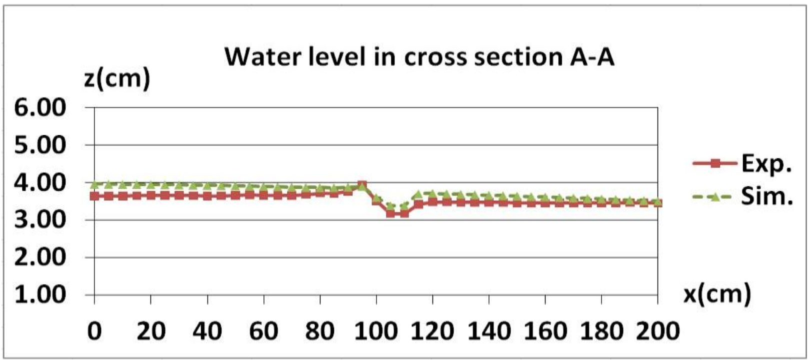

Case 1-4

Figure 3.14 Comparison of water level in each cross section (Case 1)

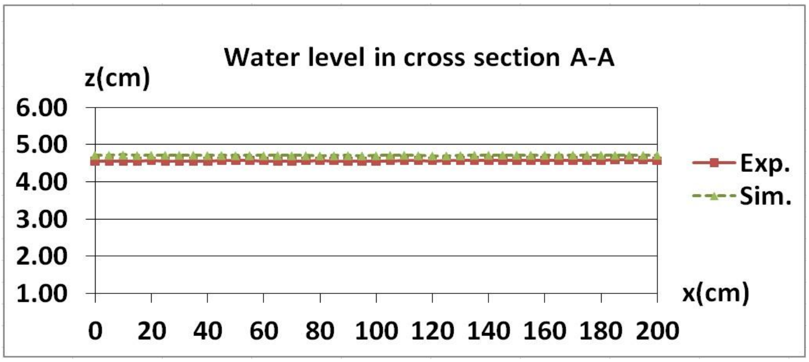

Case 2-1

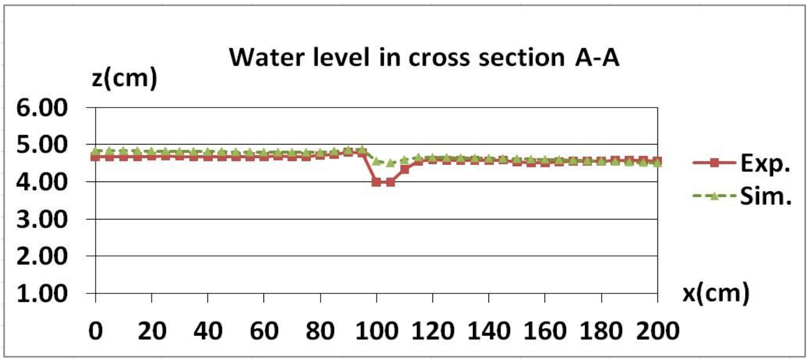

Case 2-2

Figure 3.15 Comparison of water level in each cross section (Case 2-1&2-2)

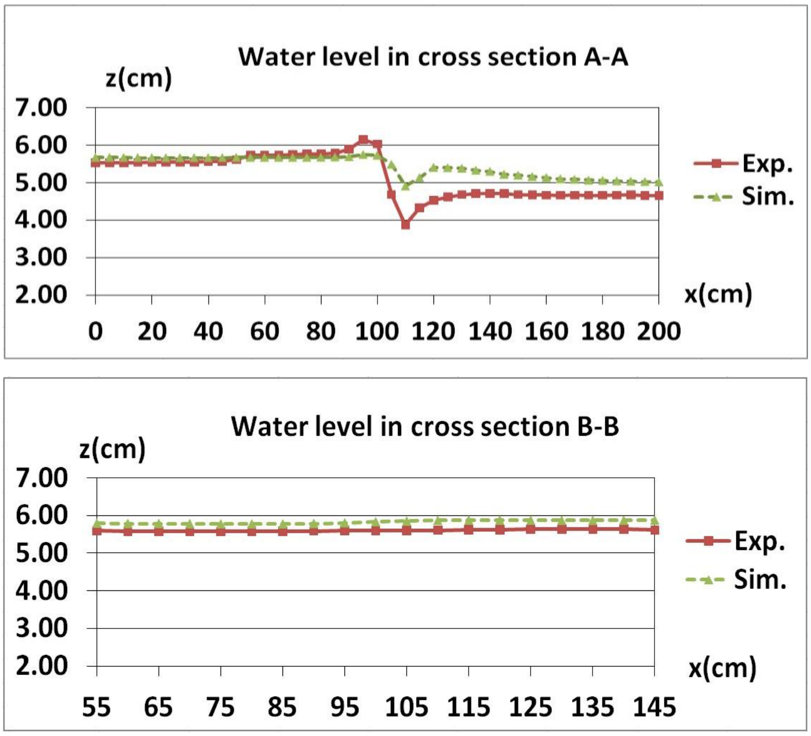

Figure 3.16 Comparison of water level in each cross section (Case 2-3)

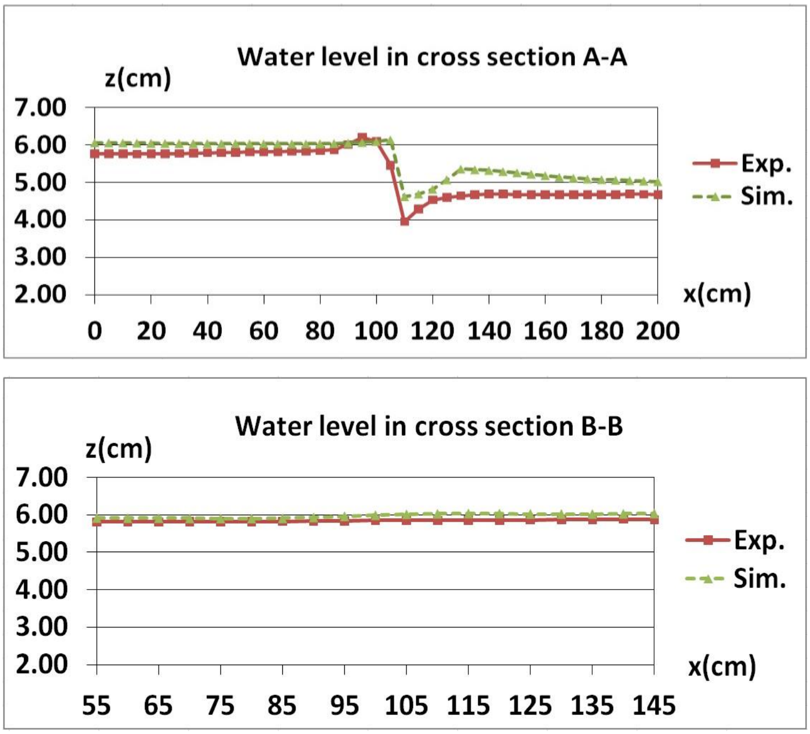

Figure 3.17 Comparison of water level in each cross section (Case 2-4)

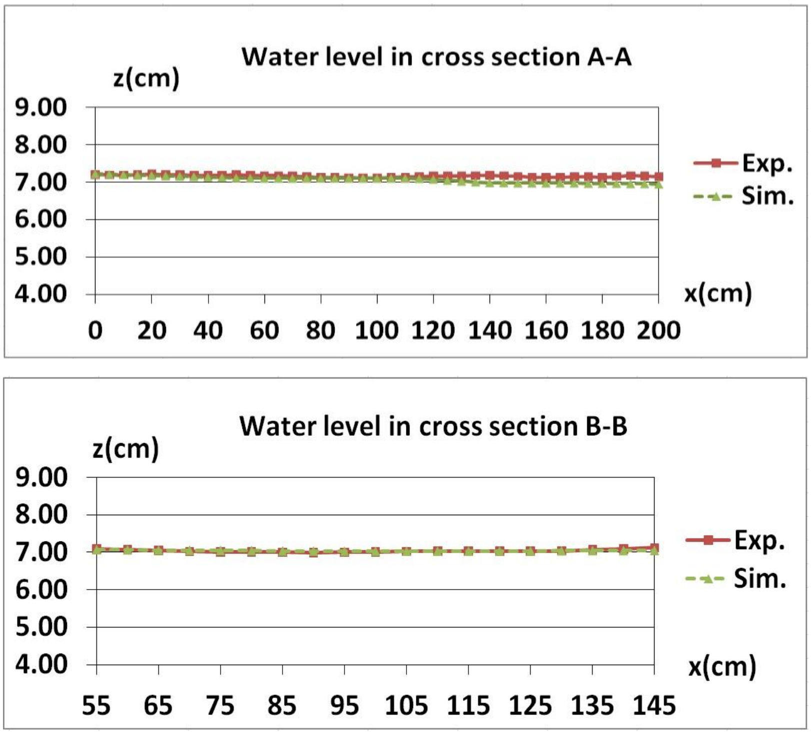

Figure 3.18 Comparison of water level in each cross section (Case 3-1)

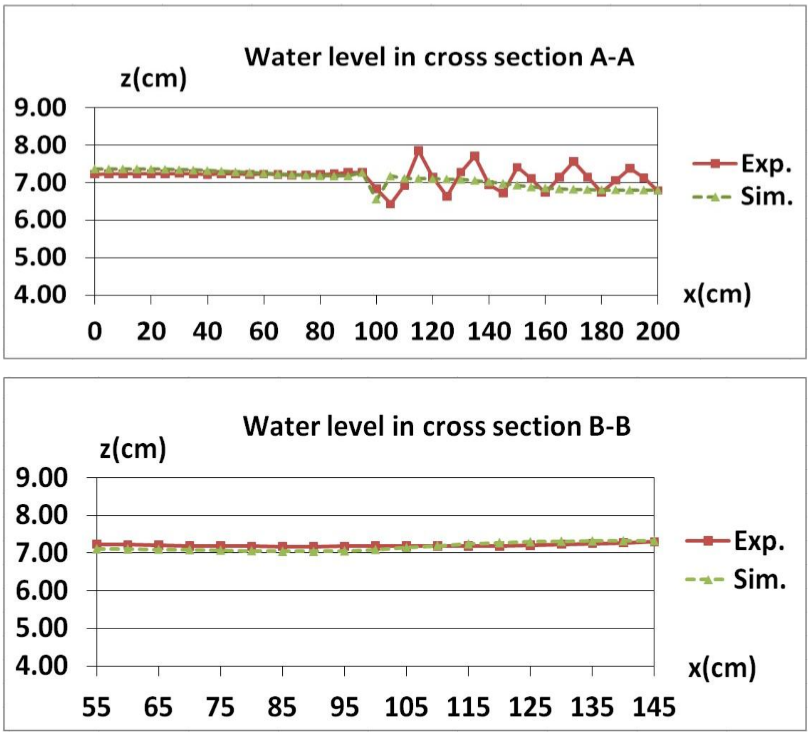

Figure 3.19 Comparison of water level in each cross section (Case 3-2)

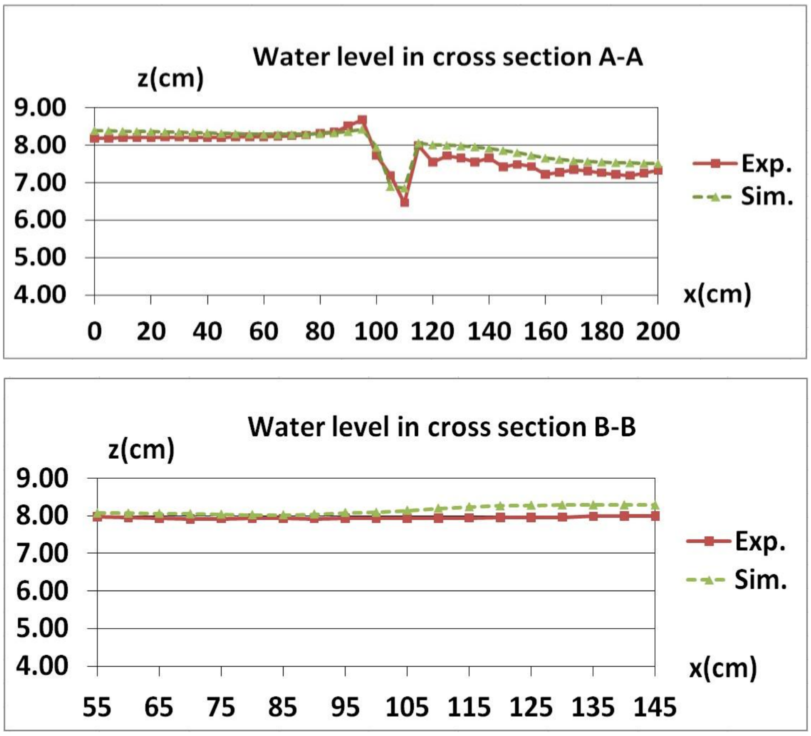

Figure 3.20 Comparison of water level in each cross section (Case 3-3)

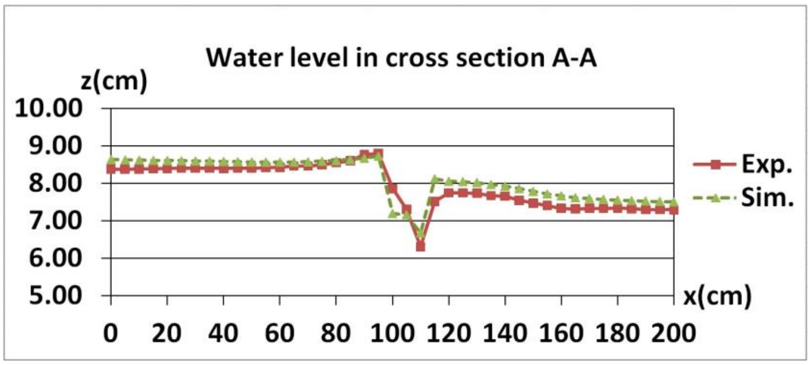

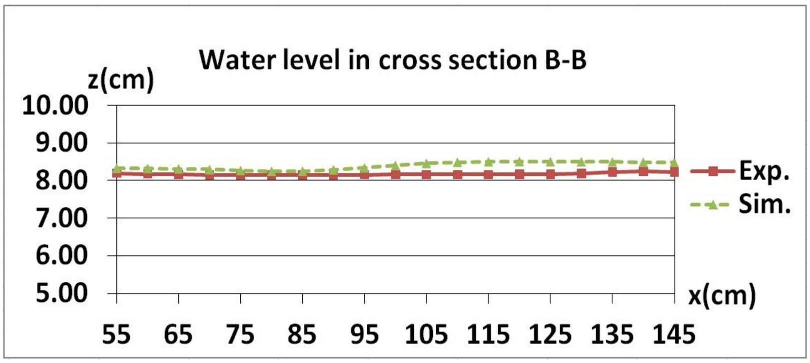

Figure 3.21 Comparison of water level in each cross section (Case 3-4)

From the results of comparison of water level along the cross-section, it is found that numerical results generally have good agreements with the experimental results although the simulation results generally are slightly overestimated than the experimental results.

3.5.2 Comparison of free-surface velocity

Figures 3.22 - 3.27 show the results of the free-surface velocity obtained from the experiments and the simulations. From the numerical results of the free-surface velocity, it is judged that variations of the free-surface velocity are generally reproduced well and have good agreements with the experimental results. And, decreases and increases of the free-surface velocity by the river structures are clearly shown.

Case 1-1

Experiment

Simulation

Case 1-2

Experiment

Simulation

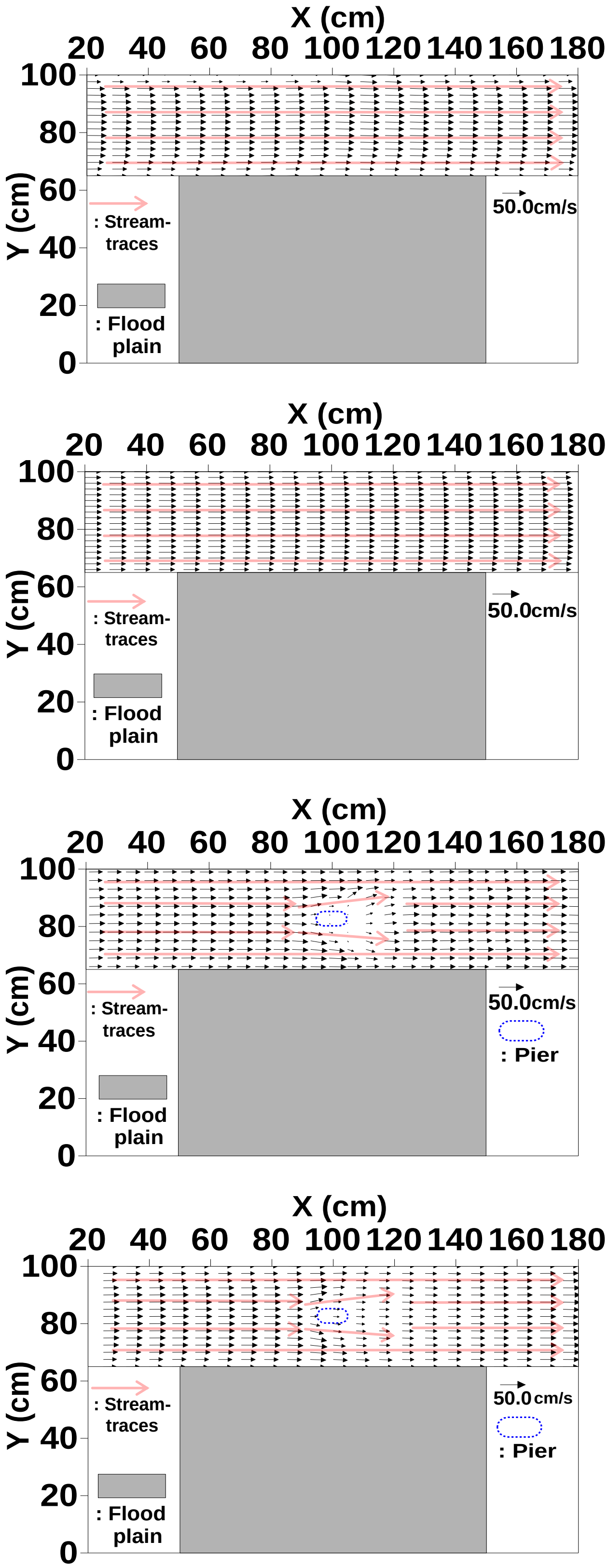

Figure 3.22 Results of water level (Case 1-1&1-2)

Case 1-3

Experiment

Simulation

Case 1-4

Experiment

Simulation

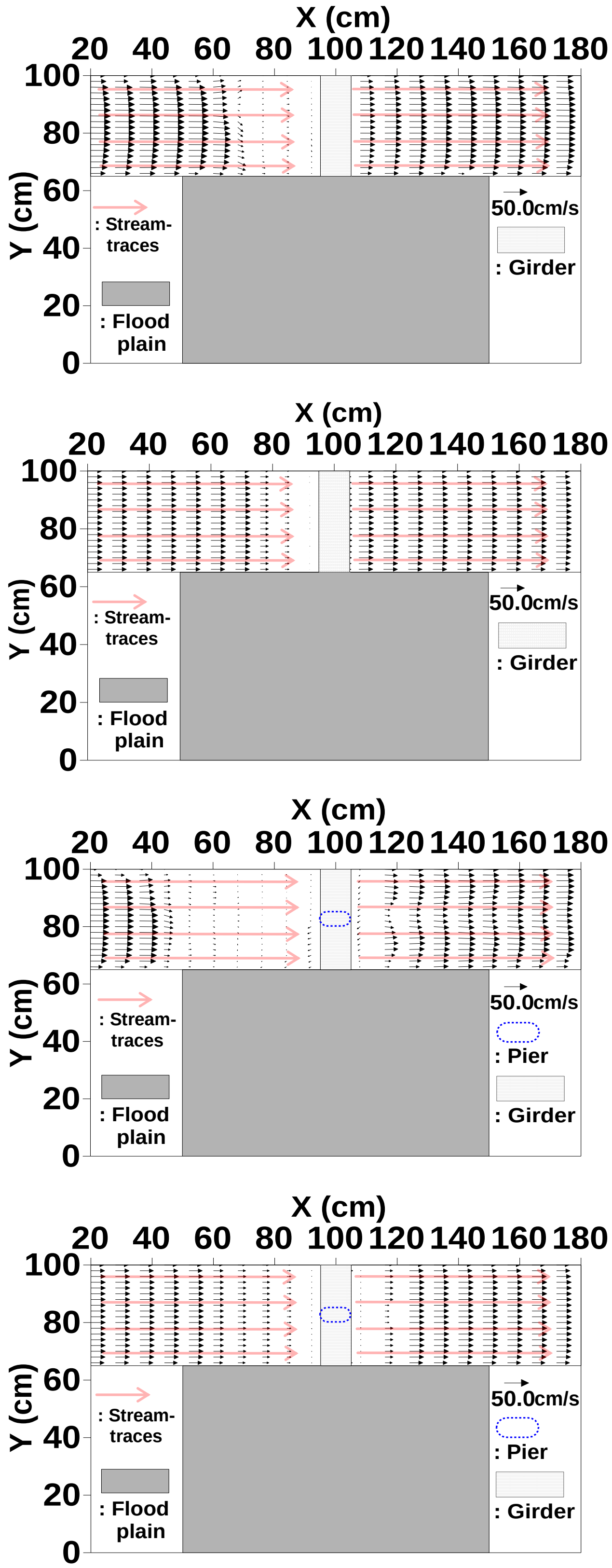

Figure 3.23 Results of water level (Case 1-3&1-4)

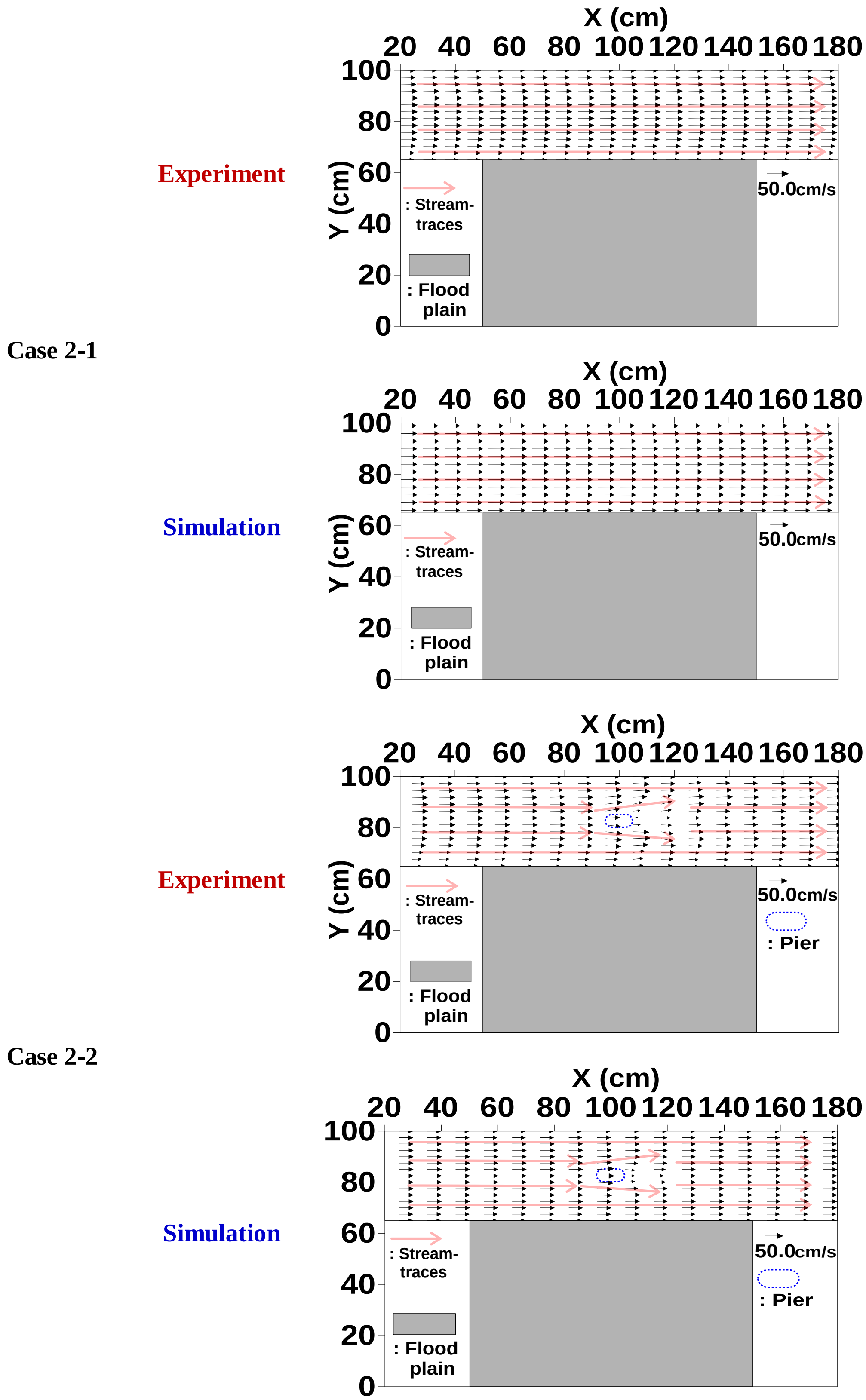

Figure 3.24 Results of water level (Case 2-1&2-2)

Case 2-3

Experiment

Simulation

Case 2-4

Experiment

Simulation

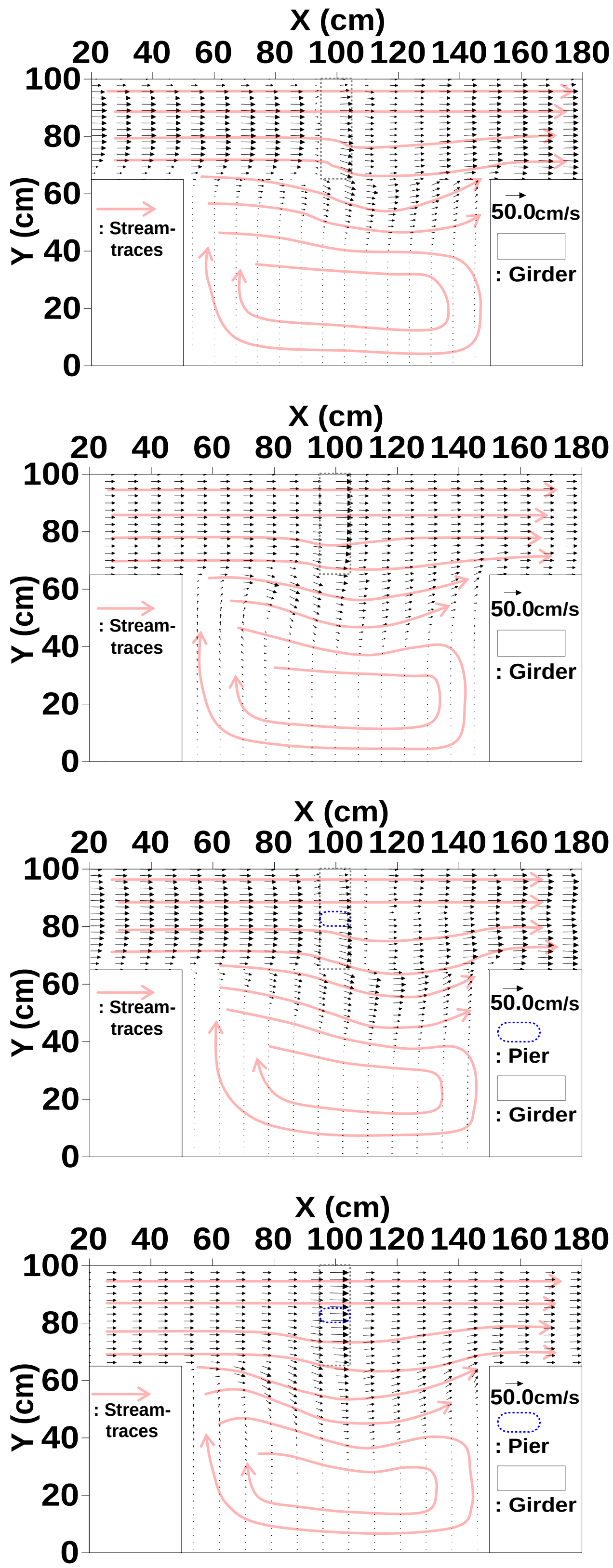

Figure 3.25 Results of water level (Case 2-3&2-4)

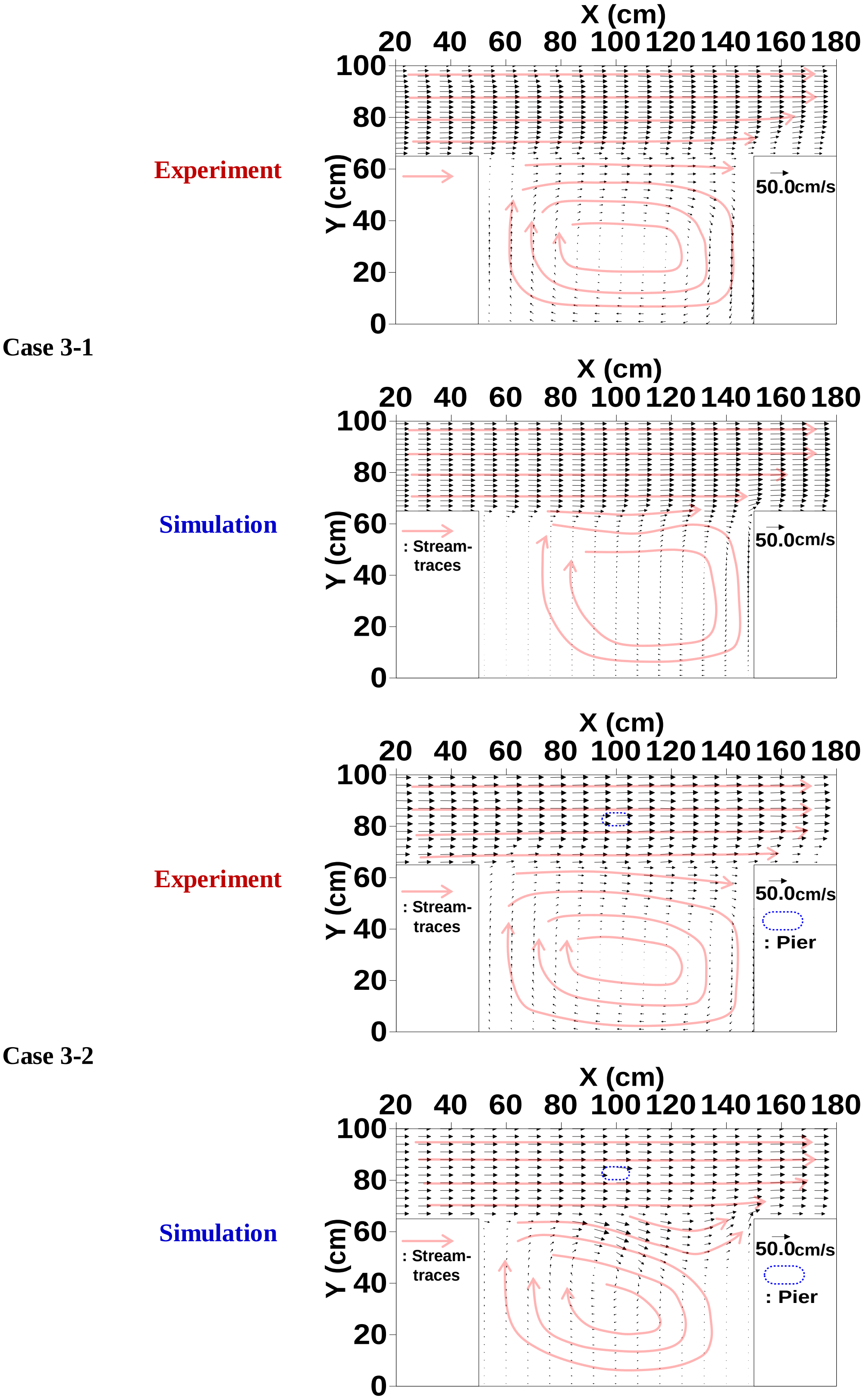

Figure 3.26 Results of water level (Case 3-1&3-2)

Experiment

Case 3-3

Simulation

Experiment

Case 3-4

Simulation

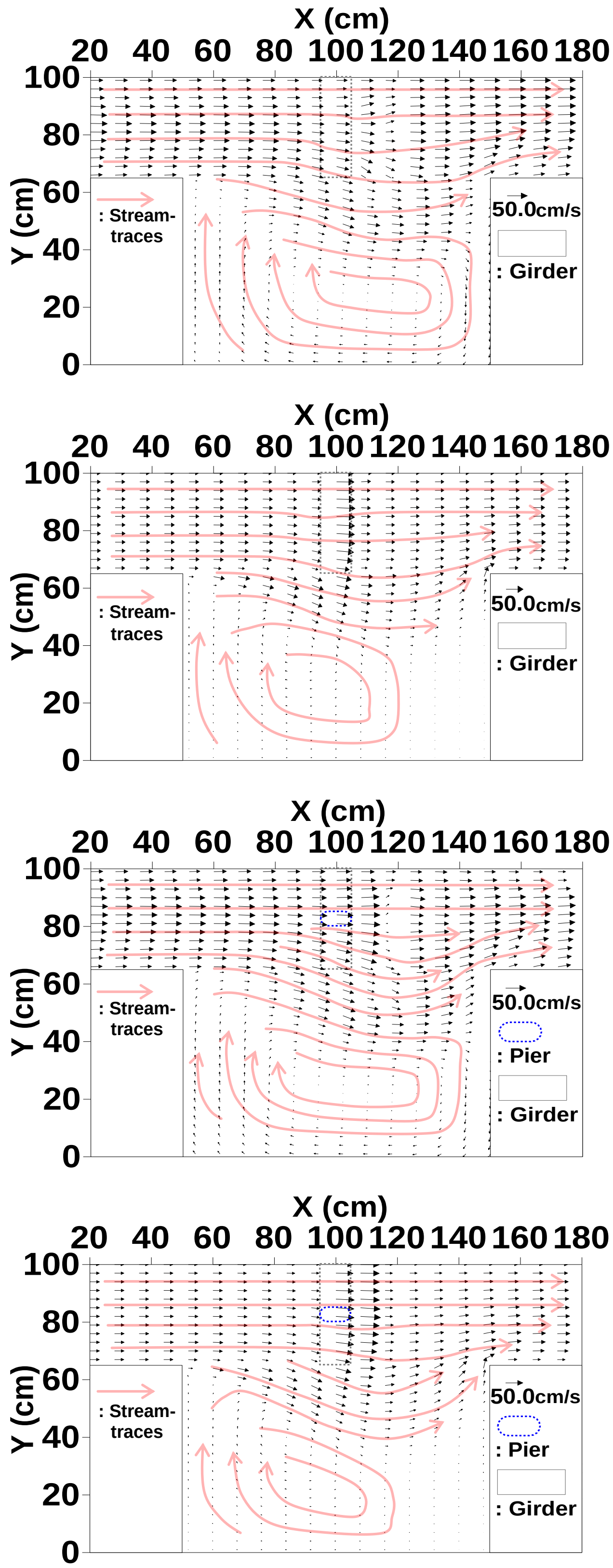

Figure 3.27 Results of water level (Case 3-3&3-4)

From consideration of the effects of river structures, the experimental results were reproduced well by the numerical simulations although the results have some differences. The causes of differences seem to be in the modeling of the turbulence and the construction of mesh in z-direction. The standard k-ε model employed in this study has several problems such as the inability to properly account for the streamline curvature, other body force effects, etc. In order to improve the proposed model, it is judged that consideration of non-linear or LES (Large Eddy Simulation) turbulence model and the construction of fine mesh in z-direction is necessary.

Summary

In this study, a numerical model for the estimation of the inundation flow considering overflow into a floodplain from a river channel was proposed and carried out. The proposed numerical coupling model could treat the inundation flow considering overflow from a river channel with river structures. The numerical results show that proposed numerical coupling model generally can reproduce well this inundation flow although the numerical results have some differences in comparison with the experimental results.

The accurate prediction of the inundation flow is important for establishment of countermeasures against inundation disasters. It is judged that numerical coupling model proposed in the present study can be helpful for estimation of the inundation flow considering overflow into a floodplain and complicated flow within a river channel with river structures.

Chapter 4

Model application

4.1 Introduction

As mentioned in the previous chapters, many disasters of river water flooding have occurred all over the world. In this chapter, the applicability of the proposed numerical coupling model is discussed by applying it to an actual area in Japan damaged by a flood disaster.

4.2 Study area

The study area is A-river basin in Japan. Figure 4.1 and 4.2 show the A-river basin and photo of the urban area around A-river.

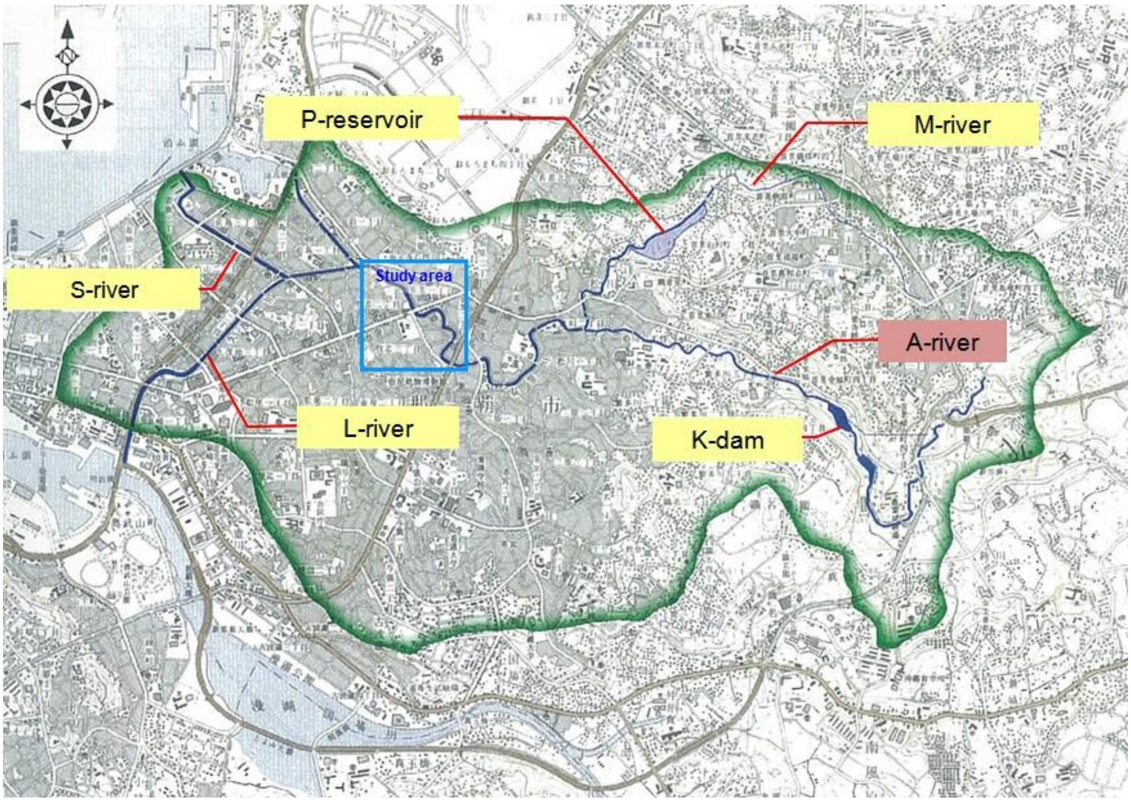

Figure 4.1 Basin of A-river

Figure 4.2 Study area (*Source: Google earth)*

The A-river has channel length 7.0*km*, average discharge 0.56m^3/s and basin area $8.6km^2$. As shown in Figure 4.1, there are four rivers, one reservoir and one dam in A-river basin. The downstream area of the A-river basin is highly urbanized.

4.3 Situations of inundation disaster

In this area, inundation disaster occurred on August 11, 2007. At that time, extreme values of the daily precipitation 427.5mm and the maximum 24 hour precipitation 431.0mm were observed at the N-observatory. Table 4.1 shows the observed extreme value compared with the past records. Figure 4.3 shows the observatories located in this area and the data obtained from the observatories.

Table 4.1 Amount of precipitation at the N-observatory

	Daily precipitation	Max. 24 hour precipitation
Past extreme value	271.7mm (Aug.15, 1952)	256.5mm (Aug.19, 1984)
Extreme value observed on Aug.11, 2007	427.5mm	431.0mm

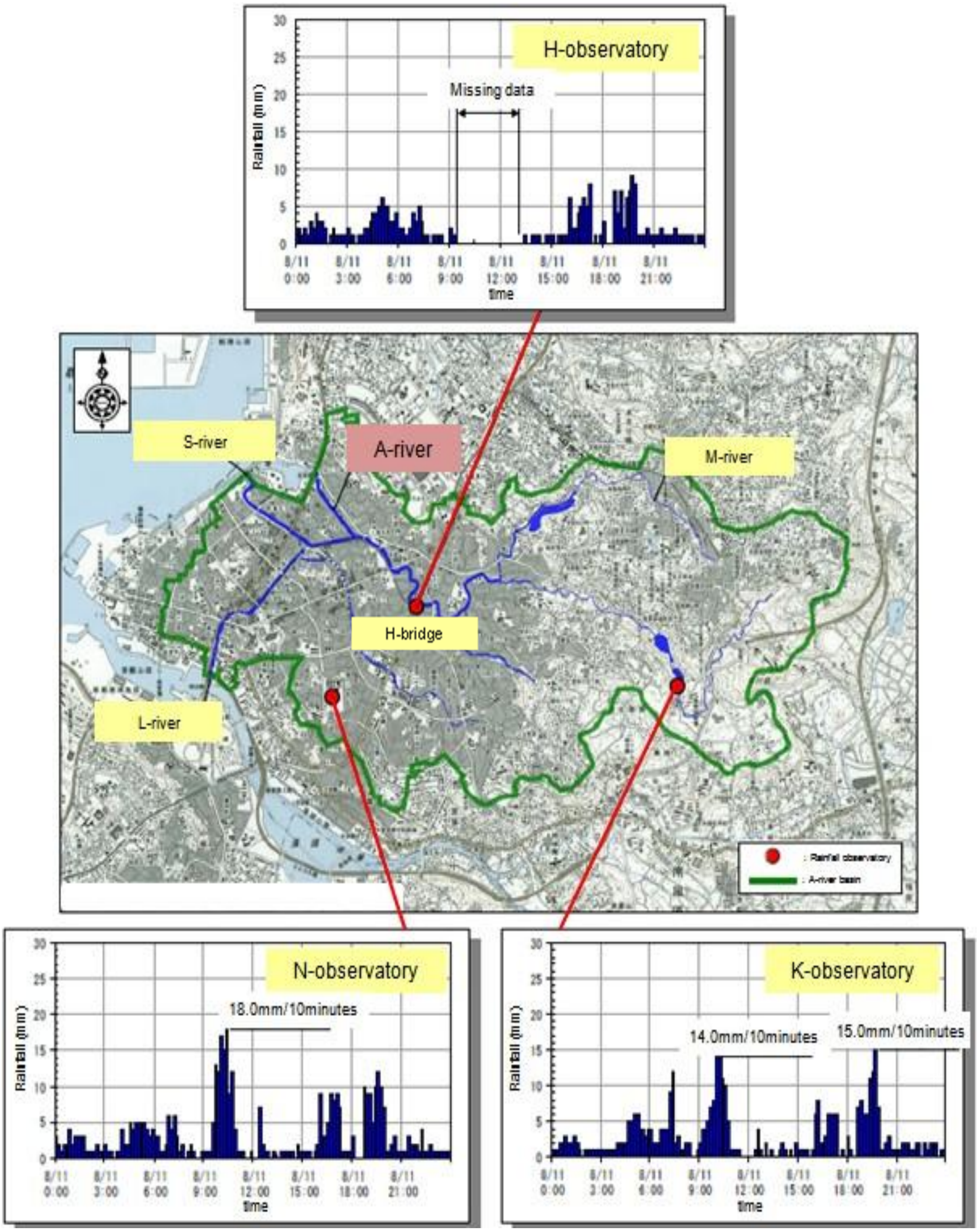

Figure 4.3 10 minute rainfall at observatories in A-river basin

Two inundations occurred in this area. The water stage observed at the H-bridge rose from about 8:00 AM. The maximum water stage reached to NP+5.90m which exceeded HWL by 100cm as shown in Figure 4.4. The overtopping flow from A-river was started around H-bridge. First inundation occurred at the time between 10:30 and 11:30 AM. The inundation depth at a street near the bridge was about 50 ~ 70cm. Hourly precipitations were 33mm/hr at 10:00 and 75mm/hr at 11:00. Second inundation occurred at the time between 19:30 and 20:30 PM. The inundation situation is almost similar to the first inundation. Figure 4.5 shows the situations of flood damages. As shown in the figure, many parts of urban area were inundated and attacked by heavy rainfall in 2007. Especially, regions near the river suffered from large damages by overflow from river channel with heavy rainfall.

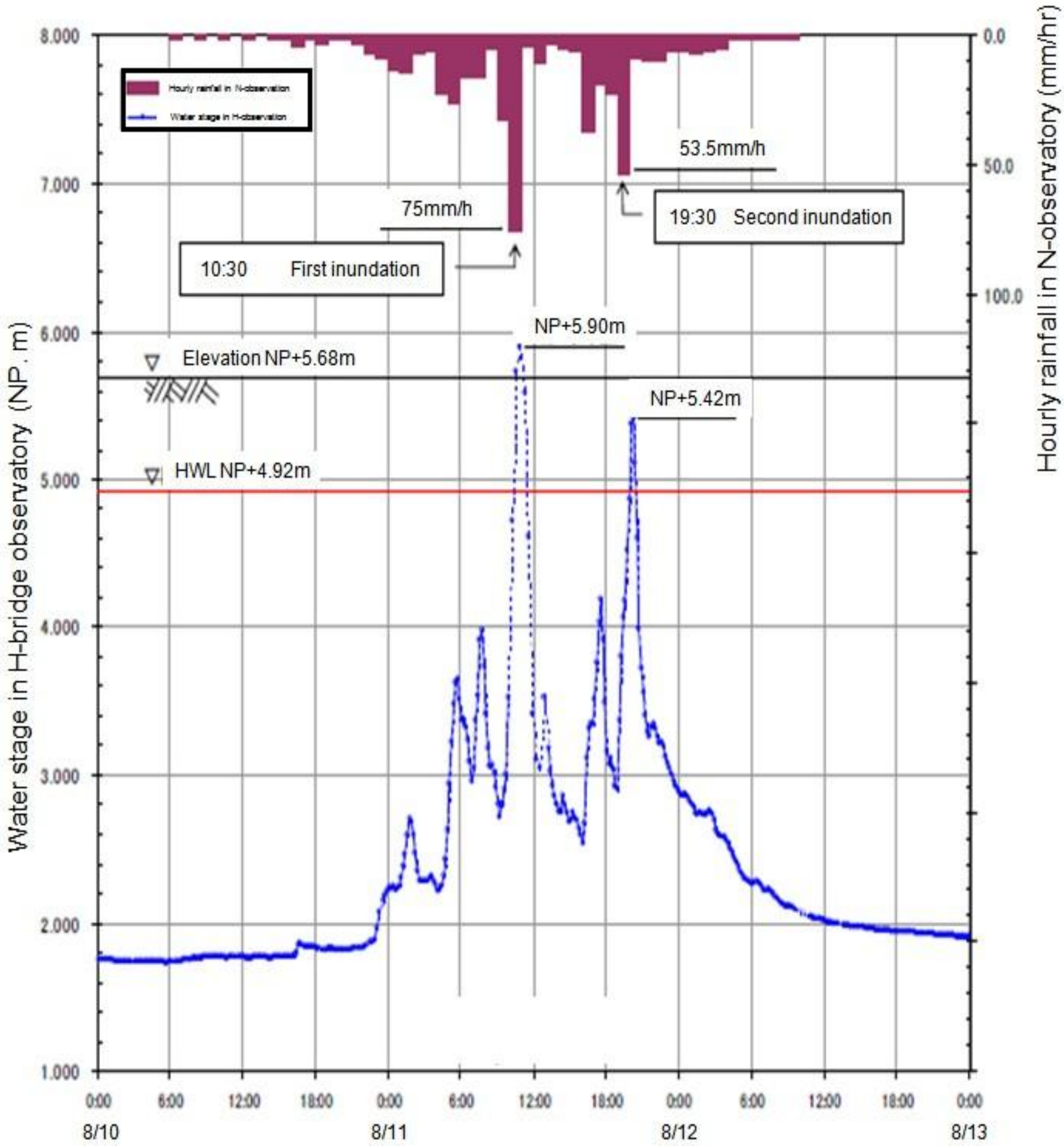

Figure 4.4 Water stage at H-observatory and rainfall at N-observatory

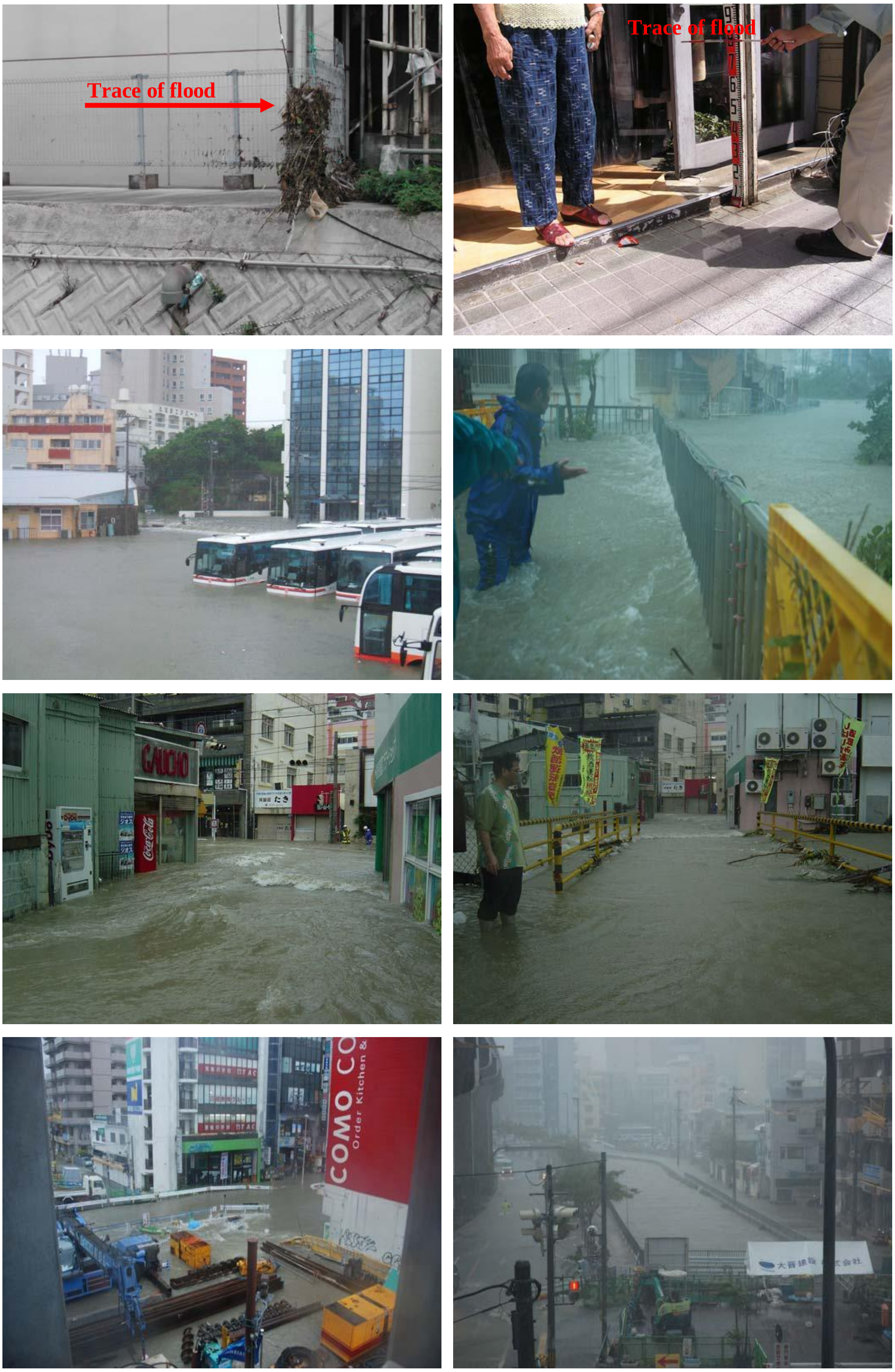

Figure 4.5 Photos of flood damages (Aug. 11, 2007)

Estimated inundation area based on hearing investigation is shown in Figure 4.6. In the figure, the region expressed by red line is inundation area due to insufficient drainage capacity. The yellow arrows show the overflow direction. As seen in the figure, it is found that overflow from the river spread into the damaged area and the region near the river with inundation due to insufficient drainage capacity has severer damage.

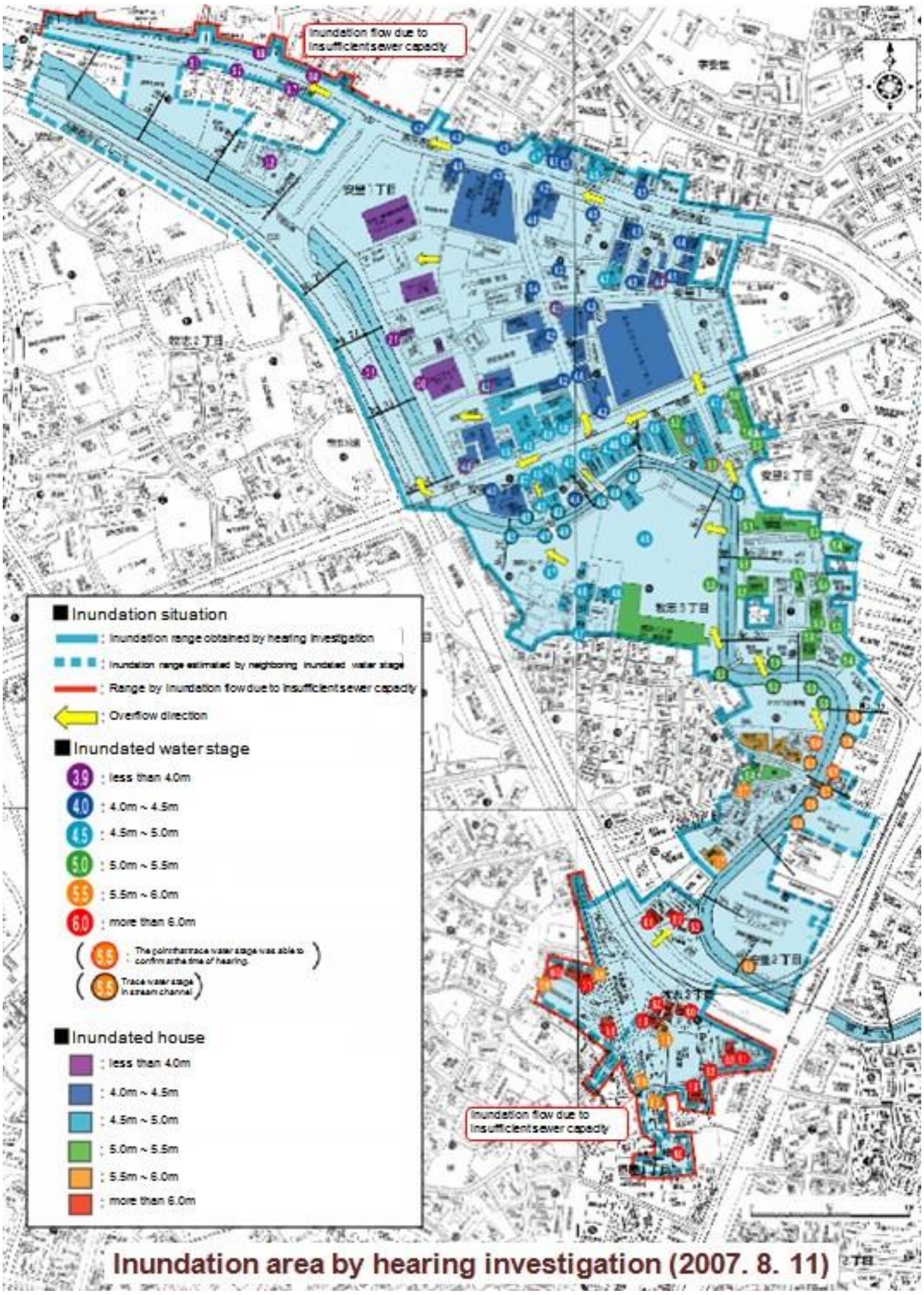

Figure 4.6 Area inundated by flood disaster

4.4 Computational domain

The numerical coupling model proposed in this study is applied to an actual urban area and its applicability is discussed. The computational mesh consists of 2D mesh for urban area and 3D mesh for river channel. And, overlapping meshes are formed between the 2D and the 3D domains. The computational meshes are shown in Figure 4.7. Total mesh numbers of the 2D and the 3D domains are 7328 and 54043, respectively.

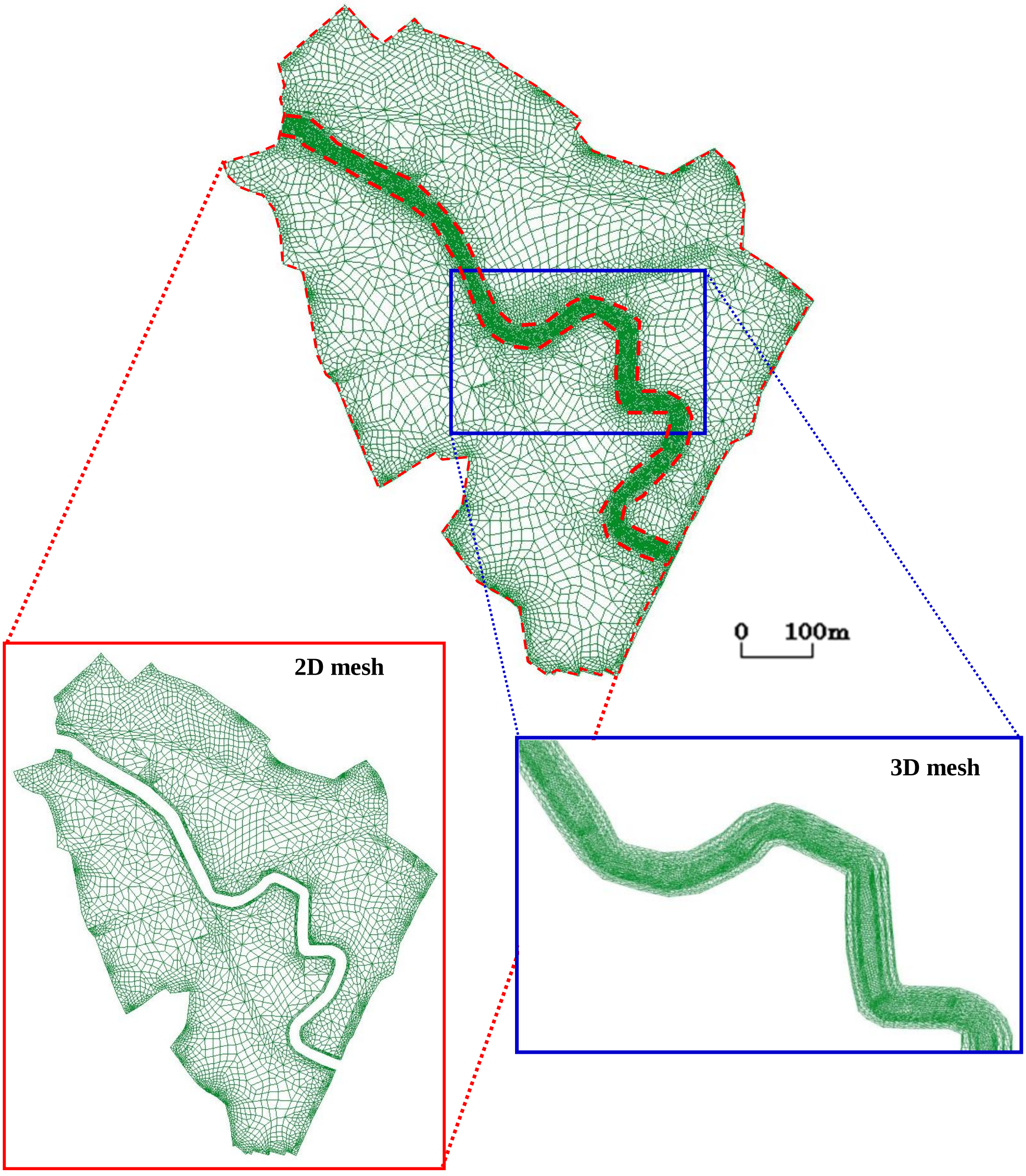

Figure 4.7 Computational meshes

In this area, the inundation disaster occurred during repairing work of river channel. Thus, effects of structures are considered in this simulation. The structures are actually H-shaped steel, but those are considered as the structure horizontally occupying one mesh Figures 4.8 shows the locations of structures considered in this study.

not considering repairing work

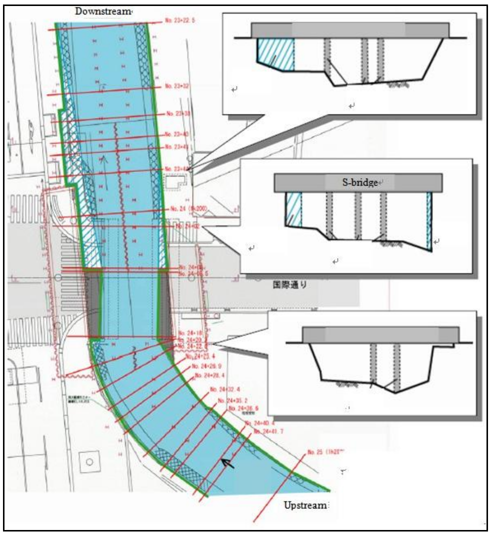

considering repairing work

Figure 4.8 Conditions with and without consideration of repairing work

4.5 Computational conditions

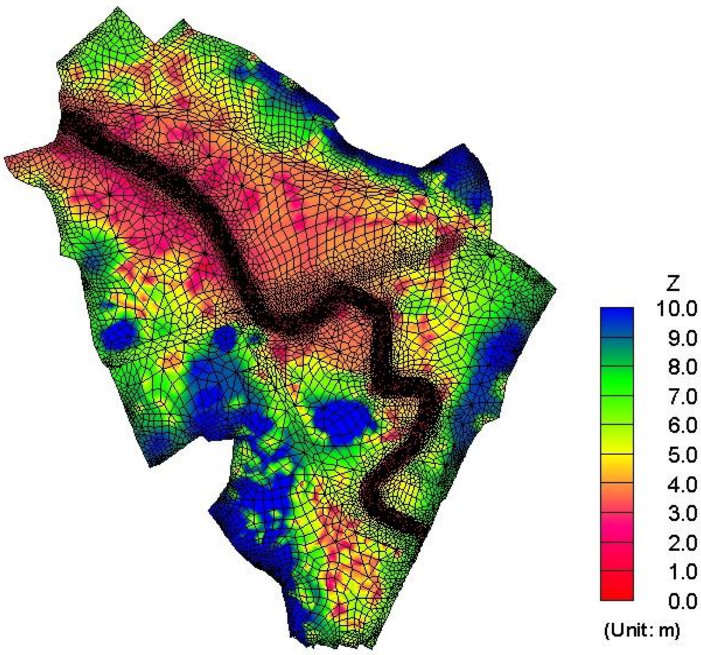

Figure 4.9 Ground elevation

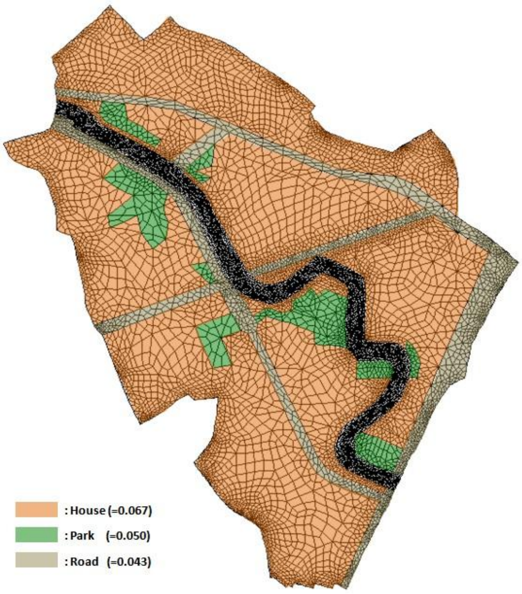

Figure 4.10 Classification of land use

Figure 4.9 and 4.10 show the ground elevation and classification of land use used in this study. In the domain of urban area, Manning's coefficient uses road (=0.043), house (=0.067) and park (=0.050). Figure 4.11 shows the locations of observatories for the boundary conditions. Figure 4.12 shows inflow discharge hydrograph at the H-observatory applied as inlet boundary condition. And, Figures 4.13 shows the water stage observed at the M-bridge for downstream boundary condition. Actually the M-bridge is not located at the downstream end of this study area, but the downstream boundary condition is approximated by the water stage hydrograph at the M-bridge because it is the closest observatory.

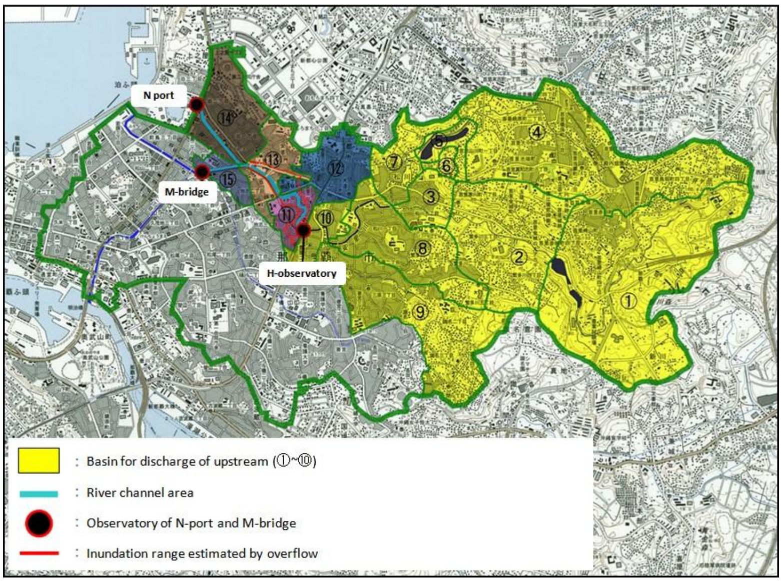

Figure 4.11 Locations of observatories for boundary conditions

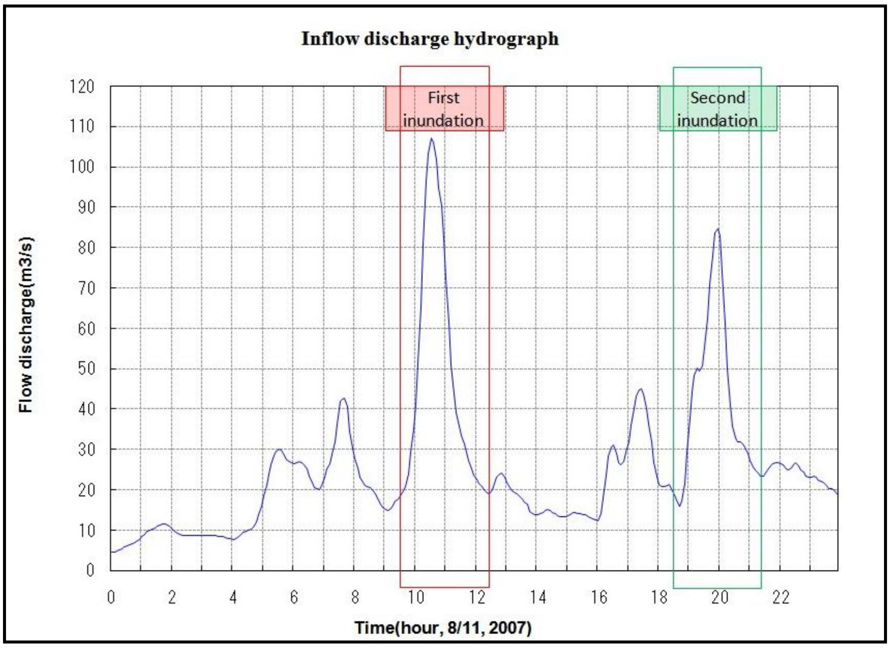

Figure 4.12 Discharge hydrograph observed at H-observatory

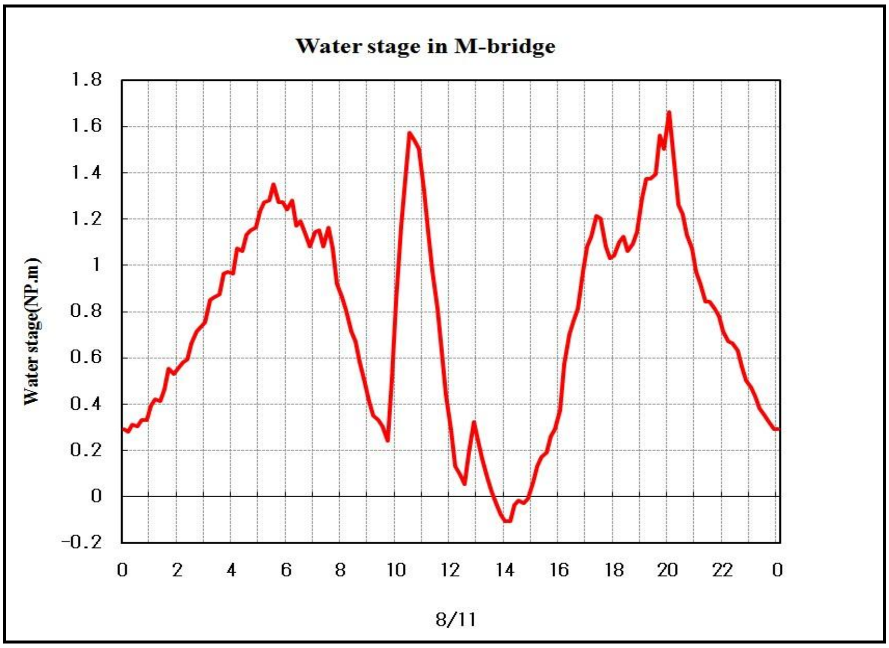

Figure 4.13 Water stage for downstream condition

In this study, in order to reproduce the inundation areas by insufficient drainage capacity indicated in Figure 4.6, the inflow discharges are given directly to the corresponding mesh. Figure 4.14 shows the regions of inundation damage by insufficient drainage capacity and the locations of mesh where inflow discharge are given. And, Figure 4.15 shows the inflow discharge hydrograph at region ① and ②.

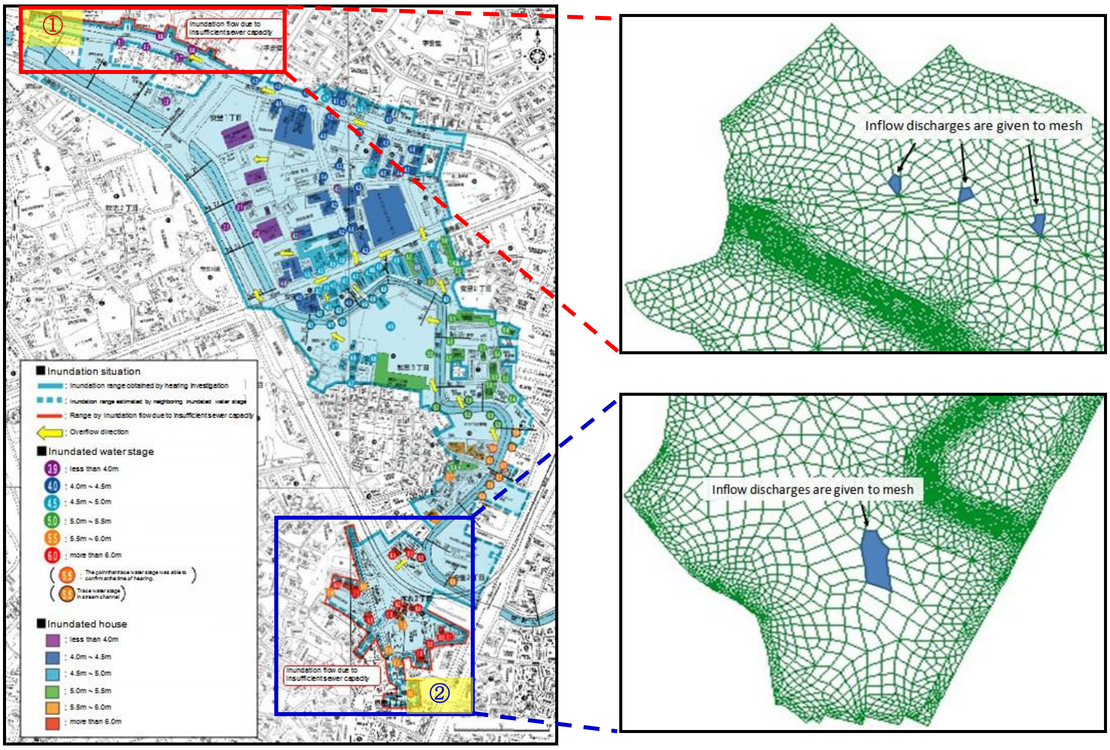

Figure 4.14 Regions of inundation by insufficient drainage capacity

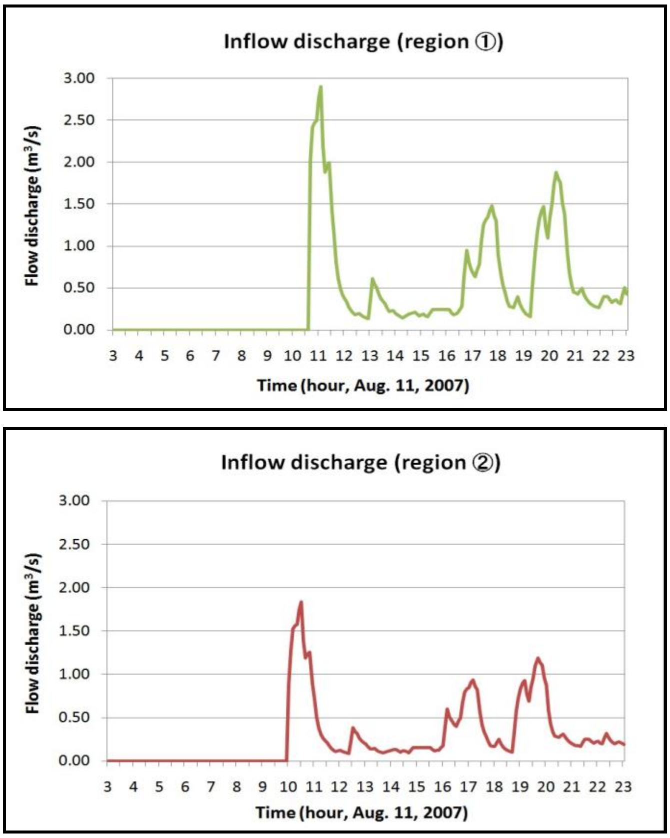

Figure 4.15 Flow discharges for inundation by insufficient drainage capacity

4.6 Results and analyses

In this study area, there is a precedent simulation result conducted by an integrated model of 1D and 2D simulation. Here, the results of present research are compared with the previous numerical simulations. Figure 4.16 shows the results of the previous numerical simulation. Figures 4.17 - 4.20 show the results of numerical simulation with and without consideration of repairing work in the river channel.

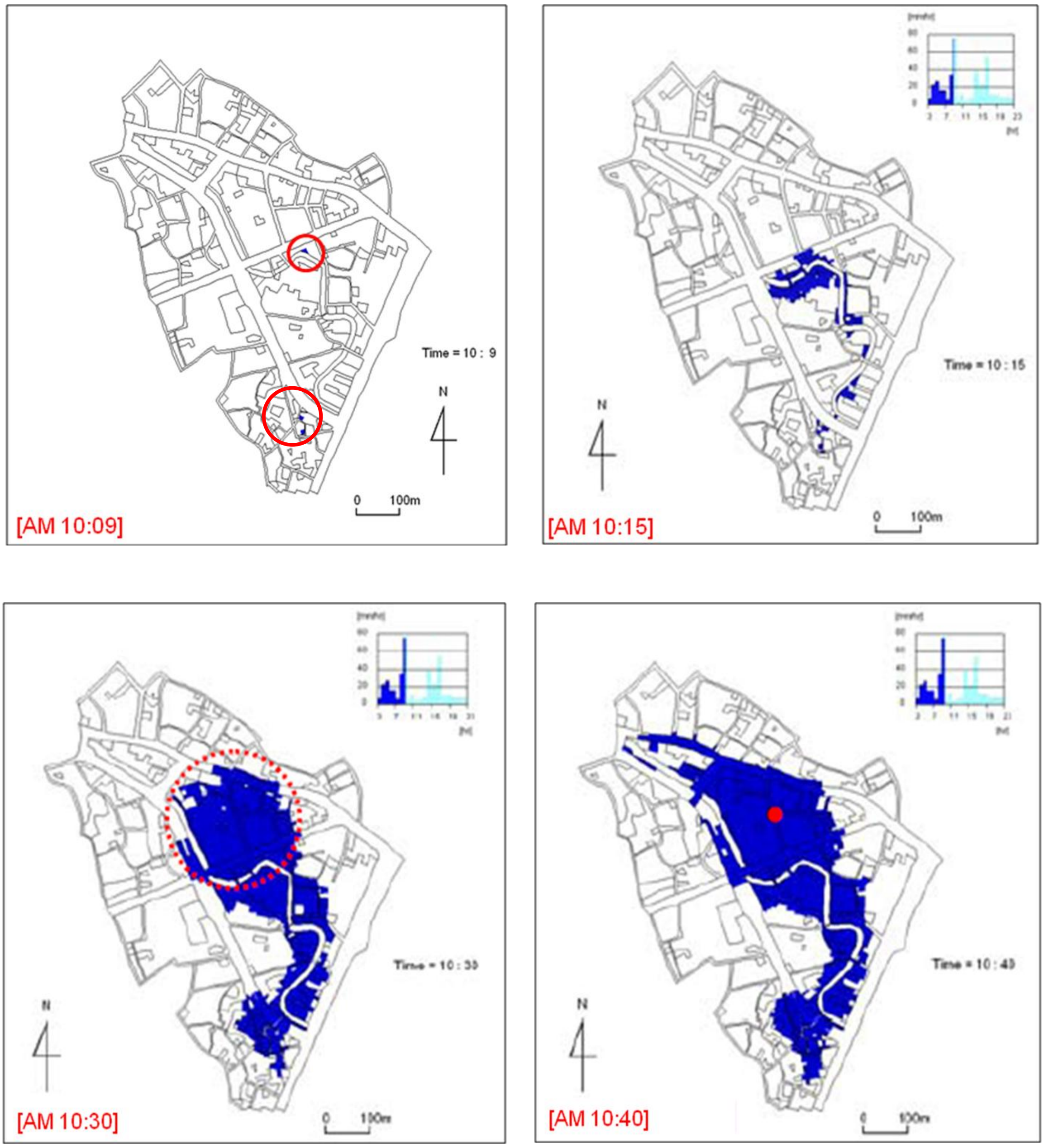

Figure 4.16 Previous numerical simulations

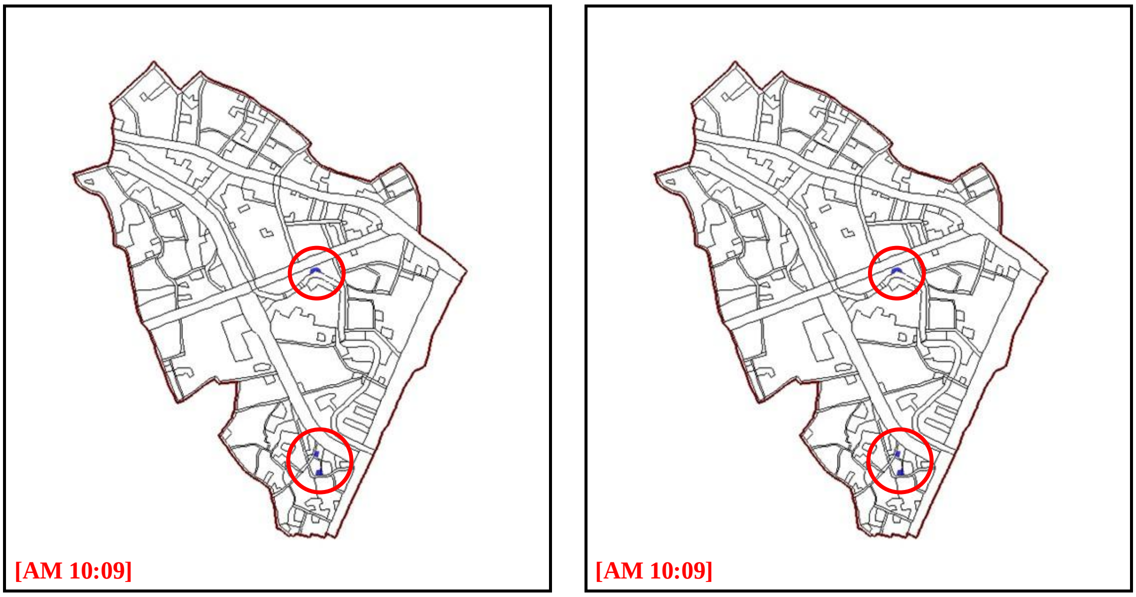

not considering repairing work considering repairing work

Figure 4.17 Comparison of results with and without consideration of repairing work (AM 10:09)

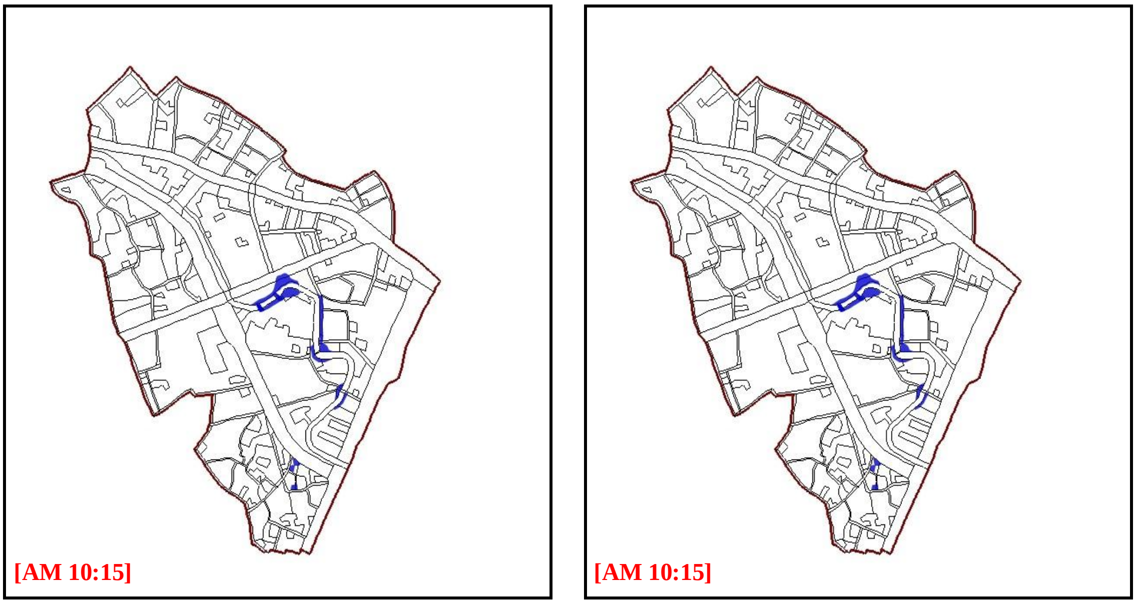

not considering repairing work considering repairing work

Figure 4.18 Comparison of results with and without consideration of repairing work (AM 10:15)

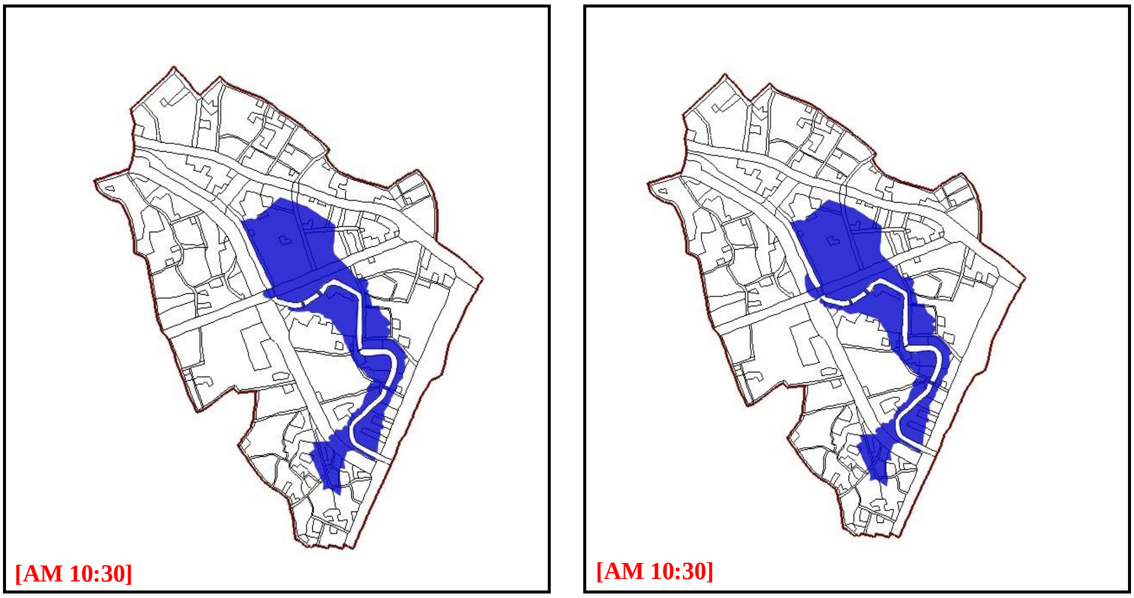

not considering repairing work   considering repairing work

Figure 4.19 Comparison of results with and without consideration of repairing work (AM 10:30)

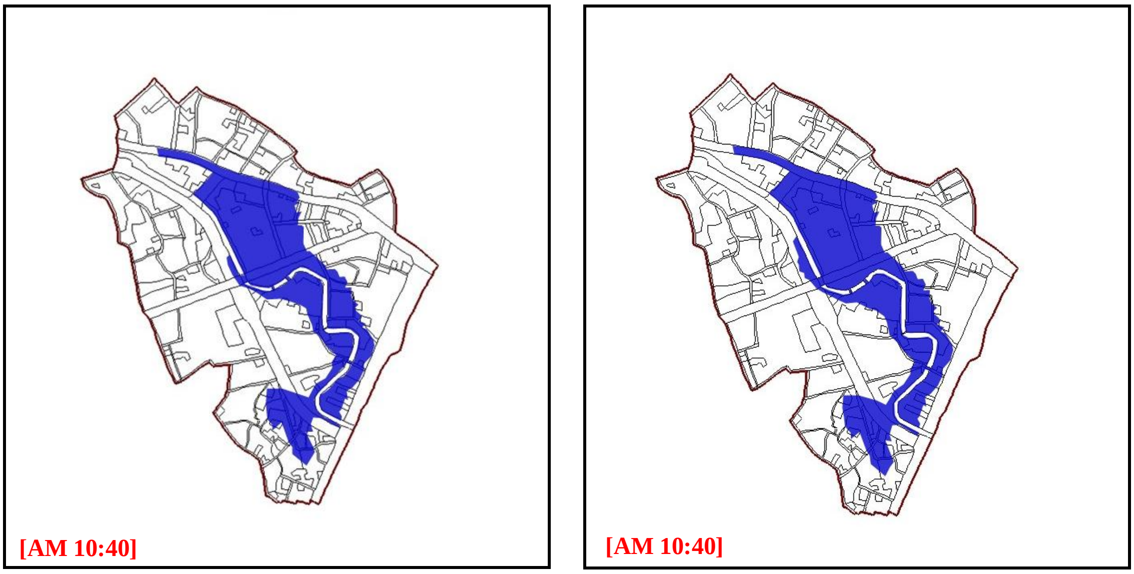

not considering repairing work   considering repairing work

Figure 4.20 Comparison of results with and without consideration of repairing work (AM 10:40)

As shown in the results, the appearance of propagation of inundation flow is similar to the previous results although inundation area showed some difference. The reason why computed inundation area of this study is different from that of the previous study is that the boundary condition at the downstream end of this study is different from that of the previous simulation. From the comparison of results with and without consideration of repairing work, it is found that starting point of overflow is the same in both results. And, it is judged that the effect of water level rise by hydraulic structures is not large.

Summary

In this chapter, the applicability of the proposed numerical coupling model was discussed through the application to an actual area. The results obtained from the simulation have good agreements in the viewpoint of flood propagation. It is judged that the proposed numerical coupling model can represent inundation disaster in actual area with appropriate accuracy. This will be helpful to establish countermeasure against inundation disasters caused by effects of hydraulic structures in river channel.

Chapter 5

Conclusions and Recommendations

In this study, in order to represent the inundation flow considering overflow from a river channel by water level rise due to effect of hydraulic structures, a numerical model was developed and verified with laboratory experimental results. For the modeling of the flow in a river channel, three-dimensional model with free-surface was proposed. The laboratory experiments were also carried out for verification of the numerical model. And then, proposed three-dimensional model was coupled with two-dimensional horizontal model for efficient calculation of the domain including a river channel and urban area. The simulated results were compared with those obtained from the hydraulic experiments. After verification of the developed numerical model, it was applied to an actual area for investigation of applicability of the model. The results obtained from the numerical simulation were compared with previous simulation. Consequently, it is found that the proposed 2D-3D coupling model is very effective to estimate overflow discharge and inundation disasters due to water level rise of the river channel.

5.1 Conclusions

The conclusions of this study are summarized as follows.

Flood flow analysis

A three-dimensional numerical model with free-surface was presented to represent the complicated flow in a river channel. The VOF (Volume of Fluid) method with CICSAM (Compressed Interface Capturing Scheme for Arbitrary Meshes) scheme was employed to be applied to discretization with unstructured meshes. For turbulence closure, the widely used standard k-ε model was employed. The proposed numerical model was applied to simple area with different hydraulic structures. For verification of the numerical model, laboratory experiments were conducted in the fixed bed condition. The simulated results of flood flow were in good agreement with the experimental results. And, the proposed numerical model represented well the water level rise due to effects of hydraulic structures. Therefore, the flood flow with free-surface can be calculated by the proposed three-dimensional numerical model.

Inundation flow analysis

A two-dimensional horizontal numerical model of inundation flow was presented with the depth-averaged equation. The two-dimensional model was coupled with the developed three-dimensional numerical model. A complicated flow around river structure should be considered by three-dimensional calculation with turbulence model. But, in order to calculate the inundation flow, conducting three-dimensional calculation on whole domain with a river channel and urban area is not effective from the viewpoint of computational time and effort. Thus, coupling of three-dimensional model with free-surface and two-dimensional horizontal model was considered in this chapter. The simulation was carried out on the unstructured mesh and used a simultaneous grid method. In this method, each domain has overlapping meshes and the computed values in this overlapping region are exchanged as boundary condition of each model. The solutions obtained from three-dimensional calculation were given as depth-averaged value in boundary of two-dimensional calculation. For verification of the proposed numerical model, laboratory experiments were carried out. The experiments were conducted on the domain including a river channel and a floodplain with three different flow discharge. The flow discharges were considered for the cases that overflow occurs or not. The hydraulic structures such as pier and girder were used to estimate the effects of hydraulic structures in a river channel. The simulated results of inundation flow are in good agreement with the experimental results. Also, inundation flow into floodplain considering the effects of hydraulic structures were reproduced well. Therefore, it is judged that the proposed model can predict the characteristics of inundation flow with complicated flow in a river channel.

Model application

In order to estimate the applicability of the proposed 2D-3D numerical coupling model, the model was applied to an actual area located in Japan. In the study area, inundation disaster by river water flooding occurred without levee failure. And, the repairing work in a river channel was conducted when the inundation disaster occurred. Thus, this region was selected as study area. In this area, the observed extreme daily and maximum 24 hour precipitation during the flood period were 427.5mm and 431.0mm, respectively. The inundation disaster started with overflow around river structures. For the application of numerical model, data of the study area were investigated and used as computational conditions. 3D mesh for river channel and 2D mesh for urban area were constructed under the unstructured mesh. In order to consider the effect of repairing work of river structures, the structures were considered in 3D mesh. The proposed 2D-3D numerical coupling model was applied to the study are using the existing data though a little different boundary condition. The simulated results were compared with existing data. The simulated results showed that propagation of inundation flow is in good agreements with existing data, but inundation area had somewhat different. However, it is judged that the proposed 2D-3D numerical model can be used to estimate inundation flow disasters.

From the results so far obtained, the 2D-3D numerical coupling model generally could predict well the inundation flow considering overflow from a river channel with hydraulic structures. It is clear that the proposed model can be used to predict the inundation flow and to support the establishment of countermeasures against inundation disasters. And, it is expected that this model would be helpful to reduce the inundation flow damages even after occurrence of inundation flow disasters.

5.2 Recommendations for future researches

Future researches are required to improve the performance of the model. The recommendations for future works are discussed here.

(a) In this study, three-dimensional model with free-surface was used for calculation of river channel. The hexahedral meshes only were used in this study. In order to calculate domains with more complex geometries, it is necessary to verify the applicability to other mesh systems.

(b) The standard k-ε model used in this study has several problems such as the inability to properly account for the streamline curvature, rotational strains and other body-force effects and the neglect of the non-local and historical effects of the Reynolds stress anisotropies. To solve those problems, it is necessary to adopt non-linear k-ε model or LES (Large Eddy Simulation) model. The proposed model should be verified through comparison with the other turbulence model.

(c) The numerical simulations used in this study require much computational time and effort. As mentioned in this study, the reason why 2D and 3D models are coupled is to reduce the computational time. Thus, in order to improve ability of calculator, it is necessary to consider the method such as the parallel computing.

(d) In this study, fixed bed was considered for all numerical simulations, but actual river has movable bed. To understand perfectly real phenomena for river flow, the consideration of movable bed is necessary.

(e) In this study, the simulations of inundation by river water flooding without levee failure were carried out. But, actually, inundations by river water flooding with levee failure frequently happen. Thus, conducting that kind of study is also necessary to understand comprehensive inundation by river water flooding.

(f) In this study, an embankment was not considered as computational condition. In order to understand the overtopping flow in actual river, it is necessary to consider the effects of embankment. In those studies, understanding the inflow discharge into urban area by the overtopping flow is very important.

(g) In this study, the proposed numerical model has been verified with limited field and laboratory experimental data. More verifications and applications are necessary for improvement of the model.

References:

Akiyama, J. and Shige-eda, M.: Predictions of overflow discharges by a dynamic inundation model and analysis of an urban inundation process due to dike breach, *Journals of the Japan Society of Civil Engineers*, Vol.63, No. 3, pp.224-237, 2007 (in Japanese).

Akiyama, J., Shige-eda, M. and Tsuzaki, S.: Estimation of overflow discharges by simultaneous analysis of flood and inundation flows in a meandering channel, *Annual Journal of Hydraulic Engineering, JSCE*, Vol. 52, pp.823-828, 2008 (in Japanese).

Ashgriz, N. and Poo, J. Y.: Flux line-segment model for advection and interface reconstruction, *Journal of Computational Physics*, Vol. 39, pp.449-468, 1991.

Caleffi, V., Valiani, A. and Zanni, A.: Finite volume method for simulating extreme flood events in natural channels, *Journal of Hydraulic Research*, Vol. 41, No. 2, pp.167-177, 2003.

Chorin, A. J.: Flame advection and propagation algorithms, *Journal of Computational Physics*, Vol. 35, pp.1-11, 1980.

Clarke, A. P. and Issa, R. I.: A numerical model of slug flow in vertical tubes, *Internal report, Department of Mechanical Engineering*, Imperial College, London, 1995.

Connell, R. J., Painter D. J. and Beffa, C.: Two-dimensional flood plain flow Ⅱ: Model validation, *Journal of Hydrological Engineering*, ASCE, Vol. 6, No. 5, pp.406-415, 2001.

Daly, B. J.: A technique for including surface tension effects in hydrodynamic calculations, *Journal of Computational Physics*, Vol. 4, pp.97-117, 1969.

Darwish, M. S.: A new high-resolution scheme based on the normalized variable formulation, *Numerical Heat Transfer, Part B*, Vol. 24, pp.353-371, 1993.

Dervieux, A. and Thomasset, F.: A finite element method for the simulation of a Rayleigh-Taylor instability, *IRIA-LABORIA report*, F-78150 Le Chesnay.

Farmer, J., Martinelli, L. and Jameson, A.: Fast multigrid method for solving incompressible hydrodynamic problems with free surfaces, *AIAA Journal*, Vol. 32, pp.1175-1182, 1994.

Ferziger, J.H and Peric, M.: Computational Methods for Fluid Dynamics, *3rd rev. ed., Springer-Verlag.*, 2002.

Fujima, K., Masamura, K. and Goto, C.: Development of the 2D/3D hybrid model for Tsunami numerical simulation, *Coastal Engineering Journal*, Vol. 44, No. 4, pp.373-397, 2002.

Fujita, I., Muste, M. and Kruger, A.: Large-scale particle image velocimetry for flow analysis in hydraulic engineering applications, *Journal of Hydraulic Research*, Vol. 36, No.3, pp.397-414,1998.

Gaskell, P. H. and Lau, A. K. C.: Curvature-compensated convective transport: SMART, a new boundedness-preserving transport algorithm, *International Journal for Numerical Methods in Fluids*, Vol. 8, pp.617-641,1988.

Ghobadian, A.: Development of a method for numerical simulation of flows with moving interfaces, *National Power report TEC/L/0077/M91*,1991.

Glimm, J., McBryan, O., Menikoff, R. and Sharp, D. H.: Front tracking applied to Rayleigh-Taylor instability, *SIAM Journal on Scientific and Statistical Computing*, Vol. 7(1), pp.230-251,1986.

Han, K. Y., Lee, J. T. and Park, J. H.: Flood inundation analysis resulting from levee-break, *Journal of Hydraulic Research*, Vol. 36, No. 5, pp.747-759, 1998.

Hirt, C. W. and Nichols, B. D.: Volume of fluid (VOF) method for dynamics of free-boundaries, *Journal of Computational Physics*, Vol. 39, pp.201-225, 1981.

Hyman. J. M.: Numerical methods for tracking interfaces, *Physica*, Vol. 12D, pp.396-407, 1984.

Inoue, K., Kawaike, K. and Hayashi, H.: Numerical simulation models on inundation flow in ruban area, *Journal of Hydroscience and Hydraulic Engineering*, JSCE, Vol. 18, No.1, pp.119-126, 2000.

Issa, R. I.: Solution of the implicitly discretised fluid flow equations by operator-splitting, *Journal of Computational Physics*, Vol. 62(1), pp.40-65, 1986.

Jasak, H.: Error analysis and estimation for the finite volume method with applications to fluid flows, *Ph.D. Thesis*, University of London, 1996.

Jasak, H., Weller, H. C., Issa, R. I. and Gosman, A. D.: High resolution NVD differencing scheme for arbitrarily unstructured meshes, 1996.

Kamrath, P., Disse, M., Hammer, M. and Kongeter, J.: Assessment of discharge through a dike breach and simulation of flood wave propagation, *International Society for the Prevention and Mitigation of Natural Hazards*, Vol. 38, No. 1/2, pp.63-78, 2006.

Kawaike, K.: Development of inundation analysis method in urban area and its application, *Ph.D. Thesis*, Kyoto University, 2001 (in Japanese).

Kawaike, K., Inoue, K., Hayashi, H. and Toda, K.: Development of inundation analysis model in urban area, *Journals of the Japan Society of Civil Engineers*, No. 698, pp.1-10, 2002 (in Japanese).

Kawaike, K., Inoue, K., Toda, K. and Noguchi, M.: Inundation flow analysis due to heavy rainfall in low-lying river basin, *Journal of Hydroscience and Hydraulic Engineering*, Vol. 22, No. 1, pp.1-14, 2004.

Kimura, I. and Hosoda, T.: A non-linear k-ε model with realizability for prediction of flows around bluff bodies, *International Journal for Numerical Methods in Fluids*, Vol. 43, pp.818-837, 2003.

Kim, S.: Effect of Large Tidal Variation on Storm Surge in the Western Coastal Sea of Korea, *Ph.D. Thesis*, Kyoto University, 2007.

Kim, S., Takayama, T., Yasuda, T. and Mase, H.: Tide-Srufge-Wave Coupling Model and Its Application to Surge and Wave Hindcast for Typhoon 0603, *Annuals of the Disaster Prevention Research Institute*, Kyoto University, No. 50 B, 2007.

Lafaurie, B., Nardone, C., Scardovelli, R., Zaleski, S. and Zanetti, G.: Modelling merging and fragmentation in multiphase flows with SURFER, *Journal of Computational Physics*, Vol. 113, pp.134-147, 1994.

Lai, C. J. and Yen, C. W.: Turbulent free surface flow simulation using a multilayer model, *International Journal for Numerical Methods in Fluids*, Vol. 16, pp.1007-1025, 1993.

Lee, D., Nakagawa, H, Kawaike, K., Baba, Y. and Zhang, H.: Inundation flow considering overflow due to water level rise by river structures, *Annuals of the Disaster Prevention Research Institute*, Kyoto University, No 53 B, 2010.

Lee, D., Nakagawa, H, Kawaike, K., Baba, Y. and Zhang, H.: Study on flood flow considering water level rise by hydraulic structures, *Annual Journal of Hydraulic Engineering, JSCE*, Vol. 54, pp.187-192, 2010.

Lee, D., Nakagawa, H, Kawaike, K., Baba, Y. and Zhang, H.: Numerical simulation of inundation flow considering overflow from river, *Proceedings of the International Symposium on Water and Sediment Disasters in East Asia*, pp.183-190, 2010.

Lee, D., Nakagawa, H, Kawaike, K., Baba, Y. and Zhang, H.: Study on inundation flow by numerical model coupling 2D and 3D flows, *International Symposium on a Robust and Resilient Society against Natural Hazards & Environmental Disasters and the third AUN/Seed-Net Regional Conference on Geo-Disaster Mitigation*, 2010.

Leonard, B. P.: A stable and accurate convective modeling procedure based on quadratic upstream interpolation, *Computational Method in Applied Mechanics and Engineering*, Vol. 19, pp.59-98, 1979.

Leonard, B. P.: The ULTIMATE conservative difference scheme applied to unsteady one-dimensional advection, *Computational Method in Applied Mechanics and Engineering*, Vol. 88, pp.17-74, 1991.

Lhomme, J., Guinot, V. and Zech, Y.: Two-dimensional shallow-water model with porosity for urban flood modeling, *Journal of Hydraulic Research*, Vo. 46, No. 1, pp.45-64, 2008.

Li, X. L.: Study of three-dimensional Rayleigh-Taylor instability compressible fluids through level set method and parallel computation, *Physics of Fluids A*, Vol. 5(8), pp.1904-1913, 1993.

Li, Y. S. and Zhan, J. M.: An efficient three-dimensional semi-implicit finite element scheme for simulation of free surface flows, *International Journal for Numerical Methods in Fluids*, Vol. 16, pp.187-198, 1993.

Li, W., Chen, Q. and Mao, J.: Development of 1D and 2D coupled model to simulate urban inundation: An application to Beijing Olympic Village, *Chinese Science Bulletin*, Vol. 54, No. 9, pp.1613-1621, 2009.

Martin, J. C. and Moyce, W. J.: An experimental study of the collapse of liquid columns on a rigid horizontal plane, *Philos. Trans. Roy. Soc. London*, Vol. A244, pp.312-324, 1952.

Mignot, E. Paquier, A. and Riviere N.: How a 2-D code can simulate urban flood situations, *Proceedings of River Flow 2004 Conference*, Federico Ⅱ University of Napoli, Italy, Vol. 2, pp.1031-1040, 2004.

Muzaferija, S., Peric, M. and Seidl, V.: Computation of flow around circular cylinder in a channel, *Internal Report, Institute fur Schiffbau*, University of Hamburg, 1995.

Nakagawa, H., Ushigaki, T., Muto, Y., Inoue, K., Toda, K., Tagawa, H., Yoshida, Y., Tatsumi, K. Zhang, H. and Yagi, H.: Flood inundation analysis in urban area using large scale inundation facility, *Annuals of the Disaster Prevention Research Institute*, Kyoto University, No.46B, pp.575-584, 2003 (in Japanese).

Nichols, B. D. and Hirt, C. W.: Improved free surface boundary conditions for numerical incompressible flow calculations, *Journal of Computational Physics*, Vol. 8, pp.434-448, 1971.

Nichols, B. D. and Hirt, C. W.: Calculating three-dimensional free surface flows in the vicinity of submerged and exposed structures. *Journal of Computational Physics*, Vol. 8, pp.434-448, 1973.

Noh, W. F. and Woodward, P.: SLIC (Simple Line Interface Calculations). *Lecture Notes in Physics*, Vol. 59, pp.330-340, 1976.

Osher, S. and Sethian, J. A.: Fronts propagating with curvature-dependant speed: algorithms based on Hamilton-Jacobi formulations. *Journal of Computational Physics*, Vol. 79, pp.12-49, 1988.

Patankar, S.V.: Numerical Heat Transfer and Fluid Flow, McGraw-Hill, New York, 1980.

Pericleous, K. A. and Chan, K. S.: The sea method for free surface problems with heat transfer and change of phase, *presented at the 1994 ASME fluids engineering division summer meeting,* Lake Tahoe, Nevada, 1994.

Ramshaw, J. D. and Trapp, J. A.: A numerical technique for low-speed homogeneous two-phase flow with sharp interfaces, *Journal of Computational Physics*, Vol. 21, pp.438-453, 1976.

Renardy, M. and Renardy, Y.: On the nature of boundary conditions for flows with moving free surfaces, *Journal of Computational Physics*, Vol. 93, pp.325-335, 1991.

Rhie, C. M. and Chow, W. L.: Numerical study of the turbulent flow past an airfoil with trailing edge separation, *Journal of AIAA*, Vol. 21, pp.1525-1532,1983.

Rodi, W.: Turbulence Models and Their Application in Hydraulics: a State of the Art Review, University of Karlsruhe, Germany, 1980.

Saad, Y.: Iterative Methods for Sparse Linear System (Second Edition), *Society for Industrial & Applied Mathematics*, 2003

Salaheldin, T. M., Imran, J. and Chaudhry, M. H.: Numerical modeling of three-dimensional flow field around circular piers, *Journal of Hydraulic Engineering, ASCE*, Vol. 130(2), pp.91-100, 2004.

Sethian, J. A.: Level set methods: Evolving interfaces in geometry, *Fluid mechanics, computer vision and materials sciences,* Cambridge University Press.

Shigeeda, M., Akiyama, J. and Ura, M.: Numerical simulations of flood propagation in a floodplain with structures, *Journal of Hydroscience and Hydraulic Engineering*, Vol. 20, No. 2, pp.117-129, 2002.

Shigeeda, M., and Akiyama, J.: Numerical and experimental study on two-dimensional flood flows with and without structures, *Journal of Hydraulic Engineering,* ASCE, Vol. 129, No. 10, pp.817-821, 2003.

Shigeeda, M. and Akiyama, J.: Predictions of overflow discharge from the river by a dynamic inundation analysis model, *Advances in River Engineering, JSCE*, Vol. 11, 2005.

Sleijpen, G. L. G. and Fokkema, D. R.: BiCGSTAB (1) for linear equations involving unsymmetrical matrices with complex spectrum, *Electronic transactions on Numerical Analysis*, Kent State University, Vol. 1, pp.11-32, 1993.

Soulis, J. V.: Computation of two-dimensional dam-break flood flows, *International Journal for Numerical Methods in Fluids*, Vol. 14, pp.631-664, 1992.

Speziale, C. G.: Analytical methods for the development of Reynolds-stress closures in turbulence, *Annual Review of Fluid Mechanics*, Vol. 23, pp.107-157, 1991.

Sussman, M., Smereka, P. and Osher, S.: A level set approach for computing solutions to incompressible two-phase flow, *Journal of Computational Physics*, Vol. 114, pp.146-159, 1994.

Takahashi, T., Nakagawa, H., Satofuka, Y. and Kawaike, K.: Flood and sediment disasters triggered by 1999 rainfall in Venezuela; A river restoration plan for an alluvial fan, *Journal of Natural Disaster Science*, Vol. 23, pp.65-82, 2001.

Takahashi, T., Nakagawa, H. and Kakehi, T.: Numerical simulation method of overland flood flow considering the existence of drainage channel networks, *Annuals of the Disaster Prevention Research Institute,* Kyoto University, No. 31 B-2, 1988 (in Japanese).

Takahashi, T., Ookubo, K. and Nakagawa, H.: Analysis of inundation due to overspilled flood water from the Nakashima river caused by heavy rainfall in Nagasaki, July, 1982, *Annuals of the Disaster Prevention Research Institute*, Kyoto University, No. 26 B-2, 1983 (in Japanese).

Takeda, M.: Development of storm surge analysis method and its application, *Ph.D. Thesis*, Kyoto University, 1996 (in Japanese).

Takizawa, A., Koshizuka, S. and Kondo, S.: Generalization of physical component boundary fitted co-ordinate (PCBFC) method for the analysis of free-surface flow, *International Journal for Numerical Methods in Fluids*, Vol. 15, pp.1213-1237, 1992.

Toda, K., Inoue, K. and Murase, S.: Numerical simulation of inundation flow due to heavy rainfall in urban area, *Proceedings of the '99 International Symposium on Flood Control*, pp.566-574, 1999.

Torrey, M. D., Mjolsness, R. C. and Stein, L. R.: NASA-VOF3D: A three dimensional computer program for incompressible flows with free surfaces, *Los Alamos National Laboratory report LA-11009-MS*, 1987.

Ubbink, O.: Numerical prediction of two fluid systems with sharp interfaces, *Ph.D. Thesis*, University of London, 1997.

Ubbink, O. and Issa, R. I.: A method for capturing sharp fluid interfaces on arbitrary meshes, *Journal of Computational Physics*, Vol. 153, pp.26-50, 1999.

Van der Vorst, H. A.: Bi-CGSTAB: a fast and smoothly converging variant of Bi-CG for the solution of non-symmetrical linear systems, *SIAM Journal on Scientific and Statistical Computing*, Vol. 13(2), pp.631-644, 1992.

Van Leer, B.: towards the ultimate conservative differencing shceme, A new approach to numerical convection, *Journal of Computational Physics*, Vol. 23, pp.276-299, 1977.

Versteeg, H. K. and Malalasekera, W.: An introduction to computational fluid dynamics, the finite volume method, *Harlow: Longman Scientific & Technical*, 1995.

Youngs, D. L.: Time-dependent multi-material flow with large fluid distortion, *Numerical Methods for fluid dynamics*, London: Academic Press, pp.273-285, 1982.

Zhang, D., Chang, H, Seaman, N. L., Warner, T. T. and Fritsch, J. M.: A Two-Way Interactive Nesting Procedure with Variable Terrain Resolution, *American Meteorological Society*, Vol. 114, pp.1330-1339, 1986.

Zhang, H.: Study on Flow and Bed Evolution in Channels with Spur Dykes, *Ph.D. Thesis*, Kyoto University, 2005.

Zhang, H., Nakagawa, H., Ishigaki, T. Muto, Y.: A RANS solver using a 3D unstructured FVM procedure, *Annuals of the Disaster Prevention Research Institute*, Kyoto University, No. 48 B, 2005.

Zhang, H., Nakagawa, H., Muto, Y., Touchi, D. and Muramoto, Y.: 2D numerical model for river flow and bed deformation based on unstructured mesh, *Journal of Applied Mechanics*, JSCE, Vol. 9, pp.783-794, 2006.

Zhang, J.: Preconditioned Krylov subspace methods for solving nonsymmetrical matrices from CFD applications, *Computational Methods in Applied Mechanics and Engineering*, Vol. 189, pp.825-840, 2000.

Zhiguo, H. M., Weiming, W. and Sam, S. Y. W.: Coupled Finite-Volume Model for 2D Surface and 3D Subsurface Flows, *Journal of Hydrologic Engineering, ASCE*, pp.835-845, 2008.

Zhou, G.: Numerical simulations of physical discontinuities in single and multi-fluid flows for arbitrary mach numbers, *Ph.D. Thesis*, Chalmers University of Technology, Gothenburg, 1995.

List of Figures

List of Tables

Curriculum Vitae

Name LEE Dongkeun

Citizenship Korea

Birth 1978 September 23, Busan, Korea

.

Ph.D. Student (2007 - 2010)
Department of Civil and Earth Resources Engineering
Kyoto University, Kyoto, Japan

M. Sc. in Hydraulic Engineering (2004 - 2006)
Department of Civil Engineering, Faculty Engineering
Inje University, Gimhae, Korea

B. E. in Civil Engineering (1997 - 2004)
Department of Civil Engineering, Faculty Engineering
Inje University, Gimhae, Korea

Papers based on the Thesis

Lee, D., Nakagawa, H., Kawaike, K., Baba, Y. and Zhang, H.: Numerical Study on Inundation Flow considering Levee Overflow due to Water Level Rise by Hydraulic Structures, *Proceedings of the 28th Annual Meeting of the Japan Society for Natural Disaster Science*, pp.65-66, September, 2009.

Lee, D., Nakagawa, H., Kawaike, K., Baba, Y. and Zhang, H.: Inundation Flow considering Overflow due to Water Level Rise by River Structures, *Annuals of the Disaster Prevention Research Institute*, Kyoto University, No. 53B, pp.607-616, June, 2010

Lee, D., Nakagawa, H., Kawaike, K., Baba, Y. and Zhang, H.: Study on Flood Flow considering Water Level Rise by Hydraulic Structures, *Annual Journal of Hydraulic Engineering*, JSCE, Vol. 54, pp.187-192, February, 2010.

Lee, D., Nakagawa, H., Kawaike, K., Baba, Y. and Zhang, H.: Numerical Simulation of Inundation Flow considering Overflow from River, *Proceedings of the International Symposium on Water and Sediment Disasters in East Asia*, pp.183-190, March, 2010

Lee, D., Nakagawa, H., Kawaike, K., Baba, Y. and Zhang, H.: Study on Inundation Flow considering Overflow from River connected with Floodplain, *Proceedings of the 29th Annual Meeting of the Japan Society for Natural Disaster Science*, pp.169-170, September, 2010.

Lee, D., Nakagawa, H., Kawaike, K., Baba, Y. and Zhang, H.: Study on Inundation Flow by Numerical Model Coupling 2D and 3D Flows, *International Symposium on a Robust and Resilient Society against Natural Hazards & Environmental Disasters and the third AUN/Seed-Net Regional Conference on Geo-Disaster Mitigation*, pp.217-226, August, 2010.

Lee, D., Nakagawa, H., Kawaike, K., Baba, Y. and Zhang, H.: Estimation of Inundation flow using 2D-3D Numerical Coupling Model, *Annual Journal of Hydraulic Engineering*, JSCE, Vol. 55 (in printing).